Republic of Iraq

Ministry of Higher Education and Scientific Research

University of Babylon

College of Materials Engineering

Department of Polymer Engineering and Petrochemical Industries

Experimental and Numerical Simulation of Rheological Properties of Hydrophobically Associated Polymer Toward Enhanced Oil Recovery

A dissertation

Submitted to Council of the College Materials Engineering /University of Babylon in Partial Fulfillment of the Requirements for the Degree of Doctorate of Philosophy in Materials Engineering / Polymer

By

Saja Haider Mohammed Jabar

Supervised by

Prof.Dr. Nizar Jawad Hadi

2023 A.M **1446 A.H**


بِسْمِ ٱللَّهِ ٱلرَّحْمَٰنِ ٱلرَّحِيمِ ١
ٱلْحَمْدُ لِلَّهِ رَبِّ ٱلْعَٰلَمِينَ ٢
ٱلرَّحْمَٰنِ ٱلرَّحِيمِ ٣ مَٰلِكِ يَوْمِ ٱلدِّينِ ٤
إِيَّاكَ نَعْبُدُ وَإِيَّاكَ نَسْتَعِينُ ٥ ٱهْدِنَا
ٱلصِّرَٰطَ ٱلْمُسْتَقِيمَ ٦ صِرَٰطَ ٱلَّذِينَ أَنْعَمْتَ
عَلَيْهِمْ غَيْرِ ٱلْمَغْضُوبِ عَلَيْهِمْ
وَلَا ٱلضَّآلِّينَ ٧

SUPERVISORS CERTIFICATION

We certify that this thesis entitled "**Experimental and Numerical Simulation of Rheological Properties of Hydrophobically Associated Polymer Toward Enhanced Oil Recovery**''had been carried out under our supervision at the University of Babylon / Collage of Material's Engineering / Department of Engineering Polymer and Petrochemical Industries in partial fulfillment of the requirements for the degree of doctor of philosophy in in Materials Engineering / Polymer.

Signature:

Prof. Dr. Qusai.F.Alsalhy

University of Technology/ Chemistry Engineering Department
Date: / /2023
(Chairman)

Signature:
Prof. Dr. A.A. Al-Zubiedy
University of Babylon /College of Materials Engineering/ Polymer and Petrochemical Industries Department
Date: / /2023
(Member)

Signature:
Assist. Prof. Dr. Salih Abbas Habeeb
University of Babylon/ College of Materials Engineering/ Polymer and Petrochemical Industries Department
Date: / /2023
(Member)

Signature:
Prof. Dr. Auda.J. Brahai
University of Babylon / College of Materials Engineering /Polymer and Petrochemical Industries Department
Date: / /2023
(Member)

Signature:
Prof. Dr. Nizar .J. Hadi
University of Babylon/ College of Materials Engineering/ Polymer and Petrochemical Industries Department
Date: / /2023
(Member)

Signature:
Prof. Dr. Haider .K. Rashid
University of Babylon/ College of Materials Engineering/Ceramics and Building Materials Department
Date: / /2023
(Member)

Approval of Polymer and Petrochemical Industries (Head of the Department)

Signature:
Prof. Dr. Zoalfokkar .K. Mezaal
Date: / /2023

Approval of Materials Engineering College (Dean of the College)

Signature:
Prof. Dr. Abd alraheem. K. Alfatlawy
Date: / /2023

ACKNOWLEDGEMENT

Praise, thank, and gratitude to the benefactor and Single-handed ALLAH who enabled and helped me to achieve this work.

I would like to express my gratitude to my supervisor, Prof. Dr.Nizar Jawad Hadi who has been guidance and advice.I would like to thank Head of Department and all Teaching staff, laboratories of Materials engineering, and staff laboratories of Basra Oil Company /Research and Quality department-Nahran Omar. Finally, I would like to thank everyone help me in any way for obtaining the present work.

DEDICATION

To

My Father and Mother

My Sisters and My Brother

My Hasbent Ms.c Wissam Hassan

My Daughter Fatima AL-Zehraa

My Boy Hassan Wissam Hassan

Raid kamel Boutros / Basra Oil Company / Research and

Quality department-Nahran Omar.

Ali Hussein Yasser / Basra Oil Company

My dear supervisor (Prof. Dr. Nizar Jawad Hadi)

with all respect My friends

Abstract:

This work aims to improve the production of residual crude oil inside the porous media (Core Samples) through the use of polymer flooding approach in experimental and numerical method. The hydrophobic associative polyacrylamide polymer (HAPAM) with concentrations of (500, 1000, 1500 and 2000) ppm, was mixed with brine water for use in polymeric tests and displacement. The rheological, physical, petrophysical properties ,and oil recovery percentage were investigated. Numerical simulation was performed using finite difference method (FDM) in the Computational Modeling Group (CMG) program and the finite element method (FEM) in Ansys Fluent software.

The measurement of rheological properties were investigated according to viscosity change with concentration, shear rate, shear stress, shear resistance and temperature. The physical properties were tested according to change in density , surface tension and interfacial tension with different HAPAM concentrations. A rig of core flooding system was design and built in this study to measure the Petrophysical properties and evaluate the enhanced oil recovery (EOR) . Porosity, permeability, Darcy velocity and capillary number of three types of carbonate rocks Core 1; Core 2 and Core 3 and two types of sandstones Core4 and Core5 were tested in this system.

Wettability study was done through the relative permeability curves with water saturation percentage and oil recovery with pore volume. The mechanical degradation was estimated from the curves of the obvious viscosity within the porous media and the shear viscosity within the rheometer with the increase shear rate, the shear viscosity with the Darcy velocity and the shear rate in addition to the pressure difference with the Darcy velocity.

Laboratory core-flood experiments have been simulated the use of CMG-STARS to research relative permeability and oil recovery percentage .Cartesian version changed into hired to expand a sturdy numerical technique to healthy flooding houses of analyzed fluids. Initially, brine water changed into simulate and HAPAM solution was injected separately. Ansys Fluent was used to estimate the contact area indicating the brine-oil or HAPAM-oil solutions as immiscible liquids in a three dimensional(3D) qualitatively. Simulations were performed depend on surface tension, interfacial tension (IFT), and viscosity effects.

The experimental results showed that all HAPAM solutions have non-Newtonian flow, Shear thinning behavior was dominant and compared with the power law model. The shear viscosity decreases and the shear stress increases with the shear rate above 7.3 s^{-1}.HAPAM 1500 ppm solution has higher viscosity, density, surface tension, shear resistance, thermal stability, aging time, consistency index(k) and improved wettability, with lower flow index (n) and interfacial tension.

The 1500 ppm HAPAM in comparison with brine water has a high Darcy velocity, and wettability. Also, low capillary number due to the delaying of the break through point of oil. Shear thickening phenomena and mechanical degradation at shear rate above 7.3s^{-1}.Experimental result for improving the ability to extract oil by using polymer instead of brine where (31,33,30.4, 30, and 29)%, while by CMG (30.85, 33.03, 30.47, 29.88, and 28.97)% respectively .The qualitative results of 3D Ansys model showed high stability and absence of viscous fingers in the contact area between this solution and the oil. Numerical simulations obtain a good compatibility with the experimental work in rheological , wettability, mechanical degradation, and relative permeability.

Table of Contents

Abbreviations

Abbreviations	Meaning
OPEC	Organization of the Petroleum Exporting Countries
EOR	Enhanced oil recovery
IOR	Improved Oil Recovery
SAGD	Steam Assisted Gravity Drainage
CSS	Cyclic Steam Stimulation
(VAPEX	Vapor Extraction
(TEOR)	Thermal methods (TEOR)
GEOR	Gas methods (GEOR
CEOR	Chemical methods (CEOR)
Eq.	Equation
HT	high temperature
HS	high salinity
HPAM	Hydrolyzed polyacrylamide (HPAM)
HAPAM	hydrophobically associating polyacrylamide (HAPAM).
HTHS	high temperature high salinity (HTHS)
CAC	critical aggregation concentration (CAC)
Mw	molecular weight (Mw).
MWD	molecular weight distribution (MWD).
TDS	total dissolved solids (TDS)

Symbols

Symbols	Meaning
M	Mobility ratio (M)
kw	relative permeability of water
ko	relative permeability of oil
IFT	interfacial tension
EV	volumetric displacement efficiency
EA	areal displacement efficiency
El	vertical sweep efficiency
fo	fractional flow of oil
Pc	capillary pressure (N/m2)
γ	Interfacial tension between oil and water (N/m)
ɵ	contact angle (degree)
Rc	radius of capillary tube (m)
Nc	capillary number
μ	viscosity (cp)
σos	$\sigma os=$ interfacial tension between oil and solid (N/m)
σws	$\sigma ws =$ interfacial tension between water and solid (N/m)
σow	$\sigma ow =$ interfacial tension n between oil and water (N/m)
∅	∅=porosity
E_V	Volumetric sweep efficiency
PV	Porous volume
E_A	Areal displacement efficiency
E_l	El is vertical sweep efficiency

Chapter One

Introduction

1.1 Oil Production

Daily cuts in reservoir oil production, have led to a severe oil crisis and a general rise in oil prices. This has resulted in the oil industry having to employ cutting-edge recovery methods to extract oil from more challenging regions, where it is less readily available. Primary production refers to the traditional method of extracting oil from reservoirs by the use of fluid energy (reservoir depressurization). To boost oil output after a drop in reservoir pressure, a secondary recovery strategy including the injection of water or gas into the reservoir is required. Capillary force prevents water flooding from releasing viscous oils or initial oil droplets from carbonate reservoirs [1-3].

The injected water will quickly spread across the fissures, and the remaining oil will be swept up in the finer crevices. As a follow-up to secondary recovery, heavy oil reservoirs can benefit from thermal treatments that reduce oil viscosity. Alkalis diminish the IFT between injection water and oil, and surfactants change its wettability to rock. These methods are called EOR processes in the industry [4].

Chemical wettability alteration in fractured carbonate reservoirs and non-thermal viscous oil recovery as an efficient EOR technology for mature, depleted light oil conventional reservoirs have increased in recent years [5].Two-thirds of a reservoir's OOIP remains unproduced after primary and secondary recovery techniques have been applied, waiting instead to be recovered using effective enhanced oil recovery (EOR) techniques. Chemical

flooding, miscible flooding, and thermal oil recovery are the three main EOR methods [6].After water flooding, leftover oil can be extracted using chemical flooding techniques, which are a subset of EOR procedures. These strategies are implemented to lessen the interfacial tension, raise the viscosity of the brine to regulate mobility, and boost the effectiveness of the sweep during tertiary recovery [7]. It is well-known that increasing the use of polymers improves the efficiency of both vertical and areal sweep, leading to increased oil recovery [8]. Polymer use also decreases the porous media's permeability, making the injected water thicker and more resistant to flow. Polymer injection reduces water-oil mobility ratios. Aqueous phase viscosity lowers mobility ratio. After water flooding, mobile oil needs a significant viscous force perpendicular to the oil-water contact to move [9]. Pumping, mobilizing, and pushing against capillary forces recovers the remaining oil [10].

Modeling chemical flooding experiments for design or optimization determines decision parameters like the cumulative oil recovery factor and net present value. A simulator had towards be chosen before any work could be done in the simulation. Two features were prioritized when selecting the best simulator. The simulator had to be capable of mimicking the polymer behavior of interest[11] and have the features needed to do so. For instance, it was crucial that the chosen simulator could mimic the deterioration behavior because of its significance. The simulator's wide adoption among the sector was another important goal[12]. It is vital that a widely used simulator can model the experimental findings [13], as the objective of these polymer tests was to learn more about their properties for potential deployments in the field.

These intricate chemical EOR processes can be modeled using a variety of available commercial reservoir simulators. CMG-STARS, ECLIPSE, and UTCHEM, with their widespread applicability, will receive the bulk of

attention. Both CMG-STARS and UTCHEM model and compare the results of core flood experiments conducted in the lab. CMG-STARS has replicated core flood experiments to study chemical flood flow dynamics [14]. These researchers then employed these parameters in field-scale simulations. In a Dalia field feasibility study using the ECLIPSE polymer module, injectivity and oil recovery improved [15–20].

1.2 Research Objectives

In view of the increasing need to develop novel chemical systems for beneficial EOR application, the current work of the thesis encompasses the application of HAPAM in a myriad range of injection formulation strategies. HAPAM serve as a useful, . The objectives of the research study include:

1- Enhanced oil recovery by polymer flooding method.

2- Using hydrophobic associative polyacrylamide (HAPAM) in EOR.

3- Measuring rheological , physical , aging time and shear resistance of HAPAM aqueous solution.

4- Design and manufacturing of relative permeability machine (core flooding test).

5- Using sandstone and carbonate as core in core flooding test . The petrophysical, relative permeability curve and oil recovery are tested.

6- Using CMG program for modeling oil recovery contour.

7- Using Ansys fluent for modeling oil volume fraction contour.

8-Perform comparison between experimental and modeling study in term of shear viscosity and shear stress with shear rate , relative permeability, differential pressure, and Apparent viscosity .

Chapter Two

Theoretical Part and Literature Review

2.1 Enhanced Oil Recovery Techniques:-

Oil output from the reservoir can be accessed in a number of different ways, as shown in Figure 2.1. Processes of primary, secondary, and tertiary recovery are used in that order because of cost constraints on the oil production process. The terms for various oil extraction techniques are as follows [21]:-

2.1.1 Primary recovery:

Pressure depletion employing reservoir energy, also known as the expansion and compaction driving mechanisms, is the primary method of oil recovery during the early stages of an oilfield's production lifecycle. It is also known as injection-free healing. Due to the inefficiency of both natural reservoir resources and the artificial lift method, oil recovery is low at less than 30%[22].

2.1.2 Secondary recovery:

The production of oil can be prolonged by reinjection water and gas into the reserve to raise pressure. Most prevalent kind of subsequent recovery is water flooding. After the reservoir has been drained via flooding, there is still a sizable amount of oil that must be recovered using tertiary recovery techniques [23].

2.1.3 Tertiary recovery:

After the reservoir's primary and secondary oil reserves have been depleted, a third recovery method, including the injection of an external energy source, is used to displace the residual oil. Secondary recovery is also addressed by EOR

methods. After water flooding, the typical oil recovery fraction is 35%. This indicates that the reservoir likely still contains a significant quantity of oil, which motivates the EOR process. Any achievement in recovering a portion of this remaining oil is regarded as advantageous. For example, an increase of 10% or from 35% to 45% in the oil recovery factor yields 1 trillion barrels of oil [24,25].

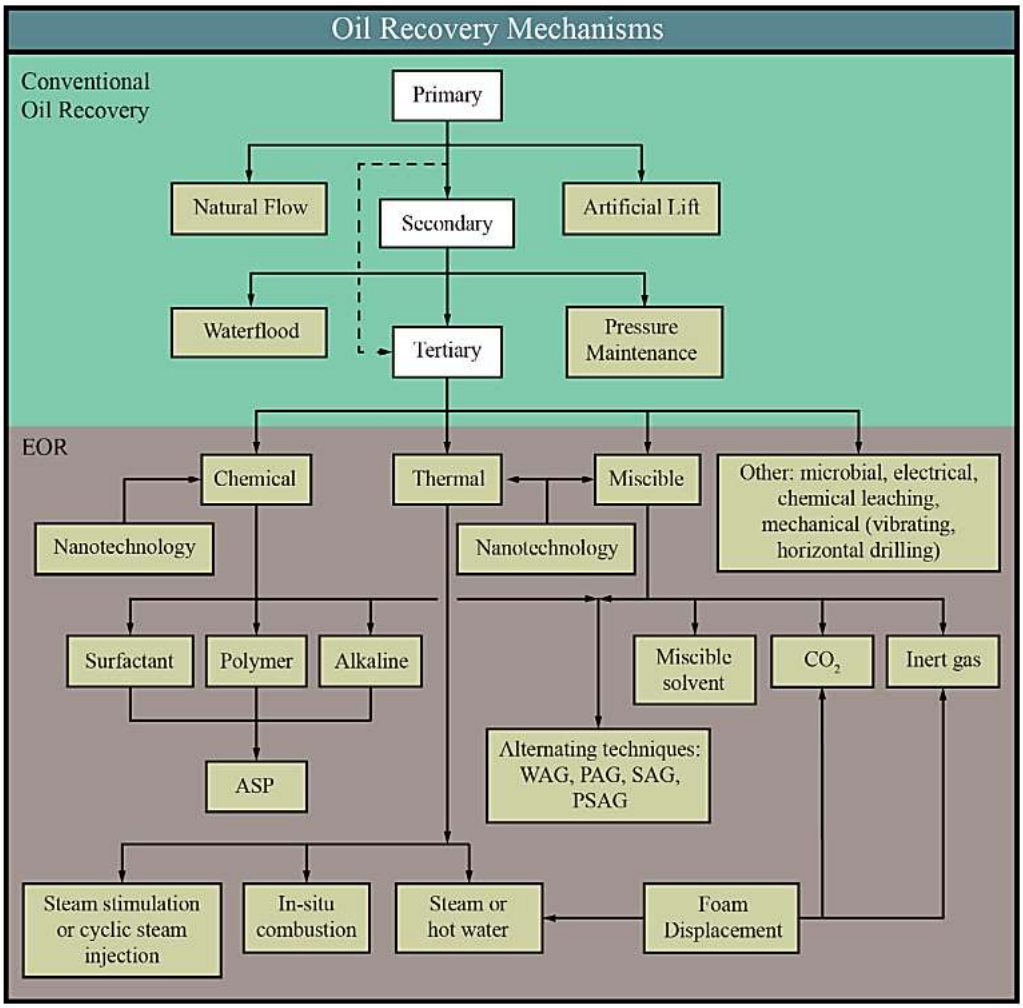

Figure 2.1:- Oil recovery Mechanisms [21].

The purpose of EOR technology is to increase oil recovery rates beyond those of primary and secondary recovery by the use of more efficient sweeping. There are times when the goal of EOR techniques is to lower the level of residual oil saturation [26]. Improved oil recovery, or EOR, is a larger process

that includes EOR technology. All techniques besides the principal method of oil recovery fall under the umbrella of IOR. Reservoir development encompasses a wide variety of techniques, including infill drilling, cutting-edge well technologies, reservoir organization, control, etc. [27]. High oil recovery could result from combining IOR and EOR strategies [28].

Enhanced-oil recovery" (EOR) uses external energy resources to establish a pressure gradient, alter rock wettability and permeability, and vary fluid characteristics and interfacial tension to regulate oil transport from the injection well to the production well (IFT) [30].The following reviews [29] outline the most common commercial recovery technologies used in EOR technology: -

2.1.3.1 Thermal methods (TEOR)

Introducing thermal energy into the reservoir can increase temperature, which in turn greatly decreases oil viscosity. Several methods exist for doing this, including as by injecting steam or hot water, or setting fire to the material on the spot. Some current assessments of TEOR can be found elsewhere [31].

2.1.3.2 Gas methods (GEOR)

Using alternative fuels such as natural gas, carbon dioxide, or nitrogen to replace oil. Some people refer to miscible GEOR as a solvent technique [32]

2.1.3.3 Chemical Methods (CEOR)

Injecting compounds that are water soluble to improve oil displacement. An integral part of CEOR is the flooding with polymers, surfactants, and alkaline surfactant polymers. The most prevalent type of CEOR is known as polymer flooding. You can find an up-to-date analysis of CEOR in another place. Other EOR processes, such as microbial EOR, hybrid EOR, and others, are yet to be confirmed or are the subject of ongoing research in addition to the primary

EOR approaches that have been given above. It is dependent on the development of the field, but in the majority of cases, it is recommended that EOR be started when the field is at an early maturity stage. The fact that one EOR strategy can be utilized in place of another gives rise to the availability of a wide range of alternative strategies. Chemical EOR methods are an alternative that might be considered in some circumstances, such as when thermal techniques cannot be employed due to the limits of those processes [33].

2.2 Polymer Flooding

Polymer flooding has been one of the most technically established and commonly used technologies in CEOR processes for over 50 years as appear in Table 2.1. This tech has reached the point of full maturity. In addition to working well in carbonate and sandstone reservoirs, this shows how flexible it is. Oil production can be improved in a number of ways, including by reducing the occurrence of viscous fingering, raising the mobility ratio, and improving oil sweep efficiency. The method works well with heterogeneous reservoirs that exhibit significant mobility ratios or permeability fluctuations. Polymer flooding seeks to improve oil recovery by 5-20% over water flooding. Its basic concept, first patented in 1944 [34], involves changing the viscosity of the water that is injected. Afterwards, testing results showed that the mobility ratio may be enhanced.

The inability to use polymer flooding in reservoirs with high salinity(HS), high temperature(HT), and strong shear is a significant technical challenge (HS). In the correct conditions, a well-designed polymer flooding method has the potential to greatly boost oil recovery rates and even outperform existing

EOR techniques. It is one of the EOR methods that saves the most money. So, polymer injectivity is an important part of how well the process works [35].

During water flooding, oil displacement is unsuccessful because water is Newtonian and the viscosity difference between oil and water is considerable. Because of this, a lot of oil is lost. There are two types of oil that make up this massive quantity: residual and bypassed. Interfacial tension(IFT) among water and oil is driving force behind capillary forces, which means that some oil will remain immobile or trapped after a flood. For reasons such as reservoir heterogeneity (low mobility) and viscous fingering, some oil may be inaccessible via water flood, earning the term "bypassed oil" [36]. There is extensive discussion elsewhere of the relationship between the sweep efficiency of the microscopic (residual oil) and the macroscopic (bypassed oil) scales and the overall displacement efficiency. The procedure of polymer flooding is often used to regulate the mobility of a polymer. Any procedure that alters the kinetic energy distribution between the injected and displaced fluids is considered a mobility control procedure. In order to decrease the relative permeability of injected water. Key methods by which polymer flooding improves oil recovery rates include[37].

Table2.1 :- Field applications polymer flooding[38]

Country	Field	Polymer Type	T (°C)	Formation Salinity (mg/L)
China	Daqing	HPAM	45.0	9000
China	Gudong	HPAM	68.0	3022
China	Bohai Bay	HPAM	65.0	6070
China	Xing Long Tai	HPAM	56.6	3112
China	Bohai oil field	HAPAM	65.0	32423
China	Henan oil field	HPAM	75.0	5060
China	Shengli	HPAM	70.0	10000
USA	Cambridge Minnelusa	PAM	55.6	Not specified
USA	Tambaredjo	HPAM	36.0	Not Specified
USA	Tanner	PAM	80.0	66800 (P)[a]
USA	West Khiel	HPAM	57.0	46,480 (P)[a]
Canada	Pelican	HPAM	23.0	6800
Canada	David pool	PAM	31.0	6660 (I)[b]
Germany	Germany Eddesse-Nord	Xanthan Gum	22.0	120,000
Germany	Vorhop-Knesebeck	Xanthan Gum	56.0	210,000
Austria	Matzen	HPAM	50.0	20,000
India	Viraj	HPAM	81.0	13,250
India	Sanand	PAM	85.0	Not specified
Russia	Romashkino (Tatarstan)	HEC	36.0	250,000

2.2.1Mobility ratio (M)

Prior to wet-through, a fluid's mobility is considered to be in parity with that of the displacing fluid (water) if the ratio is less than 1 (oil) [39].

$$M = \frac{\mu_o k_w}{\mu_w k_o} \dots\dots\dots\dots\dots\dots\dots\dots\dots\dots\dots\dots\dots\dots\dots\dots\dots\dots\dots\dots\dots\dots\dots (2.1)$$

Water and oil have different viscosities, denoted by μ_w and μ_o, respectively, and their corresponding relative viscosities, k_w besides and k_o, are shown below. Water and oil have different levels of permeability. As a result of polymer retention, increasing the viscosity of water would lessen viscosity differential between oil then water $(\frac{\mu_o}{\mu_w})$ water resistance might be improved, and relative permeability might be decreased. Since this is the case, both the mobility ratio and the sweep efficiency can be improved.

Figure 2.2 shows how the mobility ratio influences the efficiency of the sweep. Viscosity fingering can be mitigated by decreasing M. For instance, after M< 1, the water completely covers the oil zone, resulting in a "favorable" mobility ratio due to the piston-like displacement. When M is more than one, On the other hand, oil is wasted because of viscous fingering and early water breakout. With a greater M,oil is redirected around more obstacles because of severe channeling and fingering. When M is decreased, oil fraction flow is increased. It's possible that this will speed up oil production and slow down the breakthrough of water. Polymer flooding should be started early, besides perhaps even as a minor flood, when the mobility ratio of the field is high [40]. Because it’s often not feasible to change the properties of the displaced fluid or the permeability of porous media, lower mobility ratios can only be achieved by lowering the mobility of the displacing fluid. This recovers oil by increasing both volumetric and displacement sweep efficiency [41].

2.2.2 Volumetric sweep efficiency (Ev):-

Is the Porous volume (PV) of a reservoir contacted by a displacing fluid divided by the total porous volume (PV) [42]:-

$$E_v = \frac{(E_A x E_I)}{(P_v)} \quad \text{.....(2.2)}$$

Where, E_V: volumetric displacement efficiency;E_A : areal displacement efficiency. It is expressed as area sweep by displacing fluid divided by total reservoir area target; El: effectiveness of the front's vertical sweep, as a ratio of injected fluid pore space to all layers behind the front.

2.2.3 Fractional Flow of Oil :-

According to the Buckley-Leveret hypothesis of non-miscible displacement, Oil flow (fo) increases when mobility ratio among water besides oil decreases [43,44]:-

$$f_o = \frac{1}{1 + M} \qquad (2.3)$$

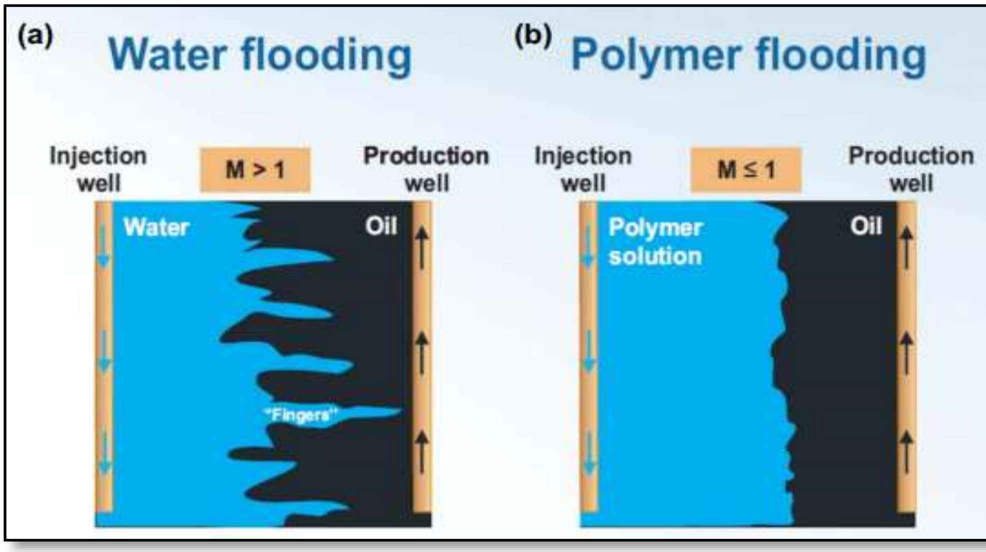

Figure 2.2 :- Comparison between water flooding and polymer flooding [44].

2.2.4 Polymer Retention

One of the most important factors in whether or not a polymer flooding project will be successful is the amount of polymer that can be retained. Using a polymer solution with low retention values improves the sweep's effectiveness. When a solution moves across a porous surface, there are a number of mechanisms 37 that prevent individual polymer molecules from blending in with the rest of the solution. Figure 2.3 depicts three retention mechanisms: adsorption, mechanical entrapment, and hydrodynamic retention. Well injectivity is hampered when polymer retention lowers polymer concentration, hence decreasing polymer viscosity or inducing polymer permeability. However, the economic viability of polymer flooding is seriously threatened if retention levels are high. Polymer retention can be deemed poor if it is less than 10 g/g, and it can be deemed high if it is greater than 200 g/g. To compensate for polymer loss due to retention, more polymer had to be injected into the reservoir than was originally planned for.

Adsorption-based polymer retention is typically thought of as a nonreversible process [45,46].

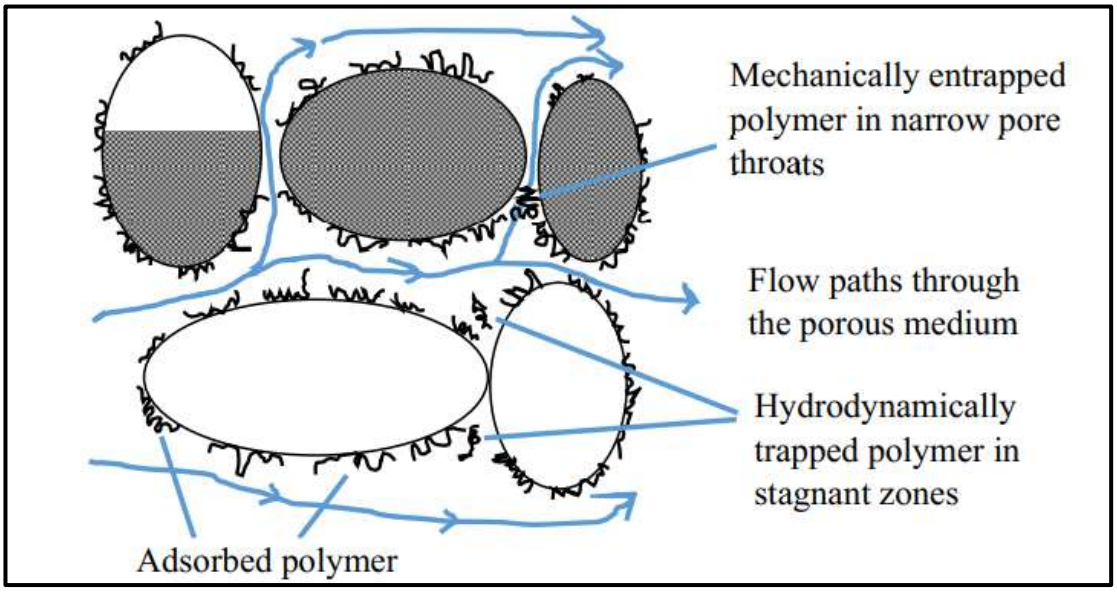

Figure 2.3: - Reprinted schematic showing polymer retention processes in porous medium [46].

2.2.5 Adsorption

After passing through porous media, polymer solutions adsorb to the rock surface due to electrostatic interactions between the molecules. Polymer molecules interact with the rock surface via hydrogen bonds and van der Waal's forces, leading to adsorption. Availability of surface area to polymer molecules is directly correlated with the degree of adsorption.The reservoir's formation also plays a role; carbonate rocks, which contain divalent ions like calcium, have a higher capacity for polymer adsorption than sandstones . Adsorption onto polymers is a common method for retention [47].

Mechanical trapping or straining of polymer molecules in narrow channels is another retention method. This occurs when the molecular size of the polymer is substantially larger than the flow channel (pore throat). At the wellbore area, mechanical entrapment is greater, and it decreases exponentially as one moves further into the reservoir. Pore-clogging may result from mechanical trapping .

Although inaccessible pore volume (IPV) is frequently cited in the same breath as retention in the literature, it is important to distinguish between mechanical entrapment and IPV. Polymer retention can be more accurately quantified if IPV is evaluated. IPV, however, is not a retaining instrument but rather a measurement of a polymer's hole volume[48].

2.3 Associating polymers (AP)

The process of polymer flooding has been modernized with the introduction of associating polymer (AP). As can be seen in Figure 2.4, along with the acrylamide monomers, it also contains a tiny number of hydrophobic monomers (1%) that bind to the polymer backbone during the polymerization process [49].

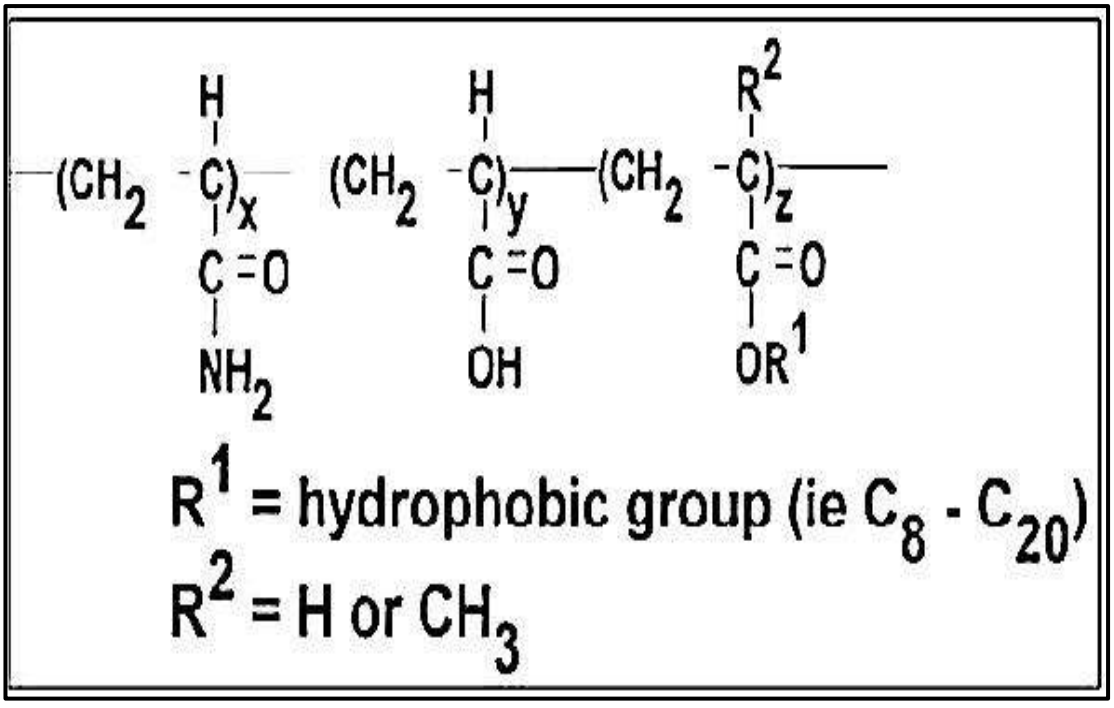

Figure 2.4:- Hydrophobic associated polymer structure [50]

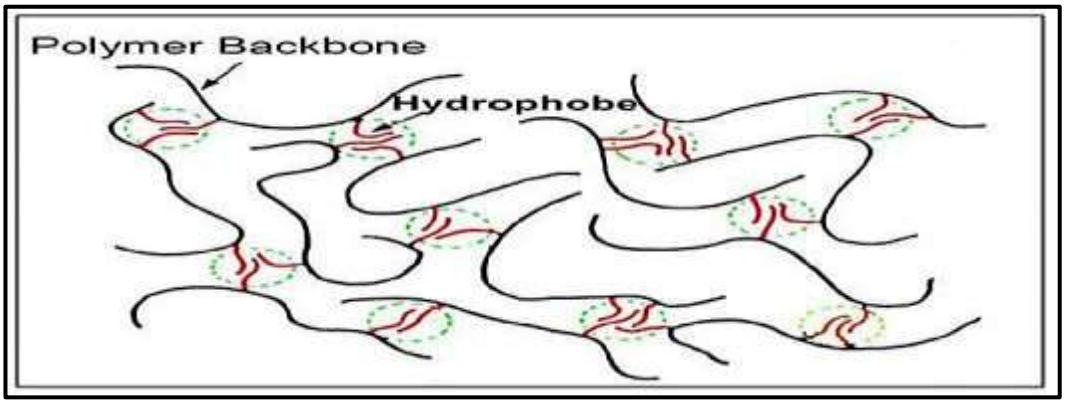

Figure 2.5:- The role of hydrophobic interactions in polymer association [51]

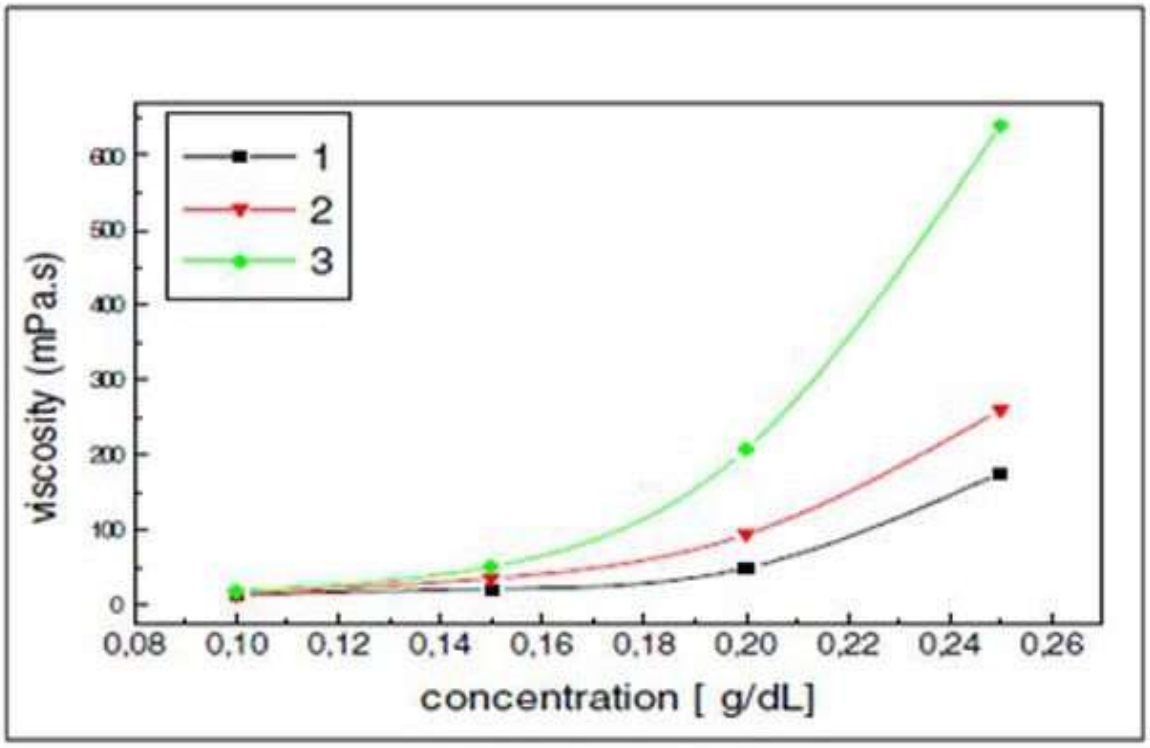

Figure 2.6:- Polymer viscosity and concentration curve of HAPAM for (1,2, and 3) at (1000, 1500, and 2000) ppm [52].

The same molecular weight, that interaction will provide better viscosities. The addition of salt has no effect on the interaction, hence the polymer's viscosity is not impacted by the concentration of salt in the environment, which is not the case for most polymers (e.g., HPAM). The viscosity of a polymer increases as a function for both the polymer concentration and the NaCl concentration, as seen in Figures 2.5 [52].

Hydrophobically associating polyacrylamides are an important derivative (HAPAM). The primary motivation for developing these derivatives was the desire to enhance polyacrylamides' thickening capacity in extremely high-temperature and high-salinity reservoir environments (HTHS). Associative polymers have more mobility reduction than HPAM polymers because of their superior thickening capabilities. When compared to HPAM polymers, associative polymers' ability to reduce high mobility results in greater incremental oil recovery [53]. Relatively recently, it has been proven that viscoelastic polymers go through a transition from laminar flow to extremely erratic flow, a state that is analogous to elastic turbulence. Elastic turbulence, also known as flow irregularities, could be triggered by a surge in the release of stored oil (capillary desaturation through destabilization of trapped oil). Greater oil recovery at flow rates above the onset for shear thickening cannot be attributed to extensional viscosity when the capillary number (Ca) is below the crucial value (Ca <1). When a set amount of oil is released from its confines, an analogous amount of elastic turbulence is generated. Therefore, the effect of intermolecular association (hydrophobic contact) on elastic turbulence for flow in porous media may account for the enhanced recovery of associating polymers [54].

Table 2.2 displays the results of several HAPAM laboratory investigations, however a comparison with Table 2.1 reveals that HAPAM has had little field applicability. As the state of knowledge in this area of research shows, HAPAM will eventually replace HPAM for polymer flooding operations, as shown by this comparison. These associative polymers can be produced or made by inserting hydrophobic comonomers along the polymer backbone. The molecular weight of polymers include the effects of hydrophobic monomers. Scientific research linking chemical flooding and the hydrophobically associating polymer has primarily focused on Regardless of changes in

temperature, salinity, or ion concentration, the polymer retains its thickening ability [55,56].

Table 2.2:- Core flooding studies on some selected polymers [56]

Polymer Type	Polymer Concentration (ppm)	T (° C)	Salinity (mg/L)	Core Type	Recovery (%)
Xanthan Gum	500	50	–	Sandstone	66 T
HAPAM	1000	50	–	Sandstone	53.6 T
HAPAM	5000	60	5000	Sandstone	8.5
HAPAM	2000	60	5000	Sandstone	11
HPAM	2000	70	10000	Sandstone	34
HAPAM	7000	60	5000	Sandstone	10.6
HPAM	1100	75	12000	Sandstone	9.8
HPAM	2500	45	508–6778	Sandstone	16.7
HPAM	4500	38	30700	Carbonate	45
HAPAM	2000	60	–	Not specifiedb	12
HAPAM	2000	60	–	Not specifiedb	18
HAPAM	2000	65	5000	Sandstone	5.7

2.4 The Rheological Properties of Polymers

Nonnewtonian liquid flow and plastic flow of solids are of particular importance to the field of rheology, which examines the deformation and flow of materials [57]. Liquids that are considered to be Newtonian are those that have a viscosity that is unaffected by the shear rate that is applied to them and have no changes in their normal stresses . The most frequent type of fluid that

falls within the category of Newtonian fluids is water. Non-Newtonian fluids are any fluids whose viscosity can be shown to depend on the shear rate of the fluid. This demonstrates that the fluid cannot be described as being Newtonian. Certain non-Newtonian fluids are not only shear rate dependent, but shear history dependent as well (time dependence). The reliance of non-Newtonian fluids on shear rate and shear history provides a useful framework for further categorization [58,59].

This class includes both shear-thinning (pseudoplastic) and shear-thickness-changing (viscoelastic) fluids (dilatant). Further examples of time-dependent fluids include thixotropic and rheopectic media, while pseudoplastic and dilatant media are examples of time-independent fluids . Shear-thickening behavior describes a rise in viscosity in response to shearing. When subjected to certain deformations, a viscoelastic fluid can take on the characteristics of either a viscous fluid or an elastic solid [60].

Non-Newtonian fluids differ greatly from Newtonian fluids in that their molecules are significantly bigger and more easily distorted or orientated by the flow (macromolecules). Perhaps this is the case because the viscosity of Newtonian fluids is invariant under shear (Figure 2.7). Differences between polymer solutions and Newtonian fluids like water can also be seen in other aspects .High-Molecule-Weight Polymer Solutions (Mw). Since the polymer solution contains molecules of varying sizes, its molecular weight distribution (MWD) is broad.In order to adapt to the current, the polymer coils can take on a variety of forms. When a polymer solution undergoes shear-thinning or thickening, the molecular configuration of the solution changes from its resting state to that of the flowing state. At high flow velocities, where the entanglement rate is greater than the disentanglement rate, polymer solutions may form a transient entanglement network. After that, shear-thinning behavior sets in [61].

For example, in porous material that allows for both shear and extensional flow, polymer reactions to exposed flow rely substantially on these non-Newtonian features.

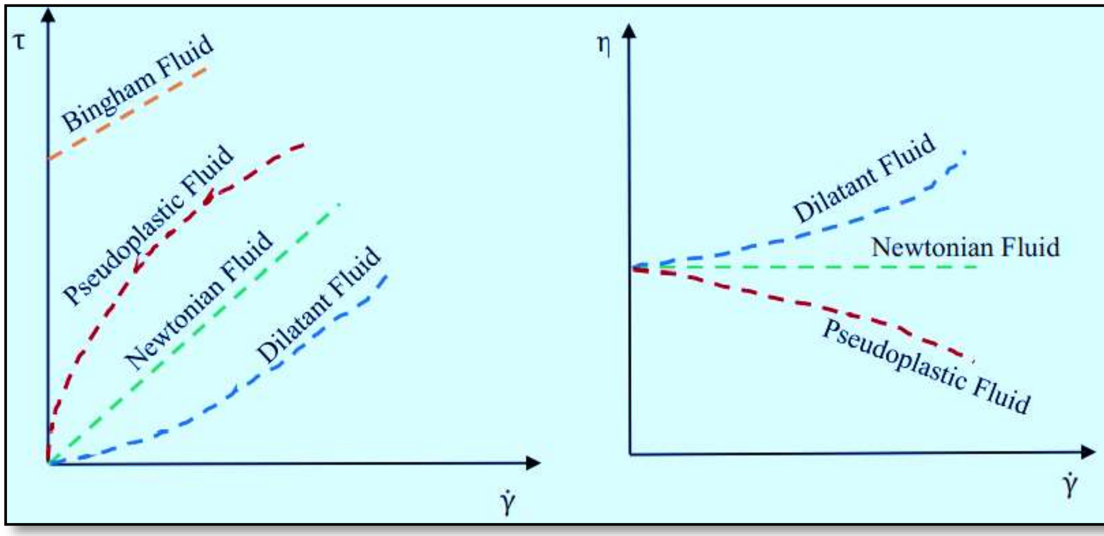

Figure 2.7:- Multiple fluid types' shear stress/strain and shear viscosities [62]

2.4.1Viscosity

The viscosity of a fluid measures how much it resists being pushed about . In the case of incompressible fluids, relationship among shear stress(τ) also shear rate(γ̇) is linear besides relatively simple, with the proportionality constant being the viscosity (η)

For shear-thinning fluids, power-law model(Ostwald-deWaele) can stand used to empirically express viscosity, giving the following [63]:

$$\eta = K\dot{\gamma}^{n-1} \ldots\ldots\ldots\ldots\ldots\ldots\ldots\ldots\ldots\ldots\ldots\ldots\ldots\ldots\ldots\ldots\ldots (2.4)$$

In which the flow consistency index K and the behavior index n are power-law constants. Power-law constants K and n have been shown to have relationships in the published literature . The shear or bulk viscosity is a term used to describe the value of. The Pa.s. (Pascal) is SI unit aimed at viscosity. The poise is another common viscosity unit used in industry; one centipoise is

equal to one millipascal-second. In order to increase the mobility ratio, Polymer flooding necessitates knowledge of polymer rheology to achieve the desired results (for example, its viscosity).Polymer flooding applications commonly utilize polymer solution viscosity as a screening or defining index due to its relevance and accessibility of measuring in the lab .

2.4.2 Shear Rate

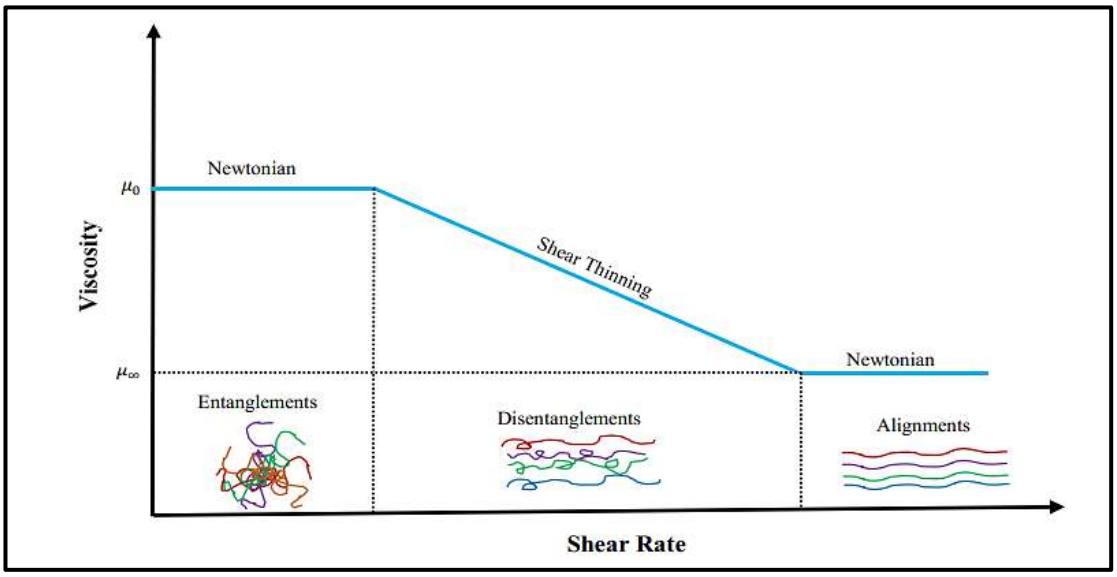

Figure 2.8 :- Shear-rate dependence of polymer viscosity [64]

A plot of HPAM polymer solution viscosity against concentration is shown in Figure 2.8. To put it another way, A viscosity for a polymer solution is constant and Newtonian at little shear rates. In presence of a growing shear rate, a fluid's viscosity gradually decreases due to molecular decoupling, a phenomenon known as shear-thinning. After being exposed to high shear rates, molecules become completely untangled and aligned with the flow, showing a second Newtonian property: a constant viscosity at its minimum. It is the physicochemical qualities of the polymer, such as Mw and concentration, and the characteristics of solvent, such as salinity besides total dissolved solids, that largely dictate the size of each flow regime for a given temperature (TDS) [64,65].

2.4.3 Concentration

In excess of the CAC, aggregation becomes impossible, A polymer chains develop intermolecular interactions (Figure 2.9). The crucial associating concentration characterizes the behavior of hydrophobically associating polymers at a certain concentration (CAC). The rheology is controlled by intramolecular contact inside the polymer chain when the temperature is below the Critical Amphibian Concentration . HAPAM's superior rheological properties over CAC are the result of the intermolecular interaction between polymerchains . However, the location of hydrophobic commoners along the polymer chain determines the strength of these interactions amongst polymer chains overhead the CAC. Whether these distributions are uniform or nonuniform, i.e., random or block-like, depends on the parameters of the synthesis process[66].

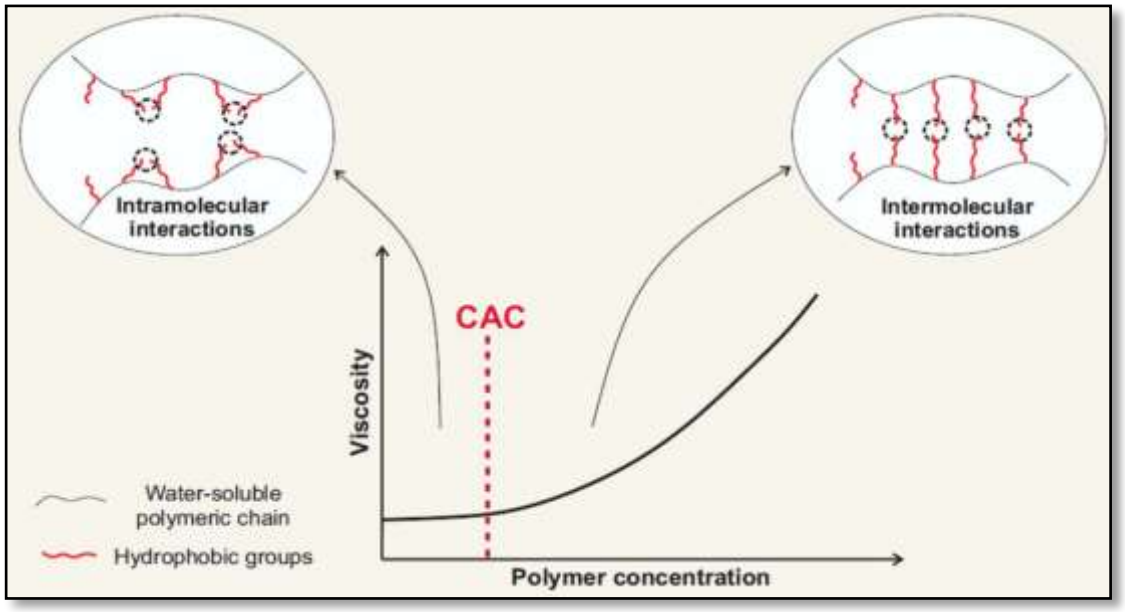

Figure 2. 9:- Viscosity changes of hydrophobically associating polymers (HAPAM) before and after the critical aggregation concentration[66].

2.4.4 Salinity

Salinity is defined as the total dissolved solids concentration in a liquid . The molecular structure and hydrodynamic volume of a polymer are what establish its viscosity in a solution. Although, HAPAM hydrodynamic volume can be negatively impacted by salt, leading to the degradation of its coil structure over time. Na+ and other salt cations can shield and neutralize the carboxyl group, which is highly reactive and susceptible to its ionic surroundings. Polymer coils shrink and coil up to compensate for the lower hydrodynamic volume, resulting in less viscosity . This is because the repulsive interactions between molecules are lessened by the shielding effect of the electrical double layer. When hard cations such as Ca2+ and Mg2+ are present, phase separation and precipitation can occur if the salt concentration exceeds a critical value . When HPAM polymer is put into porous media, gel formation (the precipitation of polymer molecules) can occur, resulting in pore blockage[67].

2.4.5 pH

Oilfield water often falls within the pH range of 7.5 and 9.5 . Viscosity of HPAM is also significantly influenced by pH , much like salinity is by the coiling mechanisms of HAPAM. A negatively charged polymer containing amino and carboxyl groups is created through the partial hydrolysis and transformation of PAM polymer. However, carboxyl groups are particularly subtle to changes in pH. Because of the abundance of hydrogen ions (H+) in a low-pH solution, the carboxyl group is rendered inert. Viscosity is reduced because electrostatic repulsion between molecules is reduced as a result of neutralization. Still, when the pH is high, the negatively charged OH in the solution makes the molecules repel each other more electrostatically, which makes the solution thicker. For polymer viscosity, soft water makes pH affects

more noticeable [69]. Low salinity solutions have a lower pH, which reduces viscosity by preventing the extension of polymer chains.

2.4.6 Temperature

Heat pressure additive (HPA) has a viscosity that reduces precipitously with increasing temperature. Indication of a behavior unique to HPAM polymer called "thermo-thinning".This is because as the temperature goes up, the speed at which HPAM molecules move increases. This makes the polymer chains less tangled and keeps the hydrogen bonds stable. This causes the viscosity of the solution to go down [70].

2.4.7 Shear Stability

The literature presents a variety of methods for enhancing HPAM shear stability. The screening of polymers for their suitability to use in the field is one such method. Key factors in this sort of screening procedure include the specific polymer being examined, its physicochemical qualities, and its chemical structure. In polymer flooding, for example, using a low Mw polymer can make the polymer solution more stable when it's being sheared .It's possible that large-scale polymer flood applications won't be cost-effective because of the enormous quantities of low molecular weight polymer needed to reach the acceptable viscosity target for polymer solution. Field procedures and well construction are another means of enhancing polymer solution shear stability. Methods that fall under this category are well treatments, horizontal wells, increasing the number of injection wells, and inducing fractures. Increased injectivity and less mechanical deterioration could preserve the polymer flooding project if fractures of, say, 15 meters in length were introduced [71]. Having more injection wells means you don't need as much space between them, and you can inject less water per well at a lower rate. Polymer injection is preferred because of the low shear rates in horizontal

wells. Thus, polymer solutions with a viscosity of up to 5000 cP can be processed by horizontal wells, whereas those with a viscosity of up to 100 cP can be processed by vertical wells. Moreover, during matrix injection, there is the potential for different flow regimes, with radial flow predominating around vertical wells and linear flow predominating in horizontal wells . Due to its inability to be applied to unplanned oilfields in terms of well type, well number, well spacing, etc., polymer flooding may not be seen as a viable solution for all field applications.

Polyacrylamide polymers can benefit from the incorporation of additives like Acrylamido tertiary butyl sulfonate (ATBS) to increase their shear stability . It is possible to increase a polymer's chemical and thermal durability by using additives such as thiourea and alcohol . The polymer solution's shear stability can be affected by varying the makeup water's salinity and quality (hardness) . Additional HPAM compounds and purpose-built modified polymers, such as thermally activated polymers , may provide even stronger shear stability. Some studies have shown that shear stability can be increased by chemically degrading polymer solutions at an early stage [72].

2.5 Methods of Test Rheological Properties

- Cone and plate rheometers
- Brookfield viscometers
- concentric cylinder viscometers

are only some of the tools that have been used by researchers. The use of specialized (and often modular) rheometers has also been considered in the polymer flooding literature .

Brookfield is the market leader in viscometers. By rotating the spindle at a fixed speed (according to a desired shear rate), a Brookfield viscometer may

measure the spindle resistance in a polymer solution (which is correlated to viscosity). Since this is a reasonably close approximation of the shear rate within a genuine oil reservoir, it is usual practice to maintain a shear rate of approximately 7 s^{-1}. during testing. This is why most reports of viscosity measurements made with a Brookfield viscometer will give a single number for a given shear rate and temperature. On the other hand, additional geometries can be added to make room for more study [73].

2.6 Physical Properties

2.6.1 Surface Tension

The term surface tension refers to the property at the surface of a liquid that causes it to behave like a plastic sheet and contract to the smallest possible area. Insects are able to walk across the surface of a pool or pond due to surface tension[74,75]. The forces of attraction between fluid molecules generate surface tension. Think of a bubble of air suspended in water. If you put a molecule within a bubble, the forces it experiences from its neighbors cancel out to zero. In spite of this, the net force at the surface is radially inward, and the sum of all radial forces acting on the entire spherical surface causes the surface to contract and the pressure to build up on the concave side. There must be a force, working solely at the surface, called surface tension, in order to keep everything in equilibrium. It does so by balancing the pressure gradient force across the surface with the radially outward intermolecular attraction force. Surface tension acts to reduce free energy by reducing an area for interface between two fluids when one of the fluids is not in the form of spherical bubbles. In liquids, the increased attraction between molecules is the consequence of cohesion; in gases, it is the result of adhesion, which explains why liquids have a higher surface tension than gases. Surface tension of water

is higher than that of most liquids (72.8% mN/m at 20 °C) due to the strong hydrogen bonding between water molecules.

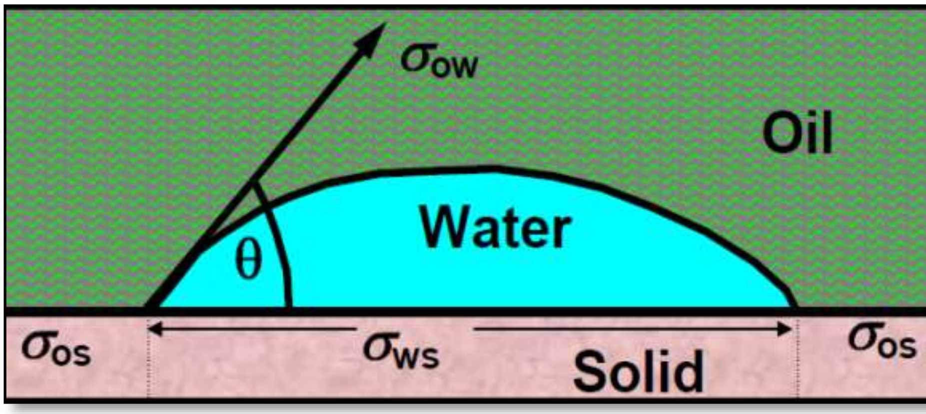

Figure 2.10 :- Interfacial tensions between solid surface, water and oil [75]

When water boils, the surface tension decreases approaching zero .Surface tension drives capillary movement. Surface tension was measured as energy per unit area or length. Surface tension, represented by the characters or, is the same as surface energy, which was used to indicate energy per unit area. It applies to both liquids and solids. cgs uses dynes per centimeter, while SI uses newtons per meter [76].

2.6.2 Interfacial Tension

Interfacial tension is the tendency of an interface to become spherical as shown in Figure 2.10, to decrease surface energy of it. Contact angle also used to determine interfacial tension by depend on equation 2.5 [77]:

$$\sigma os - \sigma ws = \sigma ow COS\theta \ldots\ldots (2.5)$$

Where, σos : interfacial tension amongst oil in addition solid (N/m) ;σws : interfacial tension amid water besides solid (N/m); σow : tension between oil

also water surfaces (N/m) ;θ: Wetness preferences of a solid are mostly determined by its contact angle, which can be either oily or watery (i.e., the wettability of a solid by a liquid).

If the angle is less than ninety degrees, water will act as the wetting fluid, meaning it will bead up on the surface more than any other liquid. If is greater than 90 degrees, Water is non-wetting, while oil is preferable .

2.7 Petrophysical Properties

2.7.1 Poropsity

The ability of a rock to hold fluids is measured by its porosity (ϕ) [78].

2.7.2 Permeability

The rock's permeability, or K, is a crucial measure of its fluid-carrying capacity. Rock permeability is measured using Darcy's law, which is described below [79].

2.7.2.1 Effective Permeability

Reservoirs can hold both water and oil or gas, but the ratio varies. Everything slows everything else down. Water is presumed to be present in the aquifer component of a reservoir system because Sw makes up only one phase of the aquifer. The granite in question is extremely permeable to water (Kab). There may be multiple fluids in a reservoir, but the rock's effective permeability to a single fluid can still be determined. There is a correlation between the fluid's saturation level and the reaction. Relative permeability to oil, gas, or water is calculated by dividing the effective permeability by the absolute permeability (Kro, Krg, or Krw). Permeability can be expressed as a percentage or as a value between 0 and 1. The relative permeability of a material depends on the wettability of its production and the kind of its pores [80].

When a pore system is saturated with a fluid, that fluid will be transported at a rate that depends on the area of the pore throat and the pressure difference between the inside and outside of the pore. The absolute size of the pore throat, A, is the intergrain distance, as shown in Figure 2.11. To facilitate the flow of oil or gas, the presence of water on the grain surface reduces the hole throat size (B) (A). Sw is almost the same as the depth of the water film that forms over the granules of rock. The effective size of the pore throat for oil or gas flow (B) grows as buoyant pressure decreases and the pore throat expands (Sw) [81] .

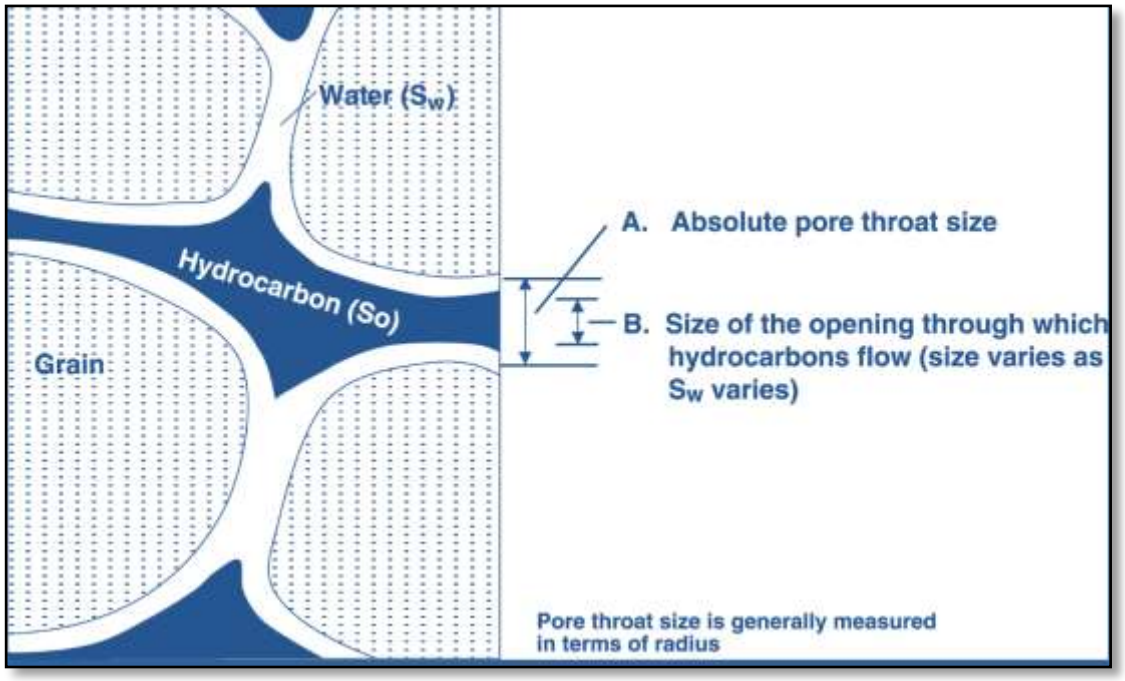

Figure 2.11: - The absolute size of the pore throat [81]

There is a smaller difference between the absolute pore throat size (D) (areas where water is present and the grain surface is wet) and pore throat size (B) aimed at oil or gas flow in a mixed sample (A).The Sw of a rock is proportional to the amount of water that coats its grains. The effective size of the pore throat for oil or gas flow (B) grows with rising buoyant pressure, while the permeability (Sw) decreases.

2.7.2.2 Single Phase Permeability

What makes a porous media permeable is the relative ease with which fluids can move through it in response to an applied fluid pressure gradient. Permeability, however, is not a directly measurable property; rather, it is inferred from a variety of other physical measurements using a wide variety of theoretical and empirical correlations. The hydrocarbon business relies on the relationship described by Equation 1, which was empirically obtained from Darcy's Law [82]. Therefore, Darcy's law is a relationship between the instantaneous discharge rate, the fluid's viscosity, and the pressure drop over a certain distance.

2.7.2.3 Relative Permeability and Multiphase Flow

The importance of defining permeability at the outset is worth noting. The absolute permeability (K) of a core sample is a measurement of the core's ability to transport fluids. therefore, it's an intrinsic characteristic of the porous material . Each fluid's permeability depends on its saturation level within the core if there are multiple fluids present. These properties, which depend on the fluid saturation and the wetting qualities of the sample, are known as effective permeabilities (i.e. kw, ko) . However, relative permeability is a more direct measurement of the porous system's ability to conduct a single fluid in the presence of many fluids. The ratio of the effective permeability of a phase to its absolute permeability [83].

Relative permeability is influenced by wettability because it plays a significant role in determining the orientation, velocity, and distribution of fluids within the interior . Due to competition between oil and water for the big pores, the oil relative permeability (kro) values are lower at low water saturation in the mixed-wet situation. The oil preferentially occupies the big pores, and as a

result, the water relative permeability (krw) at high water saturation is decreased in the water-wet situation [84] .

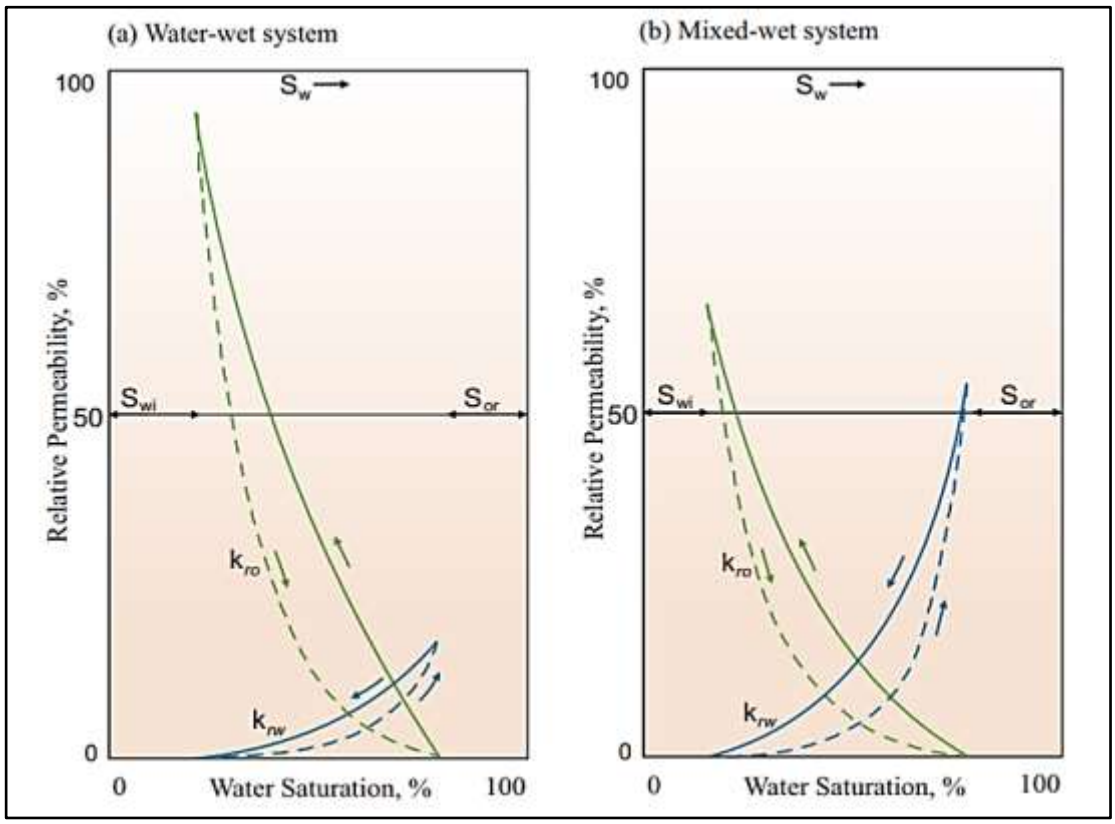

Figure 2.12: - The relative permeability curves kro (green) and krw (blue) for a water-wet and a mixed-wet system are depicted schematically [84]

If water is the preferable wetting phase, then the water will be located in the smaller pores that were not previously invaded by oil, while the oil will be located in the larger pores. In the midst of a flood, both liquid and vapor phases are in motion. Since oil travels via the biggest pores, the oil relative permeability, kro, is high and diminishes with decreasing oil saturation. Starting out small, the water relative permeability (krw) rises as the saturation level of the medium nears 100% [85].

Wetting pressures cause water saturation to rise first in the sample's smaller pore spaces. Water is replacing oil in the pore throats as the displacement process proceeds from smaller to larger pores. If the driving pressure isn't high

enough to overcome the capillary entrance pressure, then oil in a single hole or a cluster of pores can get isolated from the rest of the oil and stuck. Oil flow ceases when all possible flow channels are blocked by water. Because oil becomes trapped in the pores, the final krw is lower than the initial kro .

As before, the initial kro is high and krw is low in a mixed-wet core. However, due of the oil-wet condition of the surfaces around the biggest pores, water invades them first and remains in the center of those pores as the water saturation increases. This accelerates kro's demise since the water quickly fills the most easily accessible pathways. However, oil is not trapped by the water because it may move freely across oily surfaces and out of the virtually water-filled pores . Although there is a direct relationship between fluid flow rate and permeability as shown by the Darcy equation, it is important to note that high permeability does not necessarily imply high flow rates going through the core. In addition to affecting the flow rate, fluid viscosity affects the mobility of each phase[86].

2.8 Wettability

A distribution for fluid phases in porous media can be explained by the concept of "wettability," which is defined as the interaction of fluids and rock surfaces. The presence of water and/or a gaseous oil in the pores can be deduced from this. A rock's wettness can be determined by testing its surface for the presence of oil or gas, as these fluids have different densities and thus different attractive forces. A rock is described to be "water-wet" when water is in close proximity to it and is attracted to the rock's surface because of the presence of oil Figure 2.13. A presence of oil on surface of a rock is what's meant by the phrase "oil-wet." Additionally, at the intermediate wetting

condition, both fluid phases have a greater chance of adhering to the rock surface [87].

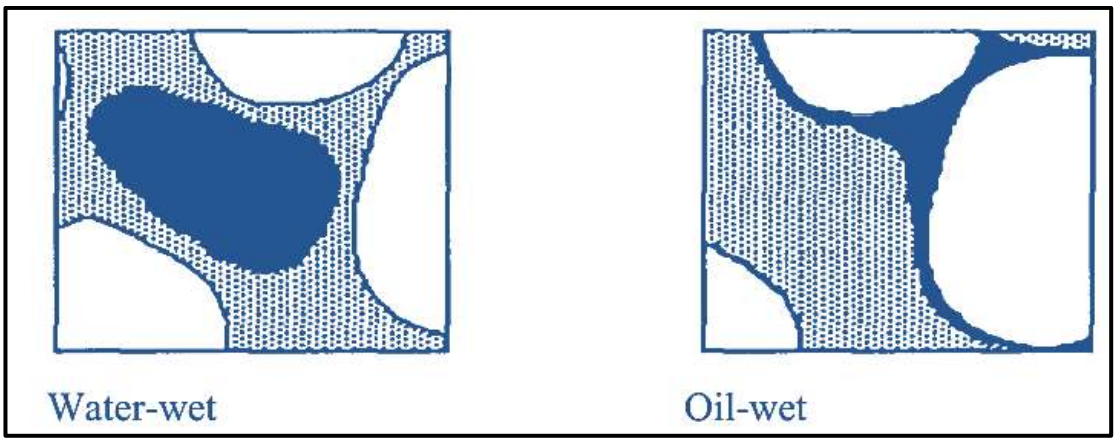

Figure 2.13: - This article provides illustrations of oil spreading in both oil- and water-wetted porous media [87].

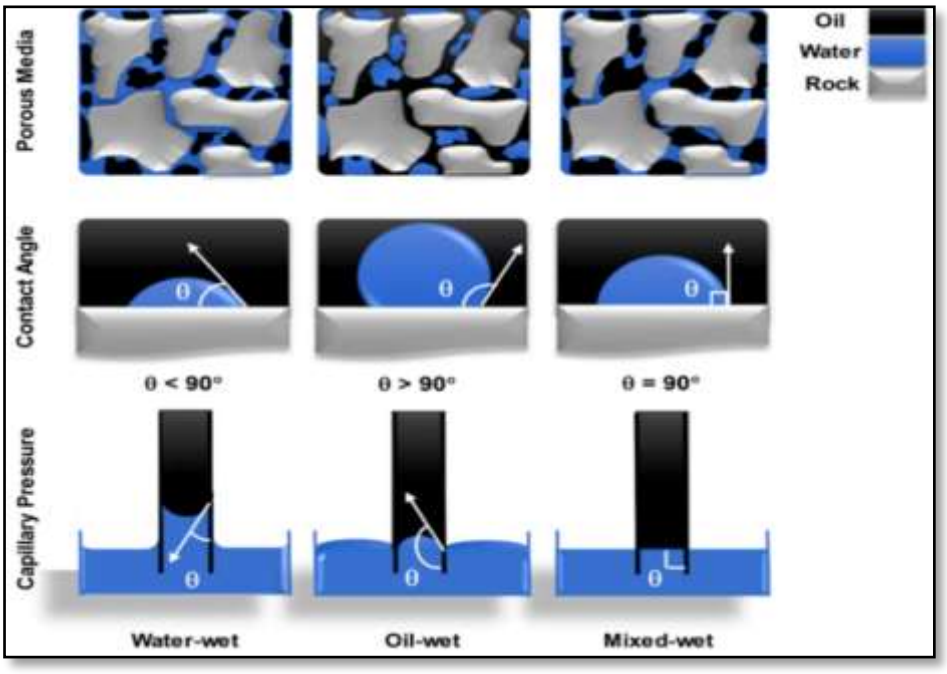

Figure 2.14:- Contact angles that result in vastly different wetting conditions [88]

The wetting phase is distinguished from the non-wetting phase by its enhanced diffusion across capillary walls. Surface tension, forces that motivate a fluid's

inclination to occupy the smallest feasible volume, and the contact angle determine a fluid's "wettability." . It is possible to manipulate the "wettability" of a fluid by manipulating its capillary surface properties (e.g. roughness, hydrophilicity). As seen in Figure 2.14, oil is typically the non-wetting phase in gas-oil systems, while water is the wetting phase. A pressure difference is always created at the curved interface between the two fluids when two fluids meet at an angle. The neutral-wet or mixed-wet conditions give the lowest residual oil saturation. This finding indicates that residual oil saturation can be decreased and hence oil recovery can be increased by changing wettability .

2.9 Resistance Factor

As a mathematical ratio, the RF connects the pressure droplet of a polymer to the mobility of water in a porous medium ($\Delta P_{polymer}$ and ΔP water, formerly the polymer reaches porous medium[89]:

$$RF = \frac{\Delta P_{polymer}}{\Delta P_{water}} \dots\dots\dots\dots\dots\dots\dots\dots\dots\dots\dots\dots\dots\dots\dots\dots\dots\dots\dots\dots\dots\dots\dots\dots (2.6)$$

2.10 Residual Resistance Factor

The residual resistance factor indicates how water traveled through the porous media before and after the polymer was injected (RRF). It shows how water can flow through a porous medium before and after polymer is added [90]:

$$RRF = \frac{K_{wi}}{K_{wf}} = \frac{\Delta P_{water\ after\ polymer}}{\Delta P_{water\ before\ polymer}} \dots\dots\dots\dots\dots\dots\dots\dots\dots\dots\dots\dots\dots\dots\dots\dots\dots\dots\dots\dots\dots\dots\dots\dots (2.7)$$

2.11 Capillary Pressure:-

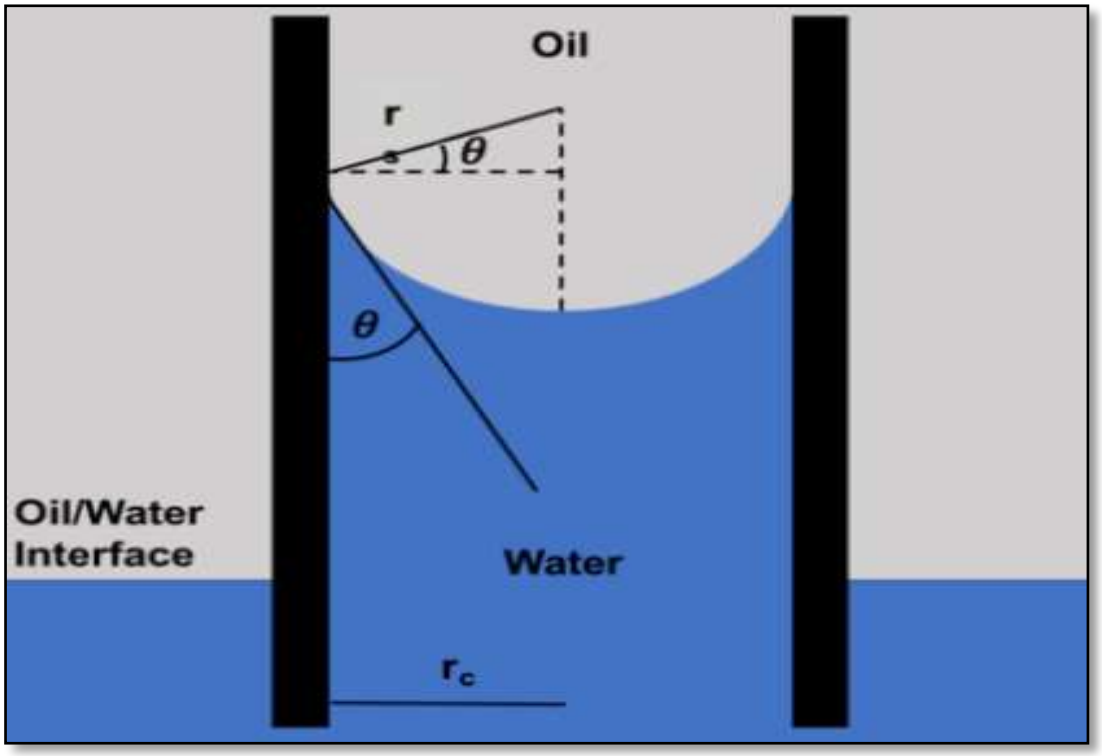

Figure 2.15:- Capillary Pressure [91]**.**

These procedures, as shown in Figure 2.15, reduce the interfacial tension between the oil and formation water, hence increasing oil output. Capillary forces keep most of the oil (residual oil) in the reservoirs' pore structures, which is crucial to the oil extraction process. It is this forces that low IFT processes are intended to overcome .The capillary pressure in reservoirs pores is given by equation 2.8 . Since the pores sizes and the contact angle are usually fixed in a reservoir, the only way to lower the capillary forces is to lower the interfacial tension. oil is forced out of pores by viscous forces, which can be altered by modifying the viscosity of the displacing fluid or by decreasing the capillary forces holding the oil in place [91].

$$P_c = \frac{2\gamma \cos\theta}{r_c} \quad \text{.....(2.8)}$$

Where ,Pc: capillary pressure (N/m2);γ: Oil-water surface tension (in Newton-meters);ɵ: angles of contact (degree); and rc: radius of capillary tube (m).

2.12 Capillary Number

One of the most important factors in achieving superior oil restoration is the capillary wide variety (Ca), which is the dimensionless ratio of viscous force to capillary force (EOR). The scaling factor between the viscous and capillary forces is a constant. There are discrepancies between the many programs and manuals, as at least 33 different Ca have been offered. The most widely used definition in EOR is the shortest one that includes velocity, interfacial tension, and viscosity. As a result, the relationship between ROS and Ca, commonly known as the capillary desaturation curve, provides the foundation for many chemical EOR applications (CDC). In order to achieve low reactive oxygen species (ROS) levels and high displacement efficiencies, the use of polymers is fundamentally terminated as a result of a wide variety of CDCs. However, after a thorough investigation of Ca and the most current experimental results, it became clear that the conventional definition of Ca is fraught with difficulties and based on misconceptions [92] .

Capillary desaturation curves (CDCs) are plotted using the capillary range to describe quantitative relationships between residual phase saturation (wetting or non-wetting) and the capillary range value. The primary challenge in EOR is to significantly and inexpensively reduce residual oil saturation (ROS), which is where CDC comes in. In EOR, CDC is considered to be a top essential curve. CDCs are often created by adjusting the Ca parameters while maintaining the same core or model. The method of acquiring such CDCs shifted to relying on correctly brought in references. Correlating ROS and Ca for a CDC is often done using different cores with similar features because it

is difficult to reuse the same core for multiple tests. The dispersion of test results took into account both the correlation and the variation between models. Figure 2.16 , demonstrates that many CDC are comparable even when based on specific criteria [93].

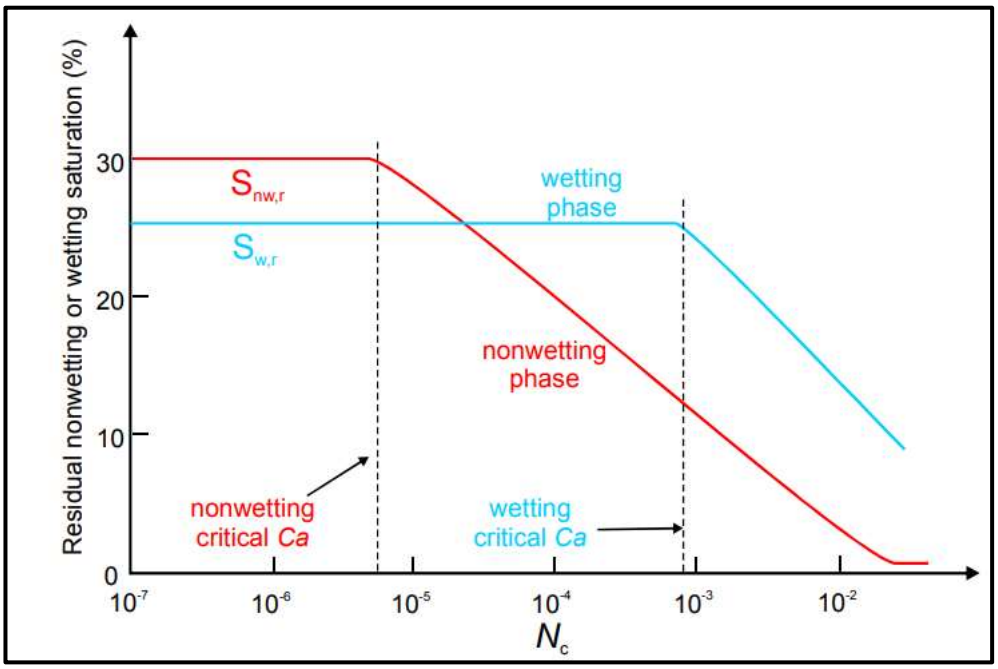

Figure 2.16:- Capillary de-saturation curve: Residual saturation of the wetting and non-wetting phase as function of the capillary number Ca [94].

2.13 Darcy Velocity

problems at both the pore and Darcy scales, and proposed a new regime of flow between them. Figure 2.17 neatly demonstrates how flow regimes shift from interconnected to isolated channels. Microscale and macroscale differences in a typical numerical simulation version are shown in Figure 2.18. On larger scales, it's easy to see that many of the microscale-specific factors are no longer relevant .

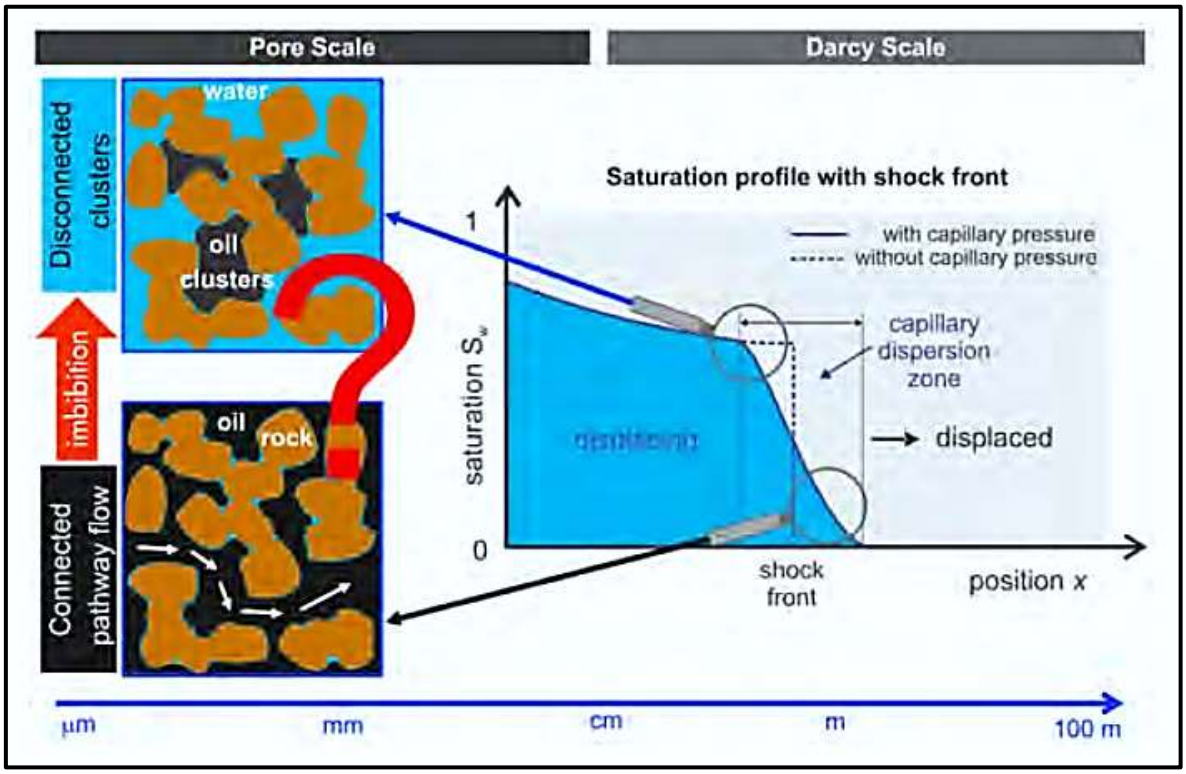

Figure 2.17:- Pore scale and Darcy velocity [95]

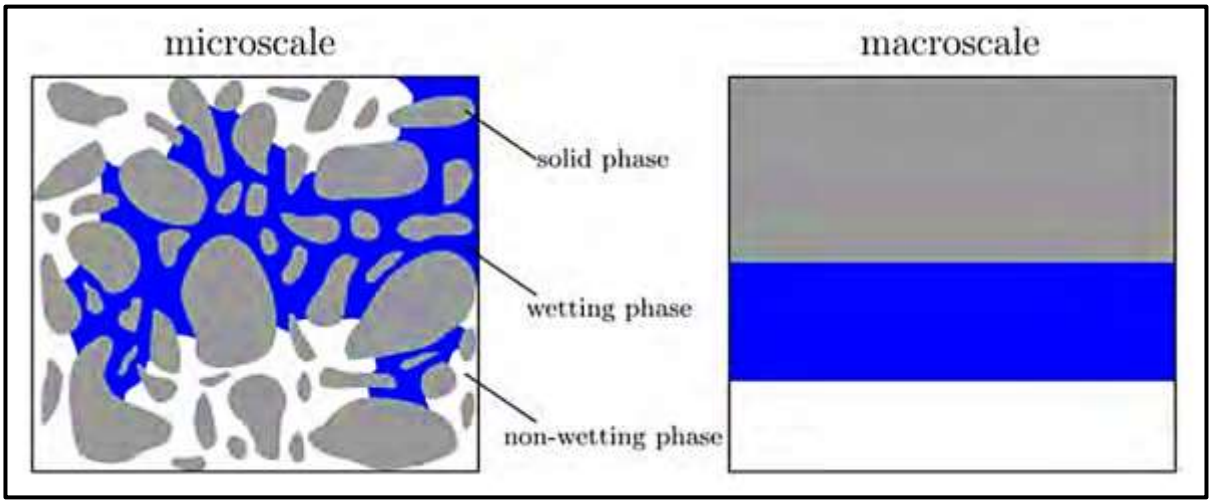

Figure 2.18:- Different Scale in Numerical Simulation [96].

2.14 Core Flooding Test

After soaking the cores in conformation water for 72 hours. Constraining pressure of 2,000 psi was applied all the way around the cores. Junk water from cores was used to calculate the volume loss caused by confining pressure

during severance. We maintained a core-holder temperature of 185 degrees Fahrenheit while storing the cores. In order to achieve water achromatism, the crude oil painting was placed in the center of the canvas for 72 hours. The permeability of an oil painting was estimated by taking into account the constant pressure point at which the core flooding shown in Figure 2.19, reached to achromatic water. The system was held steady at a confining pressure of 2000 psi, a conformation water concentration of 150,000 ppm, and a temperature of 185 °F. Core AS- 1 and AS- 2 were independently subjected to water flooding and polymer flooding(2000 ppm polymer attention) at constant pressures of 10 and 16 psi, respectively. The relative permeability of water and polymer was determined at the end of each flood tide. In order to assess the conformational damage in the core caused by the polymer flooding as a residual resistive factor, water flooding was administered after the polymer flooding as a flush on core AS-2 (RRF) [97].

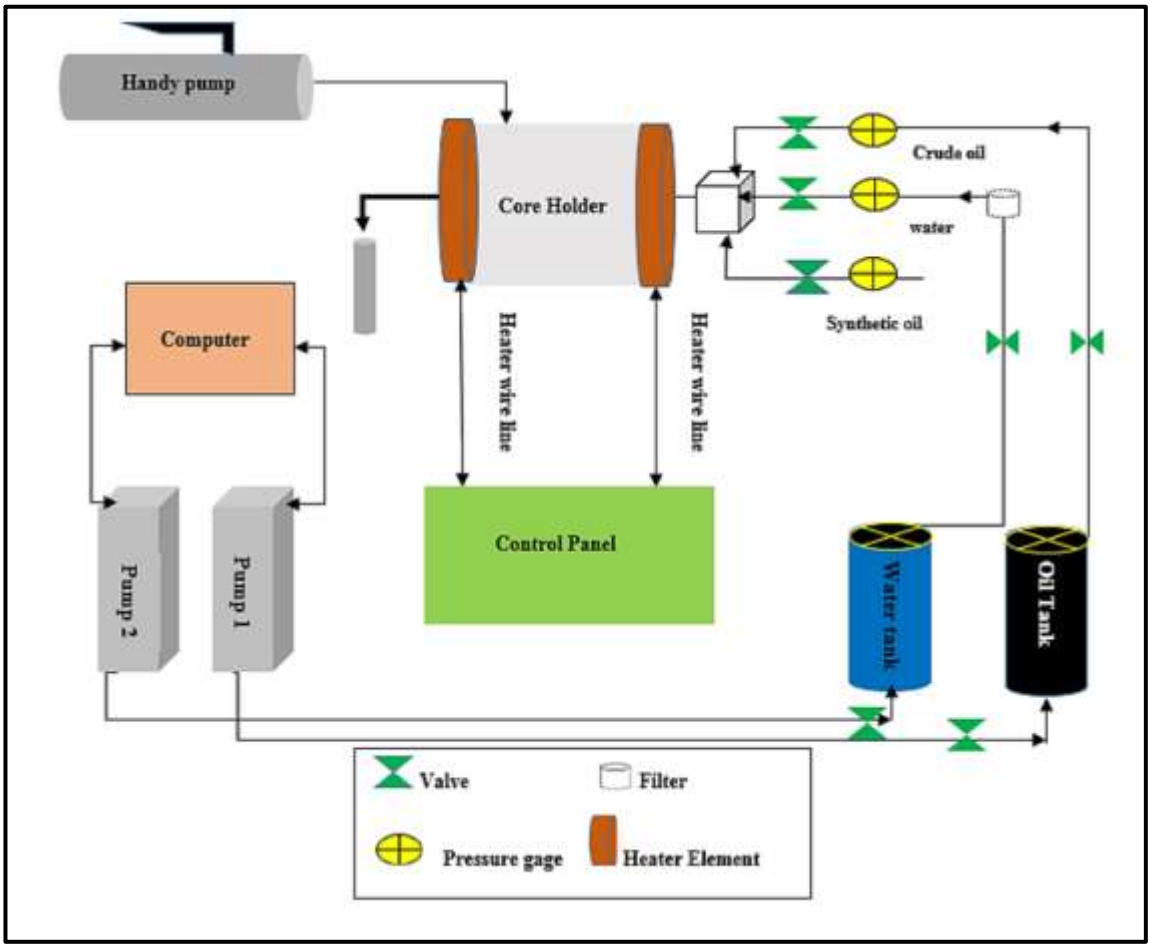

Figure 2.19 :- Scheme of core flooding test [97]

2.14.1 Oil Recovery with Pore Volume

As can be seen in Figure 2.20, the recovery factor for an oil painting subjected to water flooding was 33, but was increased to 60 when subjected to polymer flooding. More than that, the oil painting recovery factor was reached about 50 with just 1 severance volume fitted (PV- INJ). The results reveal that under HTHS conditions, this polymer performs well in pervious media and is cost-effective to boot [98].

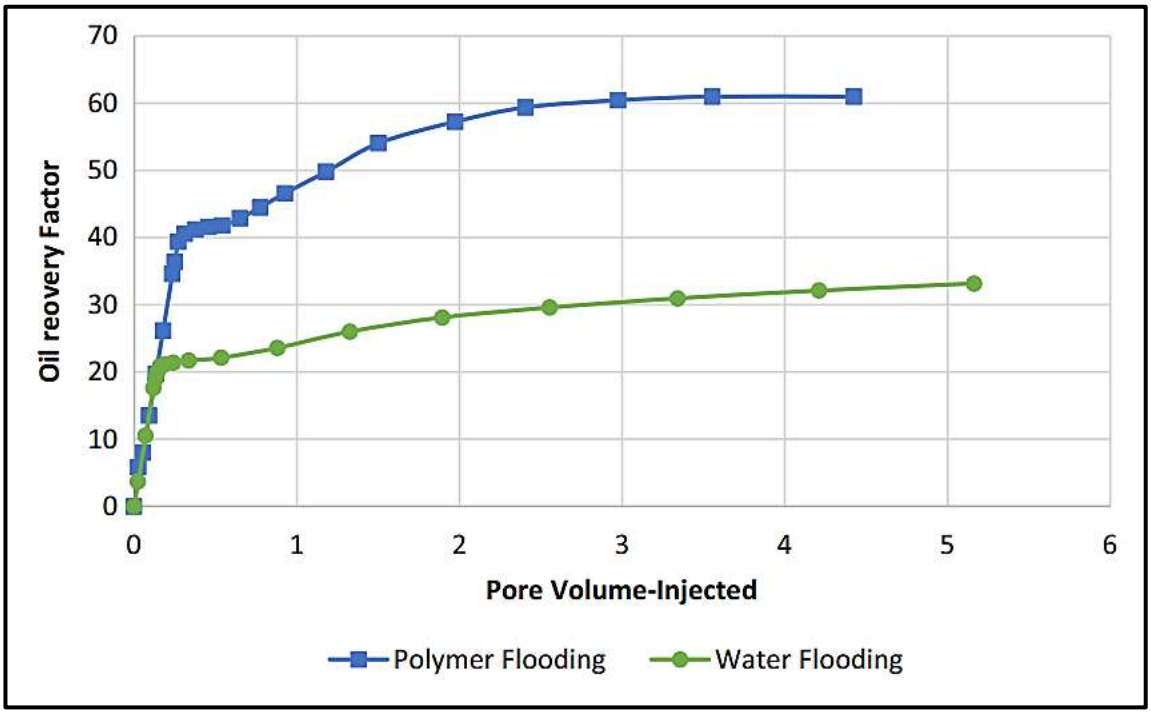

Figure 2.20:- Oil Image recovery factor for water and polymer flooding [99]

2.14.2 Oil saturation with Pore Volume

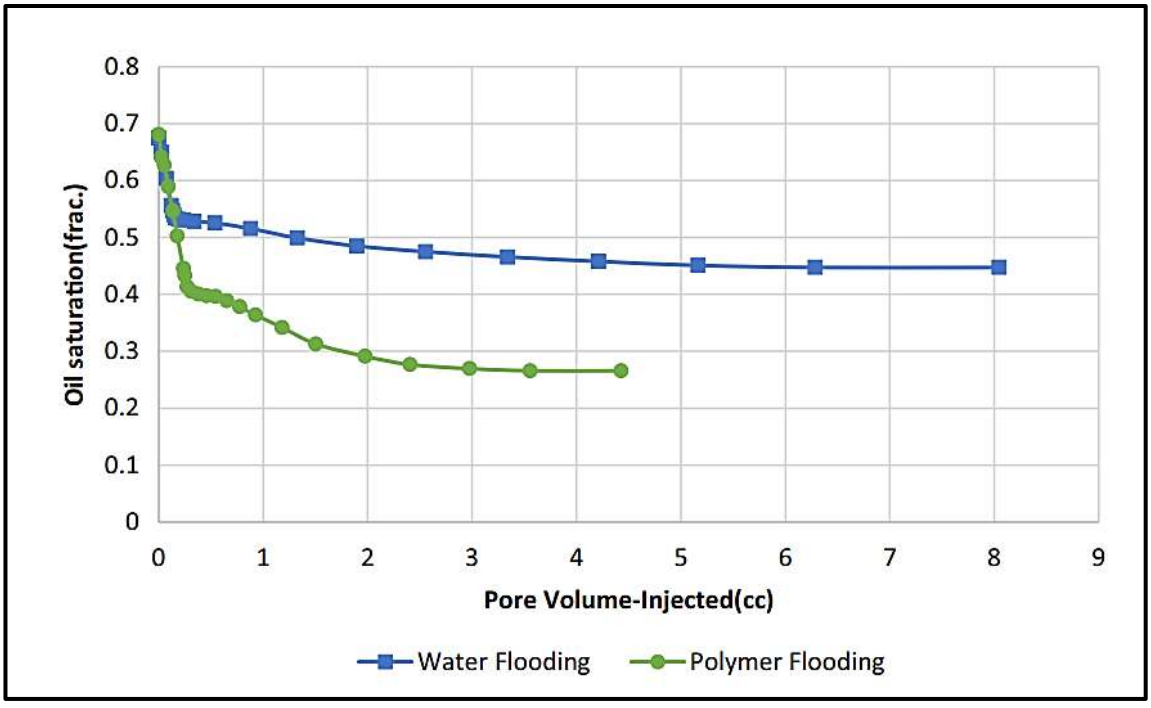

Figure 2.21:- oil saturation with pore volume for water and polymer flooding [100]

As can be seen in Figure 2.22, the residual achromatism of oil paintings was reduced by polymer flooding compared to water flooding. Due to the high value of oil painting recovery factor and the low residual oil painting achromatism in pervious media, the results show that polymer flooding utilizing Zetag 8187G was successful [100].

2.14.3 Oil Recovery with Water saturation

The recovery curves (oil recovery factor) are displayed against the injection volume of water contained in formation ports utilized for the Inundation of water Using fluids with low viscosity in Figure 2.22. For a heavily water-wet sample, the oil recovery factor is high (curve A) before the breakthrough, and the water/oil ratio climbs suddenly (curve A'). Strong oil-wetting (curve B) results in a low oil recovery factor prior to breakthrough and a gradual increase in the water/oil ratio post-breakthrough [101].

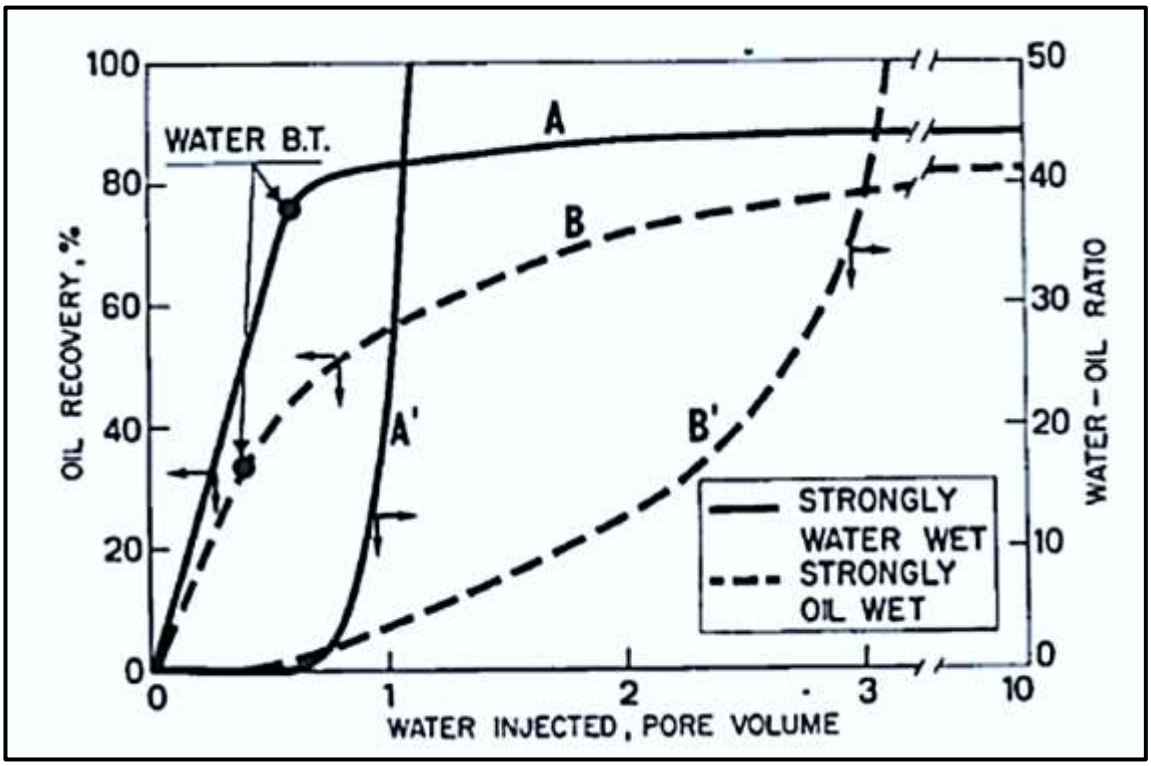

Figure 2. 22 :- Sandestone Core Samples injected by water flooding [101]

2.15 Modeling Multi Phase Flow in Porous Media

Because of the complexity of the geometry of porous media, it has been challenging to accurately predict and quantify non-Newtonian fluid flows in these media. Flows in porous media cannot be classified as pure shear flows due to the presence of converging diverging passages, which impose extensional flow fields, particularly at high flow rates, and the fact that the extension viscosity of non-Newtonian fluids increases with extension rate. As a result, the observed Newtonian and inelastic non-Newtonian tendency in the relationship between pressure drop and flow rate is frequently violated. Whether the flow is shearing, extensional, or mixed, as well as the entire history of the velocity gradient, all have a role in determining the stress for complicated fluids, adding another layer of complexity [102].Formation viscous finger as appear in Figure 2.23, result by high viscosity difference between water and oil, decrease amount of oil as reason of that[103].

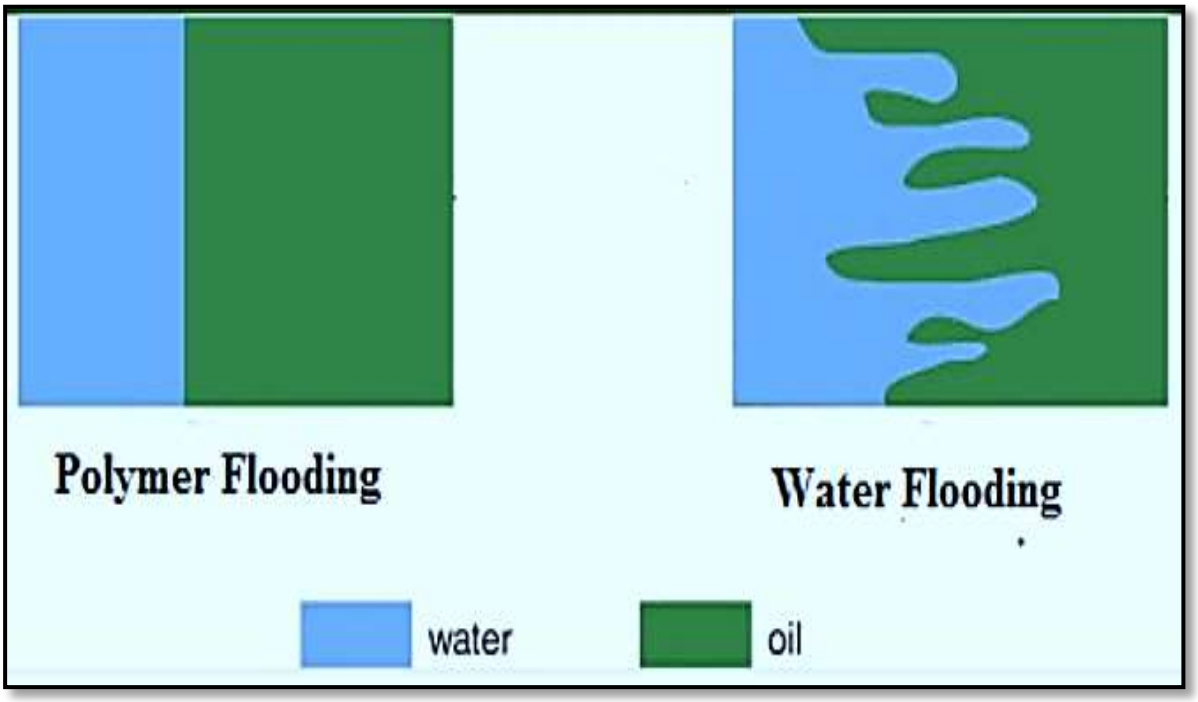

Figure 2.23:- water flooding and polymer flooding [103]

Phases in multiphase wealth are classes of materials that react to and interact with the wealth and the potential region in which they are submerged in distinct ways. This is due to the fact that a given series of patches of uniform size may all exhibit the same dynamical response to the flux field [104], for instance, stable patches of the same fabric of varying sizes can be viewed as distinct phases.

2.15.1 Ansys Fluent

A wide variety of advanced image analysis methods are now available, including X-ray. Unfortunately, like studies are time-consuming with costly, also they rarely provide a dynamic perspective. Using numerical simulation is one way around these restrictions. Recently, the chemical flooding was simulated using digital rock technology before an EOR pilot test, with the direct hydrodynamics (DHD) simulator modeling polymer, solvent, and surfactant flooding in several regimes [105]. Another approach is computational fluid dynamics (CFD), which solves the governing equations using techniques such as the finite difference method, the finite volume method, and the finite element method . CFD simulations using the fluid parameters and pore geometry from their micro model experiments . The Lattice-Boltzmann method is another CFD approach used to analyze fluid flow in a porous material (LBM). The LBM and LSM modeled fluid particles as a time-dependent distribution traveling on a regular lattice to mimic viscous flow in a physically realistic pore space without resorting to geometric simplifications. Unfortunately, capturing the pore scales experimentally is quite challenging. As a result, a computational tool that anticipates the position and geometry of fluid interfaces in common fracture geometries would be beneficial. Because they are free, free, and open source computational fluid dynamics software that has been tested for a wide range of

flow regimes, including incompressible and compressible flows, laminar and turbulent flows, and multiphase flows.Developed in computational fluid have exceeded the bottom for similarly information for dynamics of multiphase overflows. The Euler Lagrange method and the Euler-Euler method are two approaches for the numerical calculation of multiphase flows. Specifically, the Euler-Euler method is relied on in this thesis [106].

2.15.1.1 A Euler-Euler Method

A Euler-Euler method viewed a stages as a set of intertwining mathematical continuum. As a result, the idea of phasic volume fraction is introduced to account for the fact that the volume of one phase cannot be made unavailable to the other phases. It is theorized that the sum of these volume fractions is 1, and that they are continuous functions in space and time. By deriving conservation equations for each phase, we have a set of equations with the same basic structure across all phases. Constitutive relations established from experiment are used to solve these equations, or in the case of granular flows, kinetic theory is applied [107]. The volume of fluid (VOF) model, mixture model, and Eulerian model are the three types of Euler-Euler multiphase models that can be used in ANSYS FLUENT.

2.15.1.2 Volume of Fluid (VOF) Model

When applied to a static Eulerian mesh, the VOF model tracks surfaces. It's ideal for systems with two or more immiscible fluids in which the location of the interface between the fluids is of interest. The VOF model accounts for all fluids in the domain using a common set of momentum equations, while keeping track of a volume fraction for each fluid in each computing cell. A VOF model can be utilized in a wide variety of contexts, such as the prediction of jet breakup (surface tension), the steady or transient tracking of any liquid-gas interface, and the modeling of stratified flows, free surface

flows, filling, sloshing, the motion of large bubbles in a liquid, the motion of liquid after a dam break, and more. The VOF model can model two or more immiscible fluids by solving a single set of momentum equations and tracking the volume fraction of each of the fluids throughout the domain. Typical applications include the prediction of jet breakup, the motion of large bubbles in a liquid, the motion of liquid after a dam break, and the steady or transient tracking of any liquid-gas interface [108].

2.15.1.3 Volume Fraction

The description of multiphase flow as interpenetrating continua incorporates the concept of phasic volume fractions, denoted here by αq. Volume fractions represent the space occupied by each phase, and the laws of conservation of mass and momentum are satisfied by each phase individually. The derivation of the conservation equations can be done by ensemble averaging the local instantaneous balance for each of the phases or by using the mixture theory approach [109]. The volume of phase q , Vq, is defined in equation below

$$V_q = \int_v^4 \alpha_q \, dV \qquad \text{(2.9)}$$

Where,

$$\sum_{q=1}^{n} \alpha q = 1$$

The effective density of phase ^{q} is

$$\hat{\rho} = \alpha_q \rho_q$$

Where, ρ_q: physical density of phase ^{q}

Both implicit and explicit temporal discretization methods are used to solve the volume fraction problem .

2.16 Formula of Fractional Volume

In order to keep an eye on the interface(s) between the phases, one must solve a continuity equation for the extend fraction of one (or more) of the phases [110]. Volume fraction equation for qth phase written in [109]:-

$$\frac{1}{\rho_q}\left[\frac{\partial}{\partial t}\left(\alpha_q\rho_q\right)+\nabla.\left(\alpha_q\rho_q\vec{v}_q\right)=S_{\alpha q}+\sum_{p=1}^{n}\left(\dot{m}_{pq}-\dot{m}_{qp}\right)\right]\ldots\ldots\ldots\ldots\ldots(2.10)$$

Where, $\dot{m}_{pq}$: mass transfer from phase p to phase q ; $\dot{m}_{qp}$: mass transfer from q to phase p ; and $S_{\alpha q}$: zero , but you can specify a constant or user-defied mass source for each phase.

Although the primary phase's volume fraction cannot be determined by using the volume fraction equation, it can be calculated using the following [110]:

$$\sum_{q=1}^{n}\alpha q=1\ldots\ldots\ldots\ldots\ldots\ldots\ldots\ldots\ldots\ldots\ldots\ldots\ldots\ldots\ldots\ldots\ldots\ldots\ldots\ldots(2.11)$$

It is possible to solve the equation for the volume fraction either by implicitly or explicitly discretizing the time step sizes .

2.16.1 Implicit Equation

All cells, including those close to the interface, had their face fluxes calculated using common finite-difference interpolation techniques in ANSYS FLUENT, schemes such as the Modified HRIC, the Second Order Upwind, the First Order Upwind, and QUICK—when the implicit was used for time discretization [111]:

$$\frac{\alpha_q^{n+1}\rho_q^{n+1}-\alpha_q^{n}\rho_q^{n}}{\Delta t}V+\sum_{f}^{w}\left(\rho_q^{n+1}U_f^{n+1}\alpha_{q,f}^{n+1}\right)=\left[S_{\alpha q}+\sum_{p=1}^{n}\left(\dot{m}_{pq}-\dot{m}_{qp}\right)\right]V..(2.12)$$

Solving a conventional scalar transport equation iteratively for each of the secondary-phase volume fractions at each time step is necessary since this equation requires the values at the current time step (rather than at the previous step, as for the explicit technique). Time-dependent and steady-state calculations are both possible using the implicit approach .

2.16.2 Steady State and Transient Volume of Fluid (VOF)

As a polymer that can be modeled as a viscoelastic flow in porous media, HAPAM is a popular choice for usage in the oil industry. The rheological behavior of a viscoelastic fluid can be described using the upper-convected Maxwell constitutive equation if the second normal stress is small enough. Figure 1 depicts a displacement model for oil that has been left behind in a closed system. As a result of the complex structure of pores, the inclination angle between the pore and the dead end varies from 0 degrees to 180 degrees in the displacement model [112].

2.17 Computer Modelling Group (CMG)

Chemical flooding experiments must be simulated for design or optimization reasons so that decision factors like the cumulative oil recovery factor and the net present value can be calculated. A simulator had to be chosen before any work could be done in the simulation. When deciding on an appropriate simulator, two features were prioritized. The simulator required to be capable of modeling the relevant polymer behavior . Before anything further could be done with it. For instance, it was crucial that the chosen simulator could mimic the deterioration behavior because of its significance. The simulator's widespread adoption within the field was another important goal . It is vital that a widely used simulator can model the experimental findings , because

understanding polymer behavior for practical applications was the ultimate objective of the study.

Three principal simulators were examined for use: Schlumberger's Eclipse, CMG's STARS, and UTCHEM, built for academic purposes at the University of Texas at Austin. Delshad et al. had previously shown that UTCHEM could accurately describe shear-thickening how polymers act in solution . An availability of the source code was another selling point; the simulator's capacity to mimic laboratory-scale experiments and its sophistication in simulating complex chemical and polymer reactions were also noteworthy. This simulator's evident flaw is that it sees limited use beyond the academic community [113].

When it comes to reservoir simulation, the Eclipse simulator is among the most well-known products on the market. It might have been the perfect simulator for simulating the experimental results because of its widespread use in the field. Unfortunately, the technological capabilities needed to replicate the new experimental findings that motivated this work were not included in this widely used simulator. Shear-thinning behavior was all that could be simulated in the Eclipse simulator in terms of polymer viscosity when the experiment began. The simulator's inability to mimic the shear-thickening and degradation regimes meant that, despite its capacity to reflect salinity effects, adsorption behavior, and polymer concentration mixing, it could not produce an accurate simulation [114].

The STARS simulator by CMG was the last simulation tool investigated and ultimately chosen as a means of representing the experimental information. Several businesses in the petroleum sector use this simulator because of its versatility in modeling both field-scale models and laboratory and its ability to handle complex chemical behavior. The tabular format for entering the polymer apparent viscosity was a big selling point for this simulator. It was

initially unknown but hoped that the tabular input could handle all four flow regimes.

CMG-STARS to look into flow characteristics that may be implemented in pilot field tests. Multi-phase component EOR systems were studied in depth , who also determined the dynamic behavior of fluid components within the core-flood model. In order to forecast the chemical fluid's capacity to create in-situ crude oil. CMG to efficiently pull relative permeability curves, which allowed them to match the results of experimental floods [115].

Model and flooding phenomena were modeled with the aid of CMG-STARS, and experimental recovery results were corroborated with the CMOST technique. Experimental results obtained in the laboratory were simulated to corroborate the feasibility of the proposed project, whilst calculating decision variables such as cumulative oil recovery, water cut and net present value. STARS provides two main features of interest that are useful in the decision-making process related to optimal EOR strategy. These comprise of requisite capacity/functionalities associated with chemical flow dynamics in porous media; and commercial and economical usability. The degree of accuracy of simulation can be controlled by studying the behavior of surfactants and other additives employed in flooding method. Figure 2.23, illustrates an example of a five-spot pattern of production and injection wells, developed for reservoir at 9,400 feet depth with CMG-STARS tool [116].

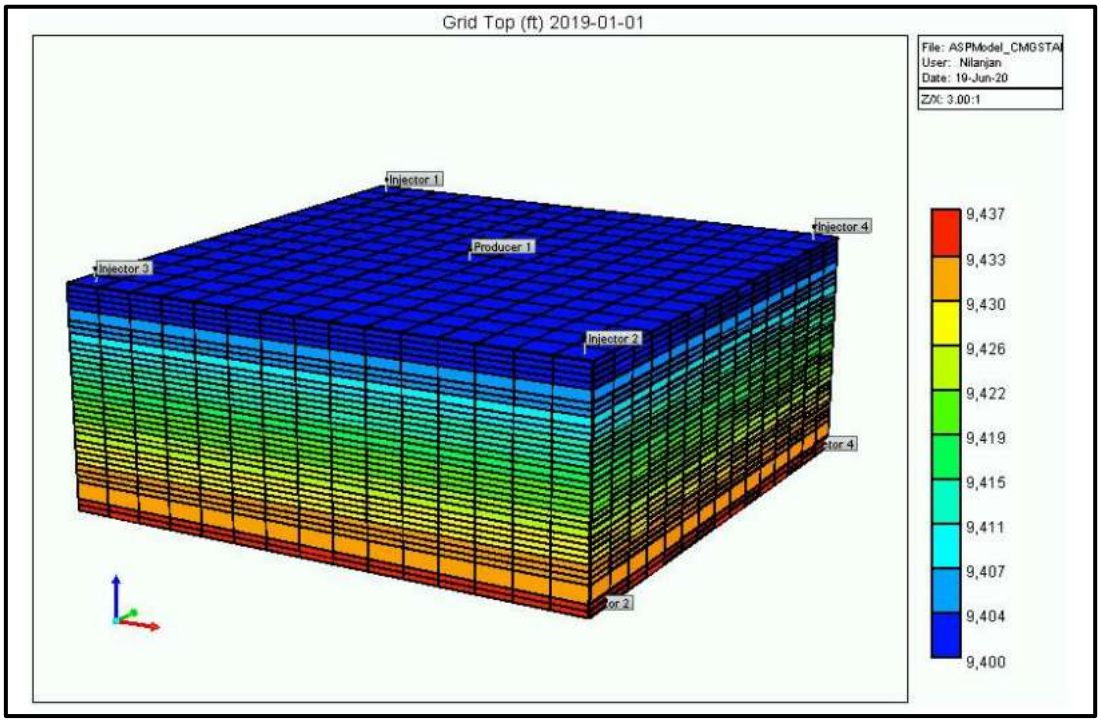

Figure 2.23: A type of reservoir model (five-spot pattern type) built with CMG-STARS [116]

2.18 Materials

2.18.1 Hydrophobic Associative Polymer

AM/AMPS (acrylamide / 2-acrylamido-2-methyl propane sulfonic acid) copolymer as hydrophobic Associative polyacrylamide (HAPAM). The AM: AMPS with mole ratio is 75:25. The thermally stable of (AMPS) monomer can be copolymerized with AM to obtain a water-soluble anionic polymer with improved thermal stability. Incorporation of the AMPS monomer in AM also improves the solubility of the polymer in the presence of divalent cations. Sulfonate makes it resistance to divalent and salinity in general [117].

Acrylamide (AM) oil recovery by acting as thickeners, stabilizers, film formers, rheology modifiers, emulsifiers, lubricity aids, conditioners, and viscosity control agents. The ability of these polymers to alter the rheology of

aqueous systems is what has led to their widespread use. The hydrodynamic volume of polymer molecules would raise viscosity, and intermolecular interaction might raise viscosity even further . If you're looking for a polymer to use as a mobility control agent, one that will hold up well in the heat and humidity of a reservoir, look for one that is thermally stable over the long run. More so, they need to be economical [118].

Poly (2-acrylamido-2-methyl-1-propanesulfonic acid) (PAMPS) reveals novel characteristics that raise the possibility of wide-ranging uses. Strongly ionizable sulfonate groups in its chemical structure are responsible for its pH-sensitivity and swelling behavior . For their low toxicity, hydrolytic stability, and antibacterial action against microbes .AMPS-containing polymers have found widespread use in polyelectrolyte membrane fuel cells [3,4], and in medical applications . In addition, they have numerous commercial applications [119], including in cosmetics, coatings, and adhesives.

There are now 2-acrylamido-2-methyl-1-propane sulfonic acid (AMPS)-containing vinyl copolymers available for industrial use. Hydrogen bonding ability and polyelectrolyte behavior in aqueous solution are provided by acrylamide copolymers with sulfonated comono-mers, particularly AMPS . Because of this, polymers with sulfonate groups are likely to be more stable in solution and resistant to the effects of high salt. Amide monomer copolymerization with other vinyl-type monomers or chemical modification of polyacrylamide itself can also be used to generate testable AM-based copolymers [120].

A typical structure of AM/AMPS copolymer is given in Figure 2.26. The AM/AMPS copolymer showed good thermal stability up to 110 C and no viscosity changes were observed after 16 days. However, at 120 C, the polymer lost 50% of its original viscosity after 10 days of aging [121].

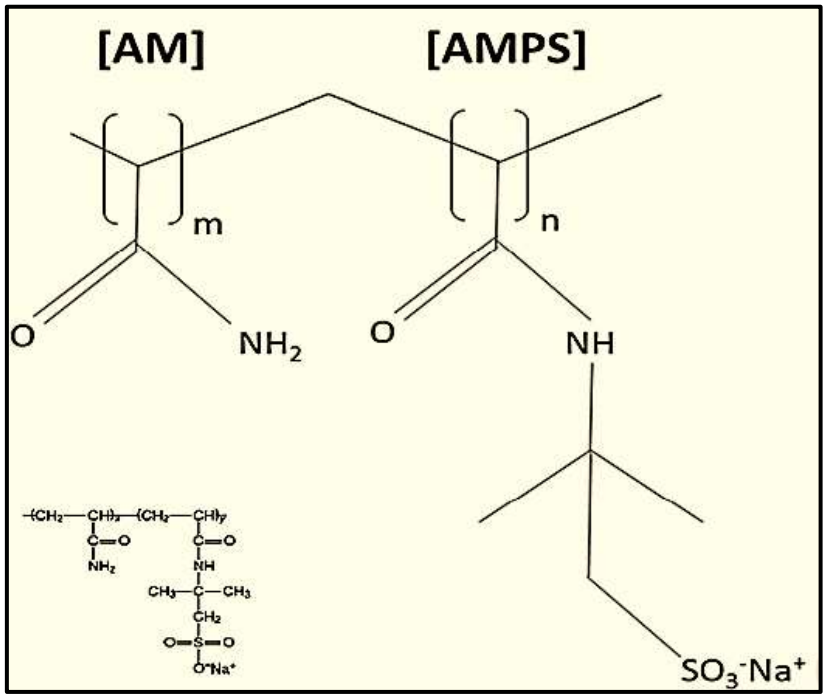

Figure 2.24:- Molecular structure of AM-AMPS copolymers [121]

2.18.2 Sodium chloride

To most people, salt is sodium chloride, an ionic molecule with the chemical formula NaCl, signifying a 1:1 ratio of sodium and chloride ions. The molar weights of the two elements in NaCl are 22.99 and 35.45, hence there are 39.34 g of Na and 60.66 g of Cl in a 100 g sample. The saltiness of seawater and the extracellular fluid of many multicellular organisms is primarily due to sodium chloride. It is often used as a seasoning and preservative in the form of table salt. Sodium chloride is a key intermediate in numerous industrial processes and a major source of the sodium and chlorine compounds that are utilized as building blocks in other chemical synthesis. Sodium chloride also has another key use: de-icing roads during cold snaps.

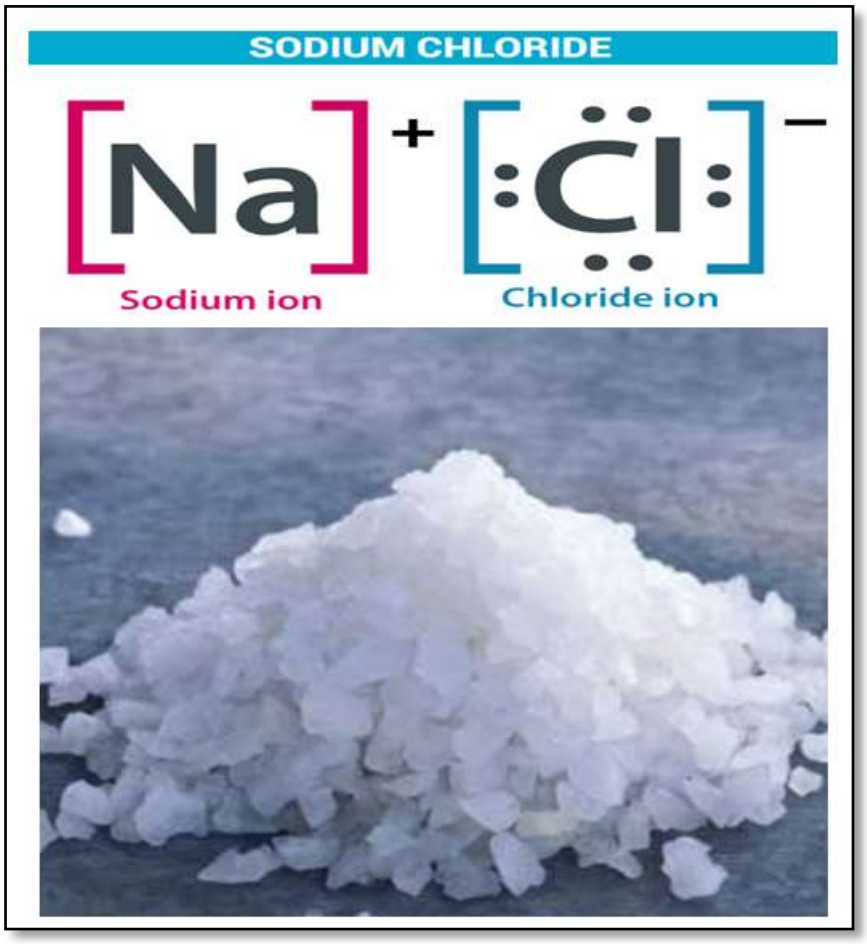

Figure 2.25:- Nacl Structure [122]

NaCl is mostly extracted from sea water, as is common knowledge. Ionic solution of sodium and chloride ions; sometimes known as sodium chloride. The amount of sodium chloride in seawater ranges from 2.79 to 2.91 percent. It plays a crucial role in maintaining the salinity of the water. As an alternative name, it is often referred to as "table salt."[123].

Sodium chloride, more often known as table salt or simply salt, is a crucial component of the food we eat. Sodium carbonate, sodium hydroxide, and other similar chemicals require it as an input. An effective freezing mixture includes sodium chloride. Soapmaking also makes use of this substance, as it is salty. Those working in the tanner and textile industries use it frequently [124].

2.18.3 Sandstone Rock

Sandstone is a common reservoir rock and is home to a large portion of the world's oil reserves. Figure 2.28 shows sandstone, a sedimentary rock formed when older rocks are eroded and broken down. Sand and sediments that eventually become sandstone reservoirs are typically carried great distances by rivers and currents before finally settling in places like deltas and beaches. Cementation occurs when a layer of loose silt is buried, compressed by the weight of the overlying material, and then cemented together [125].

Figure 2.26: - Sandstone rock [125]**.**

Transport rounds grains, and the size of grains is classified by the depositional environment. Sandstone grains are typically between 1/16 to 2 mm in size , and they are quite spherical. In comparison to carbonate rock, sandstone is quite consistent. Sedimentary rocks, however, are all heterogeneous materials, meaning they have a wide range of properties [126]. Depending on the type of rock, the degree of heterogeneity might be mild or extreme. Scale has a major impact on heterogeneity in all rocks. On a larger scale, the properties of a rock that is microscopically heterogeneous may be quite similar to those of a rock

with no such microscale differences. Reservoir modeling relies heavily on understanding how rock characteristics change as one scales down or up [127].

2.18.4 Carbonate Rock

Sedimentary rocks that are mostly made of carbonate minerals are called carbonate rocks. Dolomite rock (also known as dolostone) is formed of the mineral dolomite (CaMg(CO3)2), while limestone is built of calcite or aragonite (various crystal forms of CaCO3). Depending on a number of parameters, including water temperature, pH, and dissolved ion concentrations, groundwater can either dissolve calcite or precipitate calcite. Retrograde solubility refers to the phenomenon wherein calcite becomes less soluble in water as temperature increases, and is thus a unique property of calcite.

Calcite, when precipitated under the correct conditions, generates mineral coatings that either bind the existing rock grains together or fill fractures. Because carbonate rocks dissolve easily in weakly acidic groundwater, karst landscapes and caves can form there. Cave-forming conditions can also be produced by the cooling of groundwater or the mixing of different groundwaters. Marble, a metamorphic carbonate rock, is the rock type in question. Intrusive carbonatites and even more uncommon carbonate lava from volcanoes are the only examples of igneous carbonate rocks [128].

Figure 2. 27 :- Carbonate Rock [129]

2.19 Literature Review

Hamid et al., 2011 [130] studied the efficiency of the displacement mechanism and the displacement process were evaluated and compared between experiments using an image processing technique. Experiments were carried out to observe and track microscopic mechanisms such as the trapping of oil and polymer solution, the arrangement of wetting and non-wetting phases, the flow of continuous and discontinuous strings of polymer solution, polymer solution snap-off, distorted flow of polymer solution, emulsion formation, and the microscopic pore-to-pore sweep of oil phase. Multiple experiments indicated that recoveries in water and mixed wet media were as high as, or even higher than, those in oil wet medium. Both oil recoveries and displacement mechanisms were found to be extremely sensitive to the wettability and pore structure of the underlying media. To better understand the displacement mechanisms associated with a polymer flood process in porous media with varying pore morphologies and wetting properties, this experimental study demonstrates how glass micromodel techniques can be effectively applied to the investigation of enhanced oil recovery (EOR) processes in a five-spot pattern.

Seright et al., 2011[131] compared between associative polymer and hydrolysis polyacrylamide (HPAMs) in the rheological properties at 25°C, 2.52% TDS brine (viscosity versus concentration and shear rate, elastic and loss moduli versus frequency). Cores with permeabilities between 300 and 13,000 md did not exhibit any face plugging or internal filter cake formation for either polymer, and the resistance factors correlated well with the capillary bundle parameter. Low-shear-rate viscosities were compatible with low-flux resistance factors because HPAM polymer was employed in the devices' cores.

The associative polymer had a low-flux resistance factor that was two to three times larger than what would be predicted given viscosities throughout the same permeability range. This effect continued even after passing through a few feet of porous rock and after being subjected to significant shear degradation. The exceptionally high resistance coefficients may propagate deeply into a reservoir, resulting in larger displacement than is feasible with typical HPAM polymers, as suggested by studies of long-core propagation (up to 157 cm). In comparison to HPAM, the novel polymer shows significantly more shear thinning at low fluxes and significantly less shear thickening at high fluxes

Fathi et al., 2012 [132] summarized and discuss the effectiveness of "Smart Water" in oil recovery from carbonate rock. Using a temperature range of 70 to 120 °C. Oil recovery by spontaneous imbibition was increased by 5-10% OOIP compared to seawater by eliminating the inactive salt, NaCl, from the composition of the injected seawater. However, oil recovery decreased by 5% of OOIP when the NaCl concentration in the imbibing solution was increased. Diluting saltwater with distilled water to get a low salinity brine, 1000-2000 ppm, has been shown to systematically reduce oil recovery. Reduced active ion concentration was blamed for the drop in oil recovery. Oil recovery rose by between 5 and 18% of OOIP when SO42- was added to seawater that was low in sodium chloride. Oil recovery was unaffected by the NaCl depletion of seawater Ca2+ concentrations below 100 °C, but improved beyond this temperature. By using a chromatographic wettability test, we were able to see an increasing order in the water-wet fraction following spontaneous imbibition of seawater, seawater deficient in NaCl, and seawater depleted in NaCl spiked with sulfate, which is consistent with improved oil recovery. The

effects of the ionic double layer at the rock-brine interface and the previously proposed mechanism were explored in light of the results.

Dimitrios et al., 2013 [133] studied the comprehensive results of core flood experiments conducted on four oil-soaked limestone rocks. rocks had porosities of 25-30% and permeabilities of 0.3-28 mD, whereas the reservoir brine had a salinity of roughly 120,000 ppm, of which 10,000 ppm were divalent cations. Analysis of the bulk fluids' rheology, stability, and mixability was performed. There was only one commercial polymer that passed our tests out of the three we tried. We then ran core flood studies to measure things like relative permeability, adsorption, the amount of pores that are inaccessible, and a decrease in permeability and mobility. The 8 cP viscosity of the crude oil in the reservoir slightly impacted the mobility ratio unfavorably during the initial water flood. The chosen HPAM polymer did not severely clog any of the four low-permeability cores even at concentrations between 500 and 1,000 ppm, although it did impair mobility and permeability. Dynamic adsorption was low, at around 10-20 g/g rock, and inaccessible pore volume was high, at around 15-20%, consistent with industry norms and the results of ECLIPSE and UTCHEM models, which anticipated that significant polymer degradation did not occur. Because of its high oil content, this rock has a low adsorption. Since the polymer diffuses in water, an oily film on the rock may prevent it from adhering. Although the polymer and the impenetrable pore volume it formed were carried away in the flood, post-event research demonstrated their persistence. This was an unexpected result, one that neither UTCHEM nor ECLIPSE had considered before. The data revealed several nuances that are difficult to simulate numerically. The greatest insight from the laboratory study was the realization that polymer systems with excellent viscosifying

power can be adapted to recover oil from low-permeability carbonate rocks, lowering the permeability limit to roughly 1 mD.

Lu et al.,2014[134] Designed a surfactant mixture that showed great potential for use in reservoirs with complicated fractures. For a hard brine at a reservoir temperature of 100 °C, this new carboxylate surfactant provided ultra-low interfacial tension (IFT) and good aqueous stability. Both stationary and moving imbibition experiments made use of a fractured carbonate core. A static imbibition test only recovered 33.3% of the oil, but a fractured coreflood recovered 65.9%. The surfactant retention was quite low at 0.086 mg/g of rock. The oil recovery was remarkable despite the challenging temperature and salinity settings, the excessively vuggy and fractured core, the lack of mobility control, and the injection of a negligible amount of surfactant. The coreflood data was analyzed by building a mechanical chemical reservoir model. The results proved the significance of modifying wettability in addition to decreasing IFT for oil recovery. When combined, IFT reduction and wettability modification resulted in greater oil recovery than either technique alone.

Shi et al., 2015 [135] the effects of water/oil mobility ratio in heavy oil reservoirs and dimensionless oil productivity index on polymer flooding efficiency were examined using relative permeability curves. The results showed that polymer flooding was able to successfully regulate the growth of fractional water flow when water saturation was lower than the value where the water/oil mobility ratio was equal to 1, therefore that value should be the upper limit of water/oil ratio acceptable for polymer flooding. Meanwhile,

injecting a predetermined volume of water to build water channels in the reservoir is the most efficient method for enhancing sweep efficiency and decreasing the fractional flow of water to the value corresponding to Jmax. Taking into account the expected platform lifespan and its capacity to manage polymer mobility, the optimum time for polymer injection into heavy oil reservoirs was determined. Best results from polymer flooding were seen in reservoirs with crude oil viscosities of 123 and 70 mPa s when polymer floods were commenced with a water fractional flow of 10% and 25%, respectively. The theoretical analysis of the injection time range for polymer flooding in the Bohai Oil Field made use of relative permeability curves to determine how polymer flooding could be made more effective.

Sakthivel et al., 2016 [136] interfacial tension (IFT) of low waxy crude oil-water system (with and without salt) as a function of temperature (283.15-353.15 K) and for EOR-flooding process has been studied for six different alkyl ammonium ILs and sodium dodecyl sulfate (SDS). Polyacrylamide, a water-soluble polymer, was utilized as a polymer flood in the EOR investigation to follow the SDS/ILs flood. We call this type of flood the SDS/IL + polymer EOR flooding technique. There have been a number of EOR flooding studies performed, including those using only polymer, only SDS, alone IL, and SDS/ILS + polymer. Research on the effectiveness of ILs and SDS for EOR has also been conducted at both low (10,000 ppm) and high (>100,000 ppm) salinity levels in the reservoir. For the purposes of EOR, the study also sheds light on how the IFT of the crude oil-water system is affected by the cations and anions (alkyl chain length) of the ILs.

Hashmet et al., 2017 [137] reported the carbonate outcrop core samples were subjected to laboratory core-flood tests under reservoir conditions (120 °C and 167 g/L salinity) to evaluate the flow behavior of polymer injection. The relative permeability curves for the procedure are generated with commercial software after a baseline is established with continuous polymer injection and the experimental data is historically matched. The optimal flooding circumstances are found by adjusting a number of factors, such as the permeability of the reservoir, the size of the polymer slug, the timing of the polymer's commencement, and the flow rate. The simulation outcomes are re-validated against the experimental outcomes. It is encouraging that controlled polymer adsorption on the rock surface can recover up to 85% of the original oil in place, even with mechanical deterioration of the polymer. The potential polymer has been shown to be effective on core samples with permeabilities between 30 mD and 100 mD, although its efficacy decreases with decreasing permeability. The results also demonstrate that injecting polymer earlier helps reduce the size of the polymer slug required to achieve residual oil saturation. The optimum conditions for the polymer slug size and the polymer start time are attained after injecting 0.3 pore volume of water. In part, the reduced polymer slug size is responsible for maintaining the low values of the resistance factor and the residual resistance, 1.9 and 1.1, respectively. An important step toward increasing the number of successful polymer flooding applications is the discovery of a polymer that can withstand high temperature and high salinity conditions in carbonate reservoirs.

He et al., 2018 [138] An injection approach was developed to maximize incremental oil recovery by the use of a branched-preformed particle gel (B-PPG), polymer, and surfactant based on an examination of the process

involved in the heterogeneous phase combination flooding (HPCF) system. Different HPCF injection tactics, including simultaneous injection and alternation injection, were tested by flooding sand packs in parallel and on a wide scale with plates. Whether injected concurrently or in alternation, the HPCF is able to successfully improve oil recovery as shown by the flow rate ratio, the pressure increasing area, and the incremental oil recovery. It has been found that switching between the simultaneous injection mode and the alternation injection mode can increase the sweep efficiency and oil displacement efficiency of HPCF. When the slug of HPCF and polymer/surfactant with the comparable economical cost is injected by alternation injection mode, the incremental oil recovery improves with increasing alternate cycle. Compared to simultaneous injection, large-scale plate sand pack flooding tests showed that HPCF injections at alternating intervals retrieved more residual oil in the low permeability zone. The findings may be used to guide the development of an HPCF injection strategy to maximize oil recovery after polymer flooding of heterogeneous reservoirs when oil prices are low.

Qiannan et al., 2019 [139] tested surface-active polymer flooding using reservoirs and fluids in order to maximize oil recovery . In terms of molecular aggregation, viscosity, flow capacity, and mobility, the experimental results reveal that the surface-active polymer is different from conventional polymers and polymer-surfactant systems. The surface active polymer solution excels at both viscosifying and viscoelastic properties. Enhancing oil washing effectiveness in non-ultralow interfacial tension settings requires a surface-active polymer's ability to emulsify oil into a somewhat stable oil in water emulsion. Changing the chemical properties of the contact and reducing the

interfacial tension can make reservoir rock permeable to water. When surface-active polymer flooding occurs, two things happen to the swept volume. The surface-active polymer's mobility control impact is more important than its oil washing capability in enhancing oil recovery because it can drive residual oil by penetrating oil-bearing pores that have not been swept by water. Macroscopically, it can clog, emulsify, and block the principal channels in the high-permeability layer, diverting the injected fluid into the layer with medium or low permeability and low flow resistance, so increasing the swept volume.

Castro et al., 2020 [140] evaluated of scleroglucan (935 mgL1) and sulfonated polyacrylamide (2500 mgL1) to improve oil recovery at high temperatures for heavy oils (212 F and total dissolved solid of 3800 mgL1) in both synthetic (0.5 Darcy) and representative rock samples (from 2 to 5 Darcy). Under modest pressure difference (less than 20 psi), 18% IPV, 49 g/g dynamic adsorption, 6.17 resistance, and 2.84 residual resistance reservoir circumstances, a scenario with steady injectivity after 53.6 PV is provided by dynamic evaluation. As an added bonus, the oil displacement efficiency was increased by as much as 10% at a concentration just 2.7 times that of a sulfonated polyacrylamide polymer.

Maghsoudian et al. (2021) [141] Hydrophobically modified copolymer of acrylamide and styrene (HSPAM) was used inverse emulsion polymerization as a wettability modifier and viscosifying agent for use under severe reservoir conditions to understand synergistic oil recovery pore-scale mechanisms . A slew of analytical methods first proved HSPAM's water-soluble structure and

its superior thermal resistance compared to HPAM (FTIR, NMR, TGA, and molecular weight measurement). Under harsh reservoir conditions, the rheological investigation of HSPAM showed that the total dissolved particles in the aqueous solution had an increasing effect on the solution's viscosity, all the way up to 40,572 mg/L. Deionized water (DIW), seawater (SW), and formation brine (FB) were used in stability tests, contact angle (CA), interfacial tension (IFT), and flooding studies with a carbonate coated glass micromodel both without and with HSPAM and HPAM. HSPAM was more stable than HPAM in sea water and forming brine after 120 days at 80 oC. After 72 hours in seawater, the contact angle of HSPAM was 31 degrees, while that of HPAM was 22 degrees. The results showed that HSPAM considerably improved the efficacy of brine-based flooding and ultimately recovered roughly 82% of the original oil in place through synergic oil recovery processes proven by emulsification and coalition phenomena (OOIP).

Hincapie et al., 2022 [142] studied the effect of using three distinct sandstone outcrops were employed, all of which were similar in composition but varied in clay concentration and porosity. Both low and high TAN oils were utilized, with the latter coming from the Matzen field's potential field pilot 16 TH reservoir (Austria). Imbibition of alkaline, nanoparticle, and polymer aqueous phases has been studied, and some of the parameters contributing to increased recovery rates and final recovery have been identified. This research provides new information on how IFT, contact angle Amott imbibition, and core flooding all work together to facilitate the chemical processes evaluated.

2.20 Summery

Glass micromodel techniques can be effectively applied to the investigation of enhanced oil recovery (EOR) processes in a five-spot pattern. The result appear Multiple experiments indicated that recoveries in water and mixed wet media were as high as, or even higher than, those in oil wet medium. Both oil recoveries and displacement mechanisms were found to be extremely sensitive to the wettability and pore structure of the underlying media [130].compared between associative polymer and hydrolysis polyacrylamide (HPAMs) in the rheological properties at 25°C, 2.52% TDS brine . Cores with permeability between 300 and 13,000 md .The result associative polymer had a low-flux resistance factor, larger oil displacement. On the other hand HAPAM show more shear thinning at low fluxes and significantly less shear thickening at high fluxes [131]. Oil recovery by smart water showed spontaneous imbibition was increased by 5-10% OOIP compared to seawater [132].HAPAM showed excellent viscosifying power can be adapted to recover oil from low-permeability carbonate rocks, lowering the permeability limit to roughly 1 Md [133]. Carboxylate surfactant good aqueous stability mixture for use in carbonate reservoirs with complicated fractures. The result showed IFT reduction , wettability modification , good aqueous stability, and greater oil recovery about 65.9% [134]. Regulate the growth of fractional water flow when water saturation was lower than the value where the water/oil mobility ratio was equal to 1, therefore that value should be the upper limit of water/oil ratio acceptable for polymer flooding at crude oil reservoir between 70 and 123 mPa.s [135]. The mixture of alkyl ammonium (ILs) and sodium dodecyl sulfate (SDS) with Polyacrylamide showed lower IFT and EOR [136]. Controlled polymer adsorption on the rock surface can recover up to 85% of the original oil in place, even with mechanical deterioration of the polymer

[137].Improve oil recovery as shown by the flow rate ratio, the pressure increasing area, and the incremental oil recovery by using branched-preformed particle gel (B-PPG), polymer, and surfactant based on an examination of the process involved in the heterogeneous phase combination flooding (HPCF) system [138].The surface active polymer solution excels at both viscosifying and viscoelastic properties. effectiveness in non-ultralow interfacial tension ,ability to emulsify oil into a somewhat stable oil in water emulsion,changing the chemical properties of the contact.Also, mobility control impact is more important than its oil washing capability in enhancing oil recovery because it can drive residual oil by penetrating oil-bearing pores that have not been swept by water. Macroscopically, it can clog, emulsify, and block the principal channels in the high-permeability layer, diverting the injected fluid into the layer with medium or low permeability and low flow resistance, so increasing the swept volume [139].Scleroglucan (935 mgL1) and sulfonated polyacrylamide (2500 mgL1) was used to improve oil recovery at high temperatures for heavy oils. The result oil displacement efficiency was increased by as much as 10% at a concentration just 2.7 times that of a sulfonated polyacrylamide polymer [140].Hydrophobically modified copolymer of acrylamide and styrene (HSPAM) .Also, hydrolysis polyacrylamide (HPAM) was used in carbonate coated glass micromodel to show pore-scale mechanisms. The result HSPAM was more stable than HPAM in sea water and forming brine after 120 days at 80 ^{o}C, the contact angle of HSPAM was 31 degrees, while that of HPAM was 22 degrees, and ultimately recovered roughly 82% of the original oil in place through synergic oil recovery processes proven by emulsification and coalition phenomena (OOIP) [141].Three distinct sandstone outcrops were employed. Both low and high TAN oils were utilized. Imbibition of alkaline, nanoparticle, and polymer

aqueous phases has been studied, and some of the parameters contributing to increased recovery rates and final recovery have been identified [142].

Through this summary, it was found that the [141] is similar to this study, with some differences. Where HAPAM was used and its rheological and physical properties were examined. types of rocks were used, 3 carbonate and 2 sandestone.The core flooding test used to measure the petrophysical properties and the percentage of oil extraction was designed. Ansys and CMG were used for the purpose of comparison between the experimental and numerical results. The results showed complete agreement between the practical and numerical aspects, with an oil extraction rate of up to 98%.

Chapter Three

Experimental Part

3.1 Materials

3.1.1 Hydrophobic Associative Polyacrylamide (HAPAM)

HAPAM used as synthetic polymer provided from America, properties of HAPAM shown in Table 3.1.

Table 3.1 : Properties of HAPAM

Properties	**Data**
Chemical Name	(AM) and 2-acrylamido -2-methylpropane sulfonic acid (AMPS)
Molecular Formula	$C_7H_{13}NO_4S$
Molecular Weight,(g/mol)	(207.247)
Place of Origin	America, Sigma-Aldrich (St. Louis, MO, USA)
Color	White
Shape	Granular
Density, (g/l)	(1.45)
Water Soluble (°C)	Soluble
Melting Point, ℃	185.5 - 186 °C

CAS Number	15214-89-8

3.1.2 Sodium Chloride

Table 3.2:-Nacl Properties

Properties	**Data**
Chemical Name	Sodium Chloride
Molecular Formula	NaCl
Shape	granular
purity	98.8%

3.1.3 Core Samples

The petroleum industry generally acknowledges sandstone and carbonate core samples, such the ones shown in Figure 3.1, as the best possible materials for testing. Both of these kinds of cores are frequently utilized in the process of measuring the effectiveness of chemical floods in the laboratory. The properties of these cores listed in Table 3.3.

Before the rock specimen could be put through its paces, it had to be honed with a grinding tool and polished using a trimming machine to produce a surface that was smooth and flat. After that, polishing tools were used to smooth out the surface and reduce the roughness. The granite was washed, then dried in a vacuum to remove any impurities that might have been present.

Table 3.4 :- Core Sample Properties

Core samples	Type	Diameter (cm)	Length (cm)	Depth (m)	Oil reservoir
Core 1	Carbonate	3.8	5.2	1545	Nasiriya
Core 2	Carbonate	3.8	5.2	1956	Nasiriya
Core 3	Carbonate	3.8	5.2	2195	Nasiriya
Core 4	Sandstones	3.8	5.2	2678	Nasiriya
Core 5	Sandstones	3.8	5.2	2856	Nasiriya

3.2 Methodology

3.2.1 Brine water Preparation

To prepare the brine solution, 20% NaCl was dissolved in tap water, as shown in Figure 3.2. After that, the solution was filtered through a 0.45 μm cellulose nitrate filter. The filtered brine was used to make polymer solutions and assess the petrophysical properties of cores, such as porosity and permeability.

3.2.2 Experimental Oil

The laboratory oil was in properties are similar to the oil found in oil reservoirs in southern Iraq, where kerosene and turbines are mixed together in the same quantity . This type of laboratory-prepared oil does not contain sulfur, phosphate or gasoline, because they are heavy materials that clog the pores of the used rocks and thus make it difficult to extract the oil. After preparation, we filter the oil using filter paper with 45 μm cellulose filter to

remove the suspended materials that cause problems for the used Core samples.Viscosity, density and interfacial tension with brine water and HAPAM solution was measured

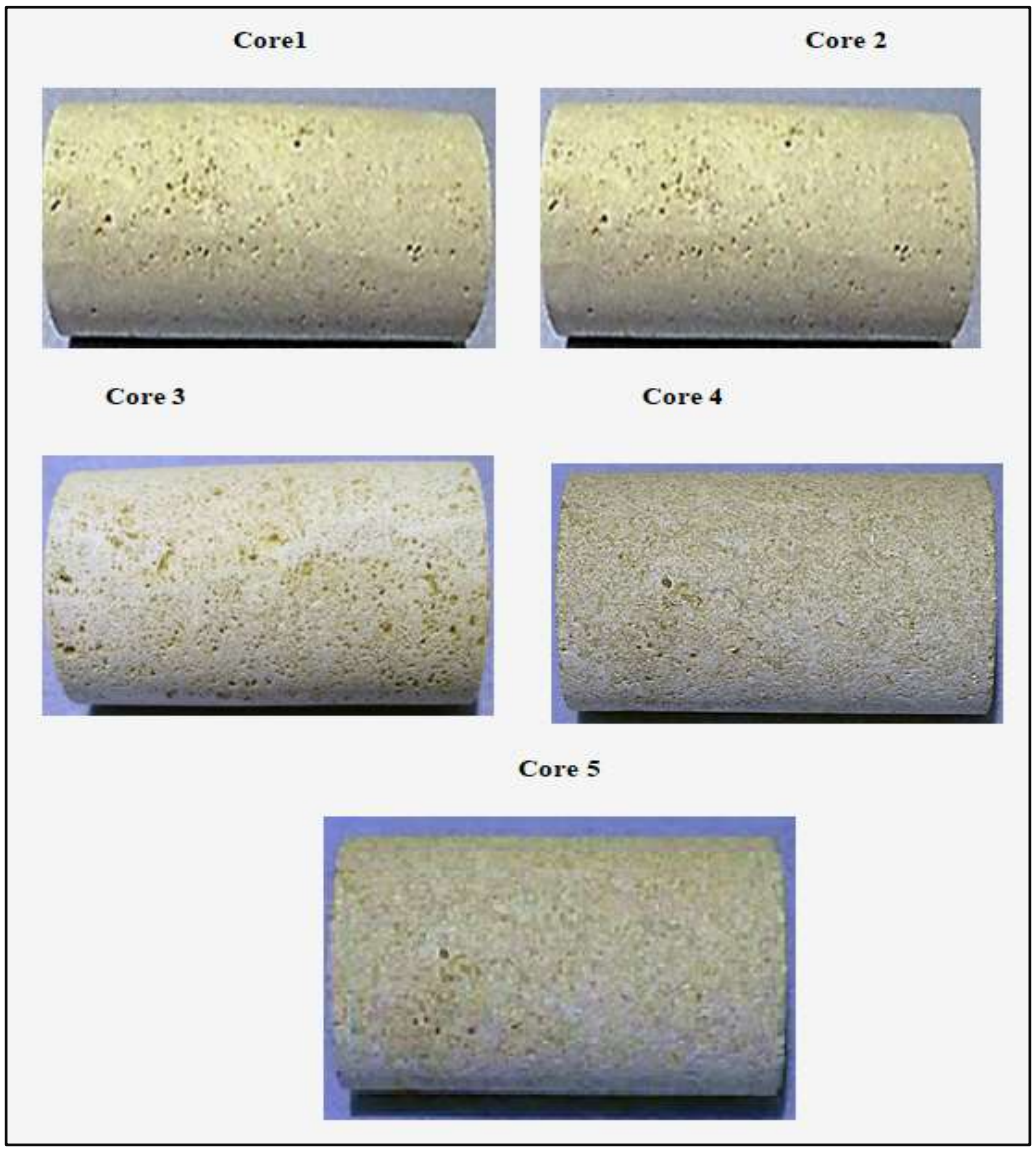

Figure 3.1:- Core samples

3.2.3 Polymer Solution Preparation

Acrylamide (AM) and 2acrylamido-2methylpropane sulfonic acid (APMS) were the monomers that were used to create the hydrophobic associative polyacrylamide, also known as HAPAM . HAPAM solutions were prepared by slowly adding 500, 1000, 1500, or 2000 ppm of HAPAM to brine water

and mixing for 30 minutes to prevent gel formation. Then filter in 0.45µm cellulose filter.

3.2.4 Core Sample Preparation

The diameter of the cores was 3.8 cm, and the length was 5.2 cm. They were soaked in methanol for 10 days in a glass jar before being cleaned with methanol and toluene to get rid of any remaining dust or dirt. After that, the cores spent 12 hours drying in a 100 °C oven. Prior to any further testing, the cores were soaked in a water solution containing 20% NaCl for 72 hours to ensure thorough saturation. The porosity was calculated by comparing the pre- and post-saturation core sample weights. The cores were initially stored in a core holder, as shown in Figure 3.2 (with a confining pressure of 180 psi). The effective permeability of the sandstone and carbonate cores was then measured by flooding them with brine water (k). To simulate an oil-saturated sandstone or carbonate reservoir in the lab, crude oil was introduced into the cores to replace the existing brine water until the irreducible water saturation state (Swi) was reached. The process was permitted to go on for 6 days.

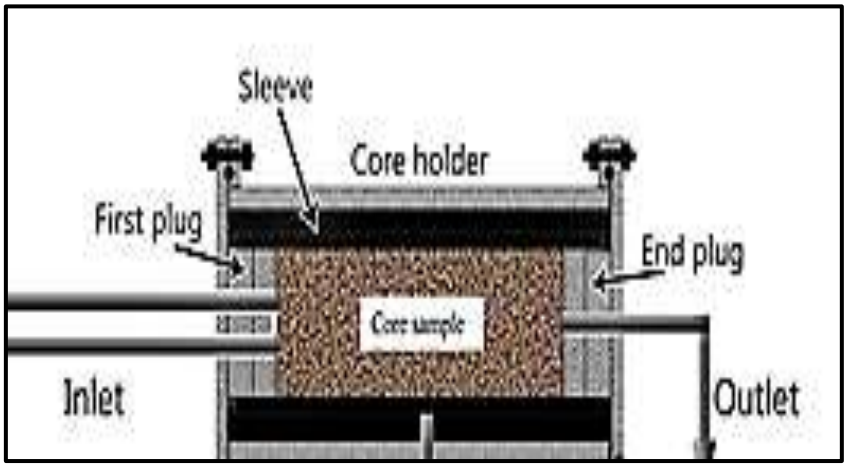

Figure 3.2:- Core sample inside core holder

3.3 Experimental Equipment

3.3.1Rheological Properties

The shear viscosity of brine water and HAPAM solutions was studied in relation to various factors, including shear rate, shear resistance, concentration, temperature, and aging time. The rheological properties were studied by Brookfield cone - plate viscometer with spindle: 41Z as show in figure 3.3.

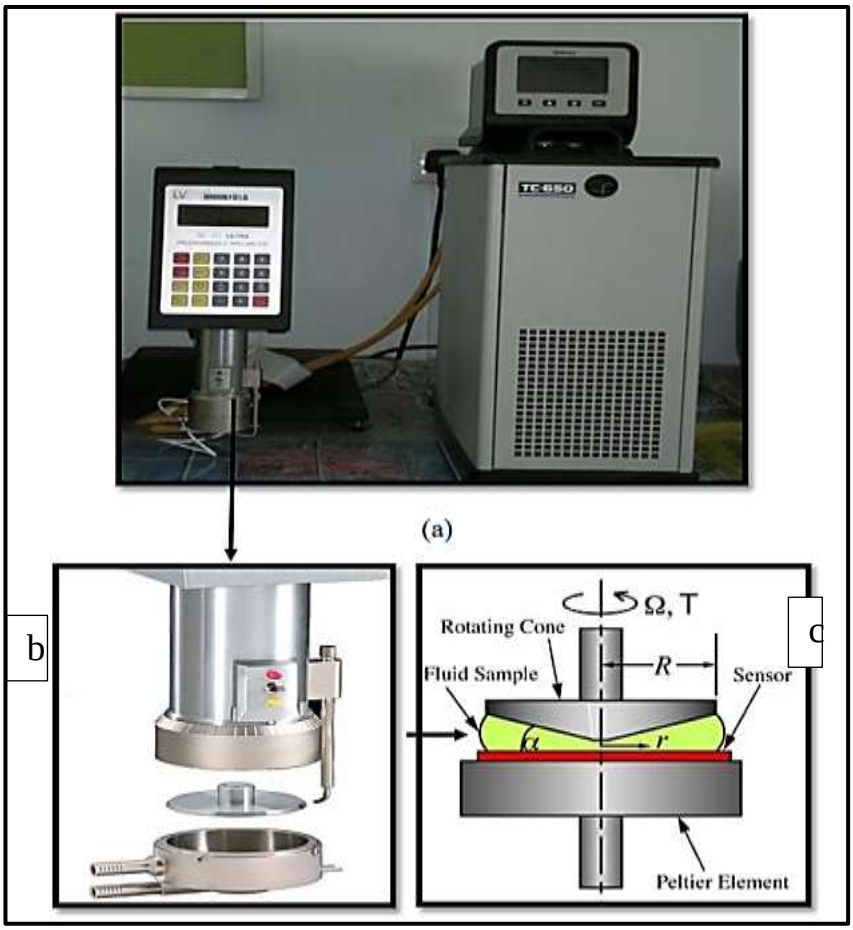

Figure 3.3:- (a) Cone- plate viscometer, b) cone and c) diagram of cone.

The rheological properties estimates executed with a cone on plate viscometer as show in Figure 3.3(a). Arrangement put in lower plate and the cone set in it as appear in Figure 3.3 (b). An electrically commutated synchronous engine drive turns the cone at a set speed and this picks the shear rate inside the

annulus. The model tends to drag the plate and the power applies on that plate (torque) is surveyed, which can be changed over shear rate.

Shear viscosity with concentration were tested for (500,1000, 1500, and 2000)ppm/brine water for HAPAM . Shear viscosity and flow curves were studied at shear rates ranging from 5 to 35 s^{-1}. Shear resistance properties were investigated by allowing the samples to rest for 48 hours and measuring the viscosity at a shear rate of 7.3 $S^{-1}$and a temperature of 25 °C. The effect of aging on the viscosity of HAPAM solutions was studied by storing them in an oven at temperatures of 25, 50, and 65 °C for periods of 2, 4, 10, 20, and 30 days, with a shear rate of 7.3 s^{-1}. An aging time of zero refers to measurements taken immediately after preparation. The viscosity measurements were fitted using the following power law model equation (2.4).

3.3.2 Physical Properties

3.3.2.1 Density

The density of brine water and HAPAM solutions was tested using a GP-120S device based on ASTM D-792 from China. The test procedure involved placing a breaker containing the sample on a testing board and removing the weight of the pothook. A standard weight was then hung on the pothook and fully submerged in the liquid being tested, and the enter button was pressed to store the measurement.

3.3.2.2 Surface Tension and Interfacial Tension (IFT) Measurement

Surface Tension:-

The JZYW-200B Automatic Interface Tensiometer from BEING UNITED TEST CO., LTD. in China was used to determine the surface tension of brine water and HAPAM solutions at a temperature of 25 °C. The process involved

using the tensiometer to bring the brine water and HAPAM solutions separately into contact with air, as illustrated in Figure 3.4.

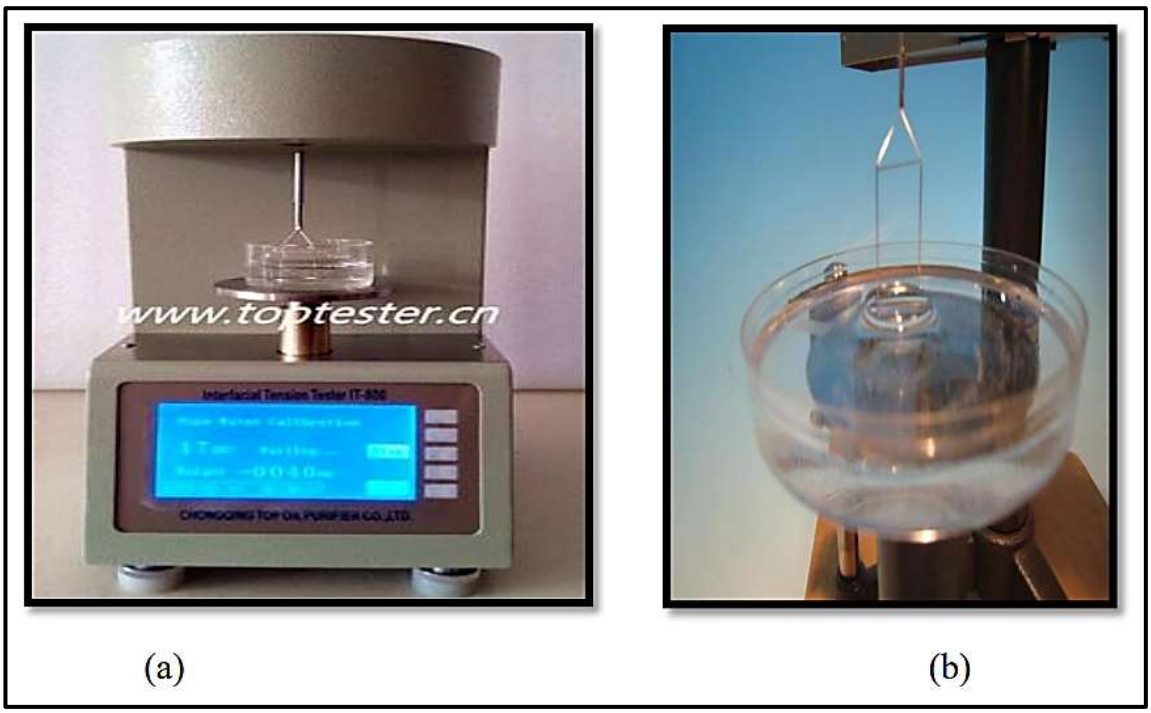

Figure 3.4:- show Du Noy ring method to measuring surface tension of solutions, (a), general shape of device and (b), high resolution on platinum ring over solution.

Surface tension measurement technique based on the force exerted by a platinum ring on a liquid's surface. By shifting the platform on which the liquid container rests, the ring is lowered below the interface. The ring is designed to pull up the meniscus of the liquid as the stage is slowly lowered. The meniscus's volume (and hence the force it exerts) reaches its maximum when it separates from the ring and then begins to decline. The surface tension of the liquid can be calculated from this occurrence.

Interfacial tension

The method relies on gauging the greatest force present at the boundary between two incommensurable fluids. In this method, it doesn't matter how

deep the ring is submerged or how high it's elevated when the draw is at its strongest. Rather, the greatest force exerted at the contact point is being recorded.

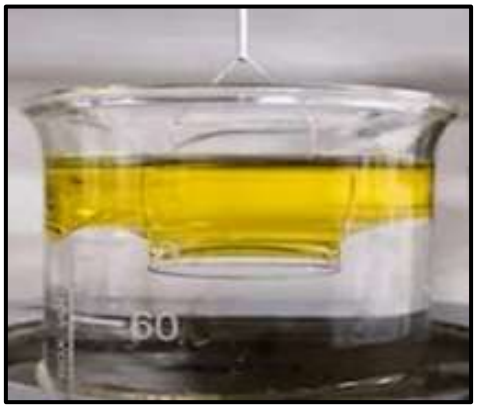

Figure 3.5:- Interfacial tension test of solution- oil by De Nouy ring method

Interfacial tension (IFT) between two immiscible fluids, specifically oil and bulk HAPAM solution, was also measured. Test samples were prepared in a 1:1 ratio by weight of oil to HAPAM solution and allowed to equilibrate for 21 days before testing. This allowed for clear and stable phase separation. The measurement of IFT between the excess oil phase and HAPAM solution is shown in Figure 3.5. and the solution adhered to the ring for a distance above the surface. When the solution broke away, the force was measured and converted to interfacial tension.

3.4 Core Flooding Device

Core flooding device as show in figure 3.6 consist of the following parts:-

Core Holder

A stainless steel core holder is used. The base is 10 cm long and its inner diameter is 5 cm. The core is placed inside the core holder. The core holder contains three tubes, the first is called an inlet, which is used to enter the solutions, the second is an outlet to exit the solutions from the core, and the third is directly connected to the compressor. The benefit of it is to exert pressure on the sleeve that is surrounded by the rock (core). As it works to make the flow in one direction from the entry area to the exit area.

The entry and exit openings of the core are covered with perforated iron pieces and linked to the core holder, which is called the first and end plug. In order for the rock to be tightened and its solutions to be introduced from the entry area.

The core holder cover in the entry area contains two holes, the first for oil entry and the second for entering brine or polymeric solution separately, while the exit area contains only one hole. On the other hand, both the entry and exit openings of the core holder contain a valve to control the incoming and outgoing solutions, as well as a gage pressure that records the incoming and outgoing pressure.

Accumulator

The device contains two types of accumulator. One of them is where oil is stored, and the other contains either brine or a polymeric solution. Where they are connected from the lower side to the compressor, and from the upper side they are connected to the core holder, and between the entry and exit points to

them, each of them contains a valve. They also contain gage pressure to record entry and exit pressure.

Collector

It is placed at the exit area of the core holder, as it contains gradations to measure the percentage of oil extraction from the rock.

Compressor

The process of pumping air into the device according to certain proportions by controlling the amount of gas coming out by means of a valve. Where it is used by pumping gas directly into the core holder to perform the process of air pressure on the sleeve. Which, in turn, works to tighten the rock (core), so it is called the confining pressure. Which is stopped by the valve after noticing that there is no increase in the pressure coming out directly from the compressor.On the other hand, it pumps air to the accumulators to push the solutions destined to the core holder to be pumped onto the core sample, where the air pressure is recorded in the entry and exit areas of the core holder.

3.4 Petro physical Properties Measurement

3.4.1 Pore volume

A mass balance, in which the weight of the dry core is weighed against the weight of the saturated core by brine water, can be used to compute the pore volume of a core. The difference in these two weights is what determines the gravimetric pore volume, and it is equal to the difference in weights divided by the brine's density. The following is a mathematical expression that may be used to describe this relationship show in equation 3.1 :-


1: gage pressure
2: core holder for core samples.
3:core holder for oil
4:core holder for solution
5:valve
6:valve
7:valve
8:compresser
9:inlet
10:outlet
2.5HP/50L AIR COMPRESSOR
INDUSTRIAL

(a)

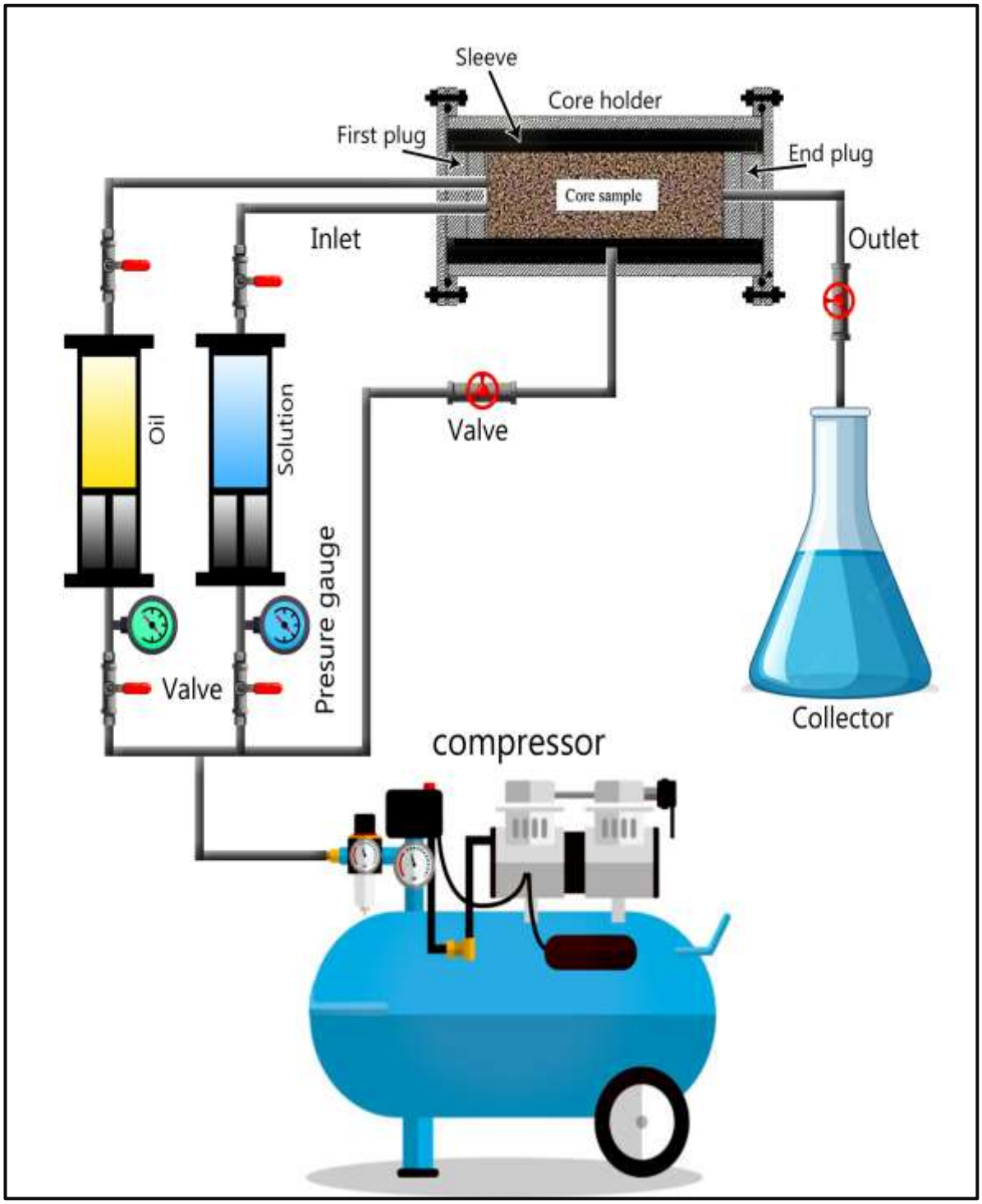

(b)

Figure 3.6:- (a)Schematic , and (b) diagram illustration of the experimental setup of the core flooding .

$$V_p = \frac{m_{sat} - m_{dry}}{\rho_w} \quad \text{……Eq.(3.1)}$$

Where, V_p: pore volume; m_{sat}: mass of core saturated with brine water;m_{dry}: mass of dried core ; and ρ_w: brine water density.

3.4.2 Bulk Volume

The total volume of the bare core can be used to calculate the bulk volume of a core:

$$V_b = \pi r^2 L \text{……..……..(3.2)}$$

Where, V_b:bulk volume; r: radius of core; and L=length of core

3.4.3 Porosity

A core's porosity is the percentage of its volume that is made up of pores relative to its total volume**.**

$$\phi = \frac{V_p}{V_b} = \frac{V_b - V_s}{V_b} \text{……..(3.3)}$$

3.4.4 Gas Permeability

Determining the gas permeability of a porous medium, a modified version of Darcy's law that takes into consideration the effect that the compressibility of the gas has on flow can be utilized. Darcy's law was used to figure out the gas permeability after the core was cleaned and the core holder was put together. Gas permeability was determined by using the injection pressure from the compressor**.** The new gas permeability equation looks like this:-

$$K_g = \frac{2q_{sc}\mu L p_{sc}}{A(p_1^2 - p_2^2)} \text{……(3.4)}$$

Where, K_g: gas permeability; K_g: gas permeability; P_1:Pressure at inlet; P_2: Pressure at outlet ; and $q_{sc:}$ flow rate at standard condition.

3.4.5 Permeability of Brine (Absolute Permeability)

After the pore volume had been measured, the core was re-saturated with 100% brine water by infusing a number of pore volumes' worth of brine water into the core. Using flow rates of(6, 10, 15, 20, 25, and 30)cm^3/min. It is possible to compute the brine permeability, which is sometimes referred to as the absolute permeability. That kind of math can be done with the help of Darcy's law, which describes how fluids move through porous media. Calculating permeability in the petroleum industry often involves using the following equation, which depicts flow in a single phase, in a steady state, and horizontally as show in Figure 3.7:-

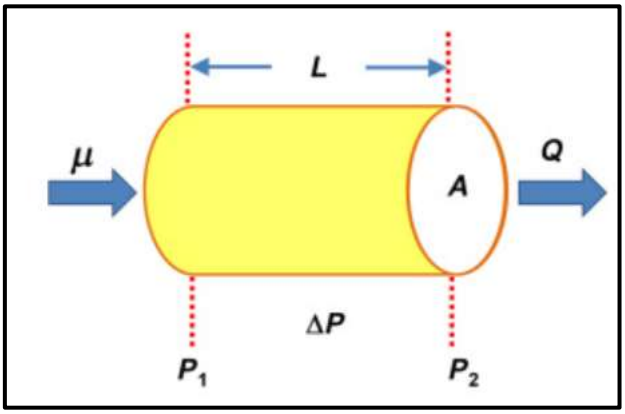

Figure 3.7 :- Calculation flow rate inside core sample

$$k = \frac{\mu L q}{A \Delta p} \text{……..……(3.5)}$$

Where, q: flow rate; ΔP:Pressure drop across core; K: absolute permeability; A: cross sectional area of core; and μ:viscosity of fluid .

3.4.6 Oil flooding

After brine water was pumped into the core, oil at ambient temperature and high injection pressure was injected into the core. The purpose of the technique known as oil flooding was to ascertain the initial oil saturation (Soi),

the irreducible water saturation (Sirw), the oil effective permeability (Ko), and the relative oil permeability (Kro).

To saturate the core with oil and properly estimate the level of irreducible water saturation, the oil flooding was carried out under a constant pressure that ranged from 50 to 180 psi. The oil was injected into the inlet end of the core. And the water displacement was measured to calculate the starting oil saturation and the final, irreducible water saturation. After the water cut, which is the percentage of water in the generated fluid, had been reduced to less than 1% and the pressure had stabilized, the oil was flooded at a constant flow rate, and the differential pressure across the core was recorded in order to compute the oil permeability.

$$S_{oi} = \frac{V_w}{V_p} \text{……(3.6)}$$

Where, Soi: initial oil saturation; and Vw: volume of water produced from oil flooding

$$S_{irw}\% = 100 - S_{oi}\% \text{.....(3.7)}$$

$$K_o = \frac{q\mu L}{A\Delta p} \text{……...……(3.8)}$$

$$K_{ro} = \frac{K_o}{K} \text{…….……..(3.9)}$$

3.4.7 Aging

Following the completion of the oil flooding process, the core was taken out of the core holder and placed in an accumulator that was filled with experimental oil. The core was allowed to age for 4 days at room temperature and an additional 4 days at a temperature of 45°C, as illustrated in Figure 3.8.

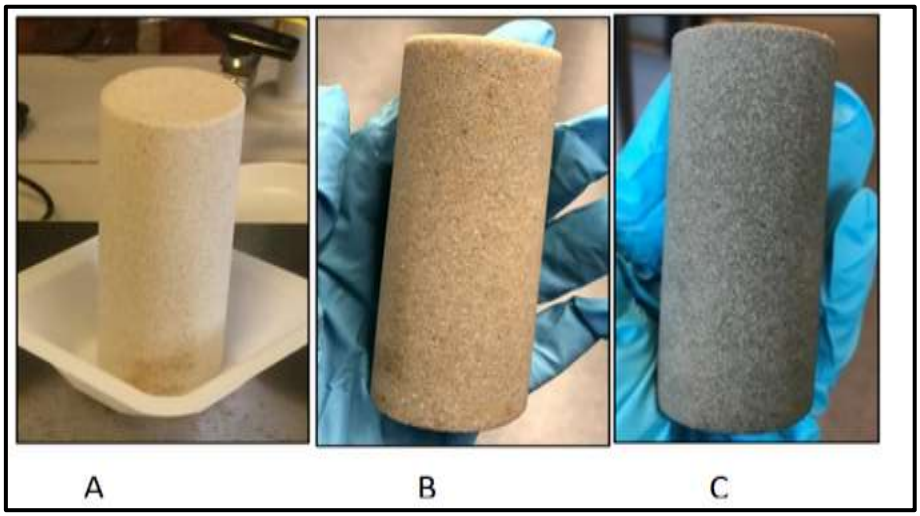

Figure 3.8:- Core sample (A): before aging, (B):after aging at room temperature and (C): after aging at 45ºC.

3.4.8 Oil Flooding after Aging

After the core had aged, it was placed back into the core holder and compressed to a pressure of 180 psi. In order to remove the oil that was trapped inside the core, oil was injected at a steady flow rate of 6 cm3/second. The difference in pressure across the core was monitored so, the oil effective permeability (Ko), and the relative oil permeability (Kro) could be calculated once it had been aged.

$$K_o = \frac{q\mu L}{A\Delta p} \text{……..……(3.10)}$$

$$K_{ro} = \frac{K_o}{K} \text{……..(3.11)}$$

3.4.9 Flooding by Brine Water

The oil flooding was carried out after the brine water flooding was completed to determine the reservoir's residual oil saturation (Sorw) after water flooding, and its relative water permeability (Krw).The flow rate of brine water flooding was carried out at (6 cm^3/min). The effluent fluids were collected in a beaker, and the water flooding was stopped when the oil cut (the percentage

of oil in the generated fluid) was less than 1% and the pressure had stabilized. In other words, when the oil cut was less than 1%, the water flooding was halted. Both the effective water and oil permeability, and the residual oil saturation were computed utilizing the total volume of oil that was collected in the beaker. The pressure difference across the core was used to determine the effective oil permeability.

$$S_{orw} = \frac{V_w - V_o}{V_p} \text{……..……..(3.12)}$$

S_{orw}= residual oil saturation after water flood

Vo= volume of oil production from water flood

$$K_w = \frac{q\mu L}{A\Delta p} \text{……..……(3.13)}$$

$$K_{rw} = \frac{K_w}{K} \text{……..(3.14)}$$

3.4.10 Flooding by Polymer(HAPAM)

HAPAM solution was injected into the core samples in order to evaluate the effectiveness of these solution of extracting residual oil from the core. At a constant flow rate of around 6 cm^3/min, HAPAM solution flooding was performed, and the process was continued until no further oil production was possible and the pressure had become stable. Then relative permeability of polymer (Krp) was determine by:-

$$K_p = \frac{q\mu L}{A\Delta p} \text{……..……(3.15)}$$

$$K_{rp} = \frac{K_p}{K} \text{……..(3.16)}$$

3.4.11 Oil Recovery

A series of core flooding tests, in which a rock core is first saturated with brine water and then flooded with oil to measure the initial oil saturation, can be used to provide an estimate of the amount of oil that can be recovered from a formation. Then, the core is flooded with either brine water or a polymer solution (such as HAPAM) and the volume of oil produced is measured.

$$Oil\ Recovery = \frac{Oil\ Production}{Initial\ Oil\ in\ Place\ (S_{oi})} \text{……..(3.17)}$$

3.4.12Water Cut

$$Water\ cut = \frac{Water\ read}{Total\ (water+oil)} x100\% \text{.....(3.18)}$$

Where, water cut:percentage of total water displaced from the rock (core); water read : the amount of water extracted from the core; and total (water + oil) : the total amount of (water + oil) extracted from the core.

3.5 Capillary Number

After calculating the velocity from Darcy's law. calculate the capillary number from the following equation:

$$Ca = \frac{\boldsymbol{\mu v}}{\boldsymbol{\gamma \emptyset}} \text{……..……..…..(3.19)}$$

Where, Ca:capillary number ; μ:viscosity (cp); γ:interfacial tension between oil and water (N/m); and ∅:porosity

3.6 Apparent Viscosity(μ_{app})

To compare the apparent viscosity of a polymer solution measured in a porous medium to the viscosity measured in a rheometer, it is necessary to establish a link between the flow velocity in the porous medium and the shear rate in the rheometer.

$$\mu_{app} = \frac{KA\Delta p}{qL} \text{……(3.20)}$$

Where, q: flow rate; ΔP:Pressure difference across core; K: effective permeability; A: cross sectional area of core; and μ:viscosity of fluid.

The apparent and shear viscosity curves with shear rate are plotted according to the following steps:-

1- Shear viscosity in cone plate viscometer is measured in the laboratory at a shear rate between (5-25) s^{-1}.

2- examine the apparent viscosity of five types of core using a core flooding test device, where the rock is injected with a polymeric solution of 1500ppm HAPAM/brine water, a range of flow rate is taken and we find the pressure difference of the core, and then we apply Darcy's law to calculate the apparent viscosity.

3- draw a relationship between the shear and apparent viscosity with the shear rate in order to compare the flow behavior of the polymeric solution in bulk with the stimulus inside the porous medium.

As for the apparent viscosity curve with shear rate and Darcy velocity, it is plotted through:

1- The apparent viscosity is measured.

2- Find Darcy's speed.

3- We draw a relationship between the apparent viscosity with the shear rate and velocity. The values of the shear rate are taken with the same values in which the viscosity of HAPAM was tested with a cone-plate viscometer, in order to compare the behavior of the flow inside the porous medium and in the case of bulk.

3.7 Differential Pressure

check the pressure difference through the Core flooding device for five types of Core sample by:-

1- Calculate Darcy's velocity for each sample.

2- Through Darcy's law, we examine the pressure difference

3- Draw a curve between the pressure difference with the velocity for each of the brine water without and after adding 1500 ppm of HAPAM to it.

Chapter Four

Numerical Simulation and Modeling

4.1 Computational Fluid Dynamics (CFD)

High complexity of to simulate immiscible two-phase flow in porous media, which containing a large number from pores variable in shapes [143]. Original exact analytical solution is not feasible option. The next best alternative to an analytical solution would be a finite-element or finite volume model, explicitly accounting for all the physical mechanisms involved. Computational fluid dynamics (CFD) methods was used to analyze and evaluate effects of different mechanisms on mobilization of trapped non-wetting fluid, analyze systems involving fluid dynamics, heat transfer ,chemical reactions and phase changes by numerical calculations[144]. Computational Fluid Dynamics (CFD) consists from:-

1-Pre-processor

2-Solver

3- Post-processor

4.1.1 Pre-processor

Pre-processor include [145] :-

a) Generation grid that defines geometry of interest.

b) Introduce physical and chemical properties that need to be simulation.

c) Definition the fluid properties.

d) Application boundary conditions.

4.1.2 Solver

Solver is to carry out the numerical calculations necessary to create satisfactory simulations of the flow problem. Solver held on finite difference, finite element, finite volume and spectral methods. The main differences between these techniques was held on how the variables of flow are approximated and on the discretization process. In this theses depend on using the commercial CFD software package FLUENT, well known for its extensive capabilities in solving a wide variety of fluid-flow problems including multiphase flow) using the finite-volume approach. This method was originally developed as a special finite difference formulation and will be discussed in the following section [146].

4.1.3 Post-processor

The post-processor include results of simulation that calculated by the solver. Today, most of the available CFD programs have developed graphical tools, which make it possible to receive a visualization of the calculated data [147].

4.2 The Finite Volume Method (FVM)

Due to the fact that FLUENT evaluation physical or engineering problem by using finite volume method in reason of [148] :-

1. Exact integration of governing equations of fluid flow over all the control volumes within the solution domain.

2. Discretization involving substitution of a variety of finite difference-type approximations for the terms in the integrated equation representing the flow processes. The terms in equation are convection, diffusion and source terms. Then this system of integral equations was transformed into a system of algebraic equations, which can be solved numerically.

Discretization methods are used to chop a continuous function (i.e., the real solution to a system of differential equations in CFD) into a discrete function, where the solution values are defined at each point in space and time. Discretization simply refers to the spacing between each point in your solution space.When a simulation intends to calculate a dynamic solution to a fluid/heat flow multiphysics problem, the finite-difference time-domain (FDTD) method is used as we need to discretize time in addition to space. In 1D, 2D, or 3D systems without time dependence (i.e., the steady-state solution), the finite element method (FEM) is used for discretization. An alternative method for 3D systems is the finite volume method (FVM), in which the system is discretized in units of volume rather than as sets of points forming a mesh.

Solution algorithms produce varying convergence and are only adaptable to certain discretization methods. The most common solution methods include:

- Iterative methods: Picard, Newton, Newton-Raphson, and Uzawa methods are the common methods used to linearize systems of CFD equations and solve their finite difference equations. These linearization schemes are similar to small-signal analysis for circuit simulations.
- Eulerian method: This can be used to solve the linearized Navier-Stokes equations for inviscid fluids and produces results that are largely equivalent to iterative techniques for inviscid fluids.
- Network techniques: This involves defining different regions with different material properties in a system as elements in a network, where the interface between network elements is the spatial boundary between neighboring regions. A related technique is the additive Schwartz technique, which splits a CFD problem into multiple boundary value problems in different domains and adds up the results.

- Transformation methods: These are linearization techniques that are only applicable in specific geometries. By applying an analytical or numerical transformation, the system can be linearized and solved easily using an iterative method.
- Adaptive meshing: This involves using one of the previous methods in a grid with fine to coarse meshing in the system. Critical areas of the system that require high accuracy use fine mesh size, while other areas where lower accuracy can be tolerated use coarser mesh size.

3. Solution of the algebraic equations by an iterative method. It is the first step that the finite volume method differs from the other numerical techniques. The finite volume method expresses the conservation of relevant properties for each finite size cell. It is clear that relationship between the numerical algorithm and the physical principal of conservation that makes the finite volume method easier to apply and understand than finite element and spectral methods.

4.3 CFD Analysis by FLUENT 20

4.3.1 Modeling

Geometry in Figure 4.1(a). Geometry consist of 3D in. Same dimension of core sample that used in experimental flooding (3.8x5.2x3.8) cm. Oil is found in core by filled it firstly. Introduced brine water or HAPAM solutions from inlet zone.

4.3.2 Main Assumptions

a) Steady state and laminar flow.

b) Viscosity dependent on shear rate for polymer aqueous solutions

, but brine water viscosity independent on shear rate.

c) Polymer aqueous solutions depend on non-Newtonian power law model.

d) Two phase flow.

e)Porous media.

f) Complex pore structure

Table 4.1:- Rheological and Physical Properties

Material	**Shear viscosity , cp**	**Power law index, n**	**Consistency index, cp.s^{n-1}**	**Density, g/cm^3**	**Interfacial tension, N/m**
Brine water	2.3	-	-	1.2	18.3
Oil viscosity	5.6	-	-	0.93	-
HAPAM/ Brine water,ppmm	6.4	0.59	17.5	0.99	4.1

Table 4.2:-Petrophysical Properties of Core Samples

Properties	Core1	Core2	Core3	Core4	Core5
Diameter, cm	3.8	3.8	3.8	3.8	3.8
Length, cm	5.2	5.2	5.2	5.2	5.2
Porosity, %	15	13	16	20	22
Permeability, mD	51	41	48	55	61

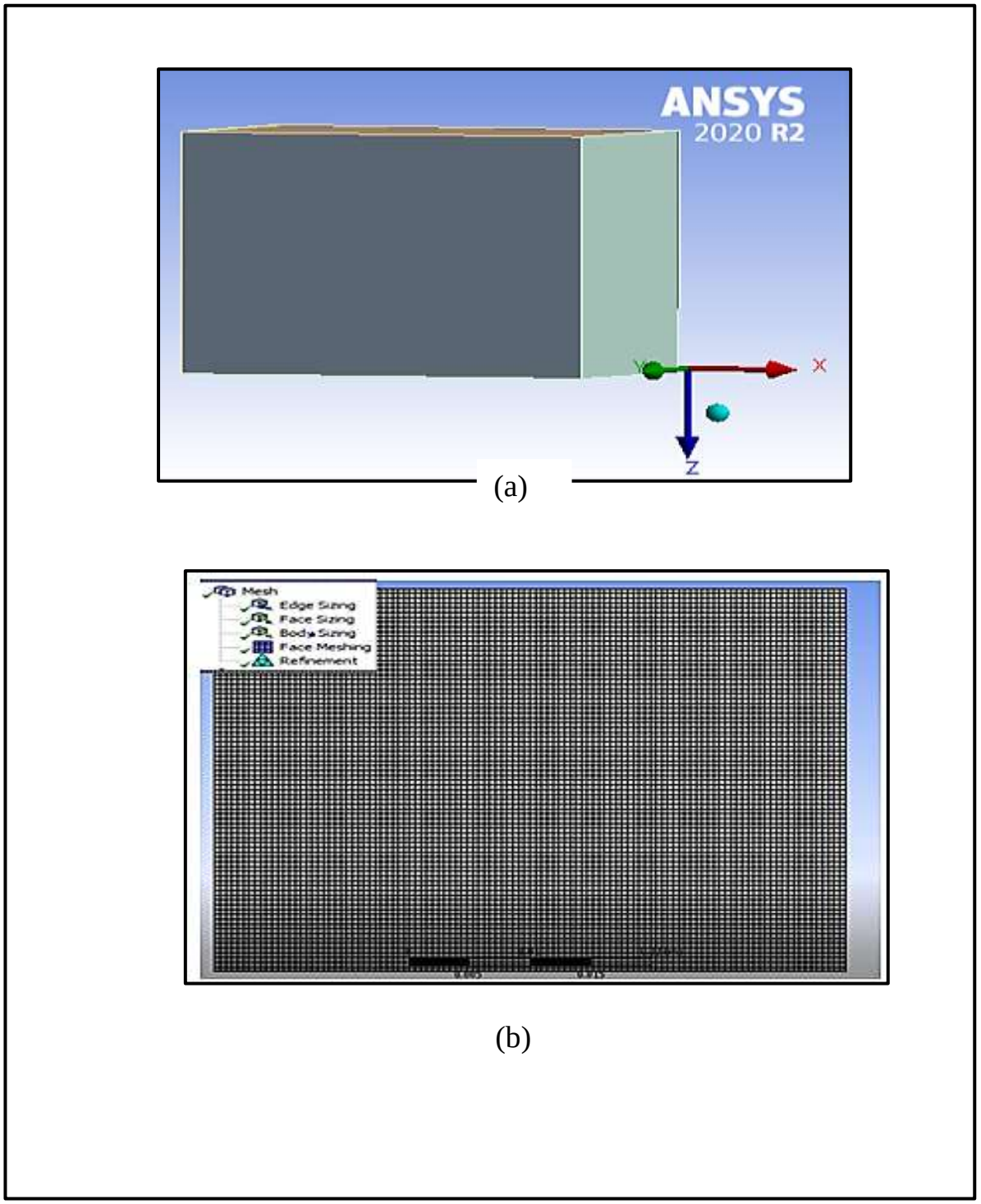

Figure 4.1:- a) Geometry and b) Meshing model

4.3.3 Governing Equations and Mathematical Model for Ansys Fluent

The flow is isothermal, incompressible, two-dimensional, and immiscible in a complex pore structure. Based on the VOF method, the mathematical model of a two-phase flow was established.

Continuity Equation [149]:-

$$\nabla . U_i = 0 \quad \text{……..……..(4.1)}$$

Where, U_i: is the velocity vector, cm/s. And subscript i denotes the x and y directions, respectively.

Momentum Equation [150]:-

$$\frac{\partial_\rho U_i}{\partial_t} + \nabla . (\rho U_i U_I) - \nabla . \mu \nabla U_i = -\nabla_P + F_\sigma \text{……(4.2)}$$

The surface pressure drop F_σ , of a two phase interface through the continuum

Surface Force (CSF) Model is as follows [151]:-

$$F_\sigma = \sigma k \nabla_\alpha \text{……..……(4.3)}$$

The formula of curvature *k* is

$$k = \nabla . \left(\frac{\nabla_\alpha}{|\nabla_\alpha|}\right) \text{……..……(4.4)}$$

Where, *t*: indicates the time, s; p :is the pressure, Pa ; ρ : density of fluids, kg/m^3; μ : viscosity of fluids, Pa.s ; σ : surface tension coefficient, N/m ; k :two phase interface curvature, m^{-1}; and α : phase volume fraction, which represents the saturation of water.

The polymer solution is non-Newtonian fluid, and exhibits shear thinning characteristics. The relationship between the viscosity and shear rate of

polymer solution is described using a constitutive equation of the power law model as appear in equation 2.4.

With VOF, α is the phase volume fraction, which is defined as follows:

$$\alpha = \begin{cases} 1 \\ 0 < a < 1 \\ 0 \end{cases} \text{.....(4.5)}$$

Where,

α = 1, for a point inside the polymer or water solution

$0 < a < 1$, for a point in the transitional region

$a = 0$, for apoint completely in the oil.

Basic on the definition of a , and the continuity equqtion the phase equation can be expressed as [152]:-

$$\frac{\partial_\alpha}{\partial t} + \nabla . \alpha U_i = 0 \text{.....(4.6)}$$

4.3.4 Boundary conditions

Boundary conditions for Figure 4.2, are shown below:-

a)Volume Of Fluid (VOF) model is selected with number of phases=2. Then select Implicit of VOF.

b) Viscosity, density, interfacial tension, n and k taken from experimental

data that used to define fluids, physical and pertophysical properties shown in Table 4.1.

c) Operating pressure is set as (101325) and gravity is consider in Y-direction as (-9.81) m/s2

d) Flow rate of brine water and polymer aqueous solutions 6 cm^3/s.

e) Wall be stationary and No-slip.

f) Select pressure as outlet.

g) Number of iteration is 150.

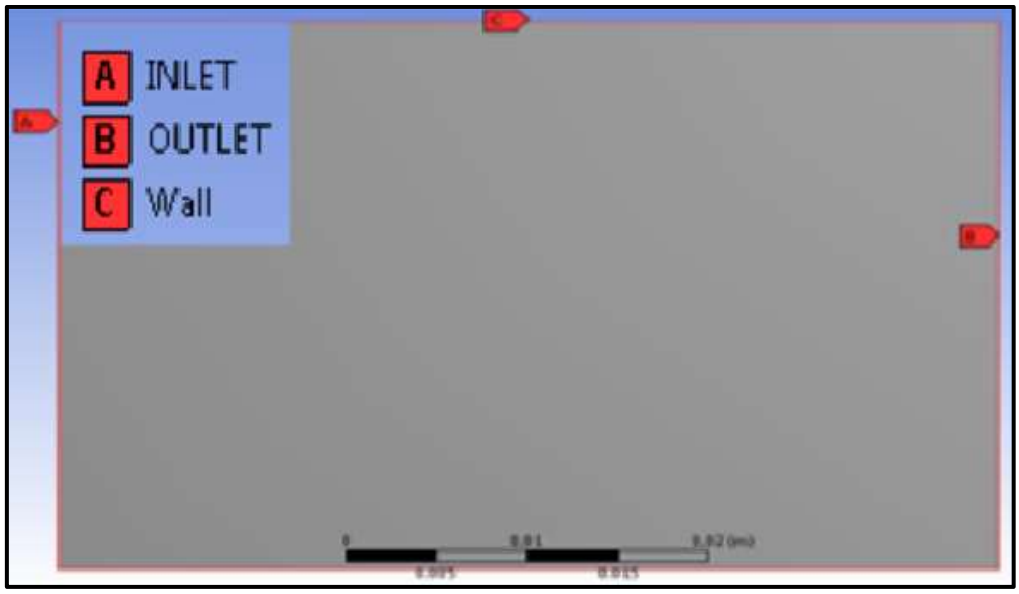

Figure 4.2:- Boundary conditions of Core sample by Ansys

4.4 Computer Modeling Group (CMG)

The reservoir data (temperature , pressure, porosity ,permeability ,depth) and fluid properties (viscosity ,density) had been collect from laboratory core flood experiment for core samples taken from Basra oil reservior, to establish simulation model through CMG software in order to predict the effect of HAPAM in oil recovery.

Abbreviated as CMG, is a software company that produces reservoir simulation programs for the oil and gas industry. It is based in Calgary, Alberta, Canada with branch offices in Houston, Dubai, Caracas and London. The company is traded on the Toronto Stock Exchange under the symbol

CMG. The company offers three simulators, a black oil simulator, called IMEX, a compositional simulator called GEM and a thermal compositional simulator called STARS[153].

Today, CMG remains focused on the development and delivery of reservoir simulation technologies to assist oil and gas companies in determining reservoir capacities and maximizing potential recovery[154].

4.4.1.CMG Components

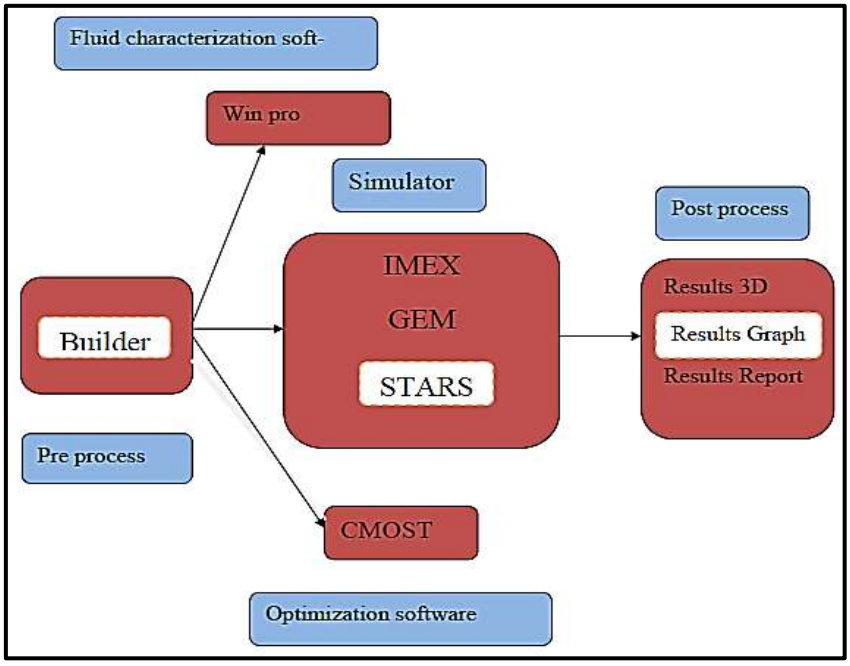

Figure 4.3:- CMG Components [153]

4.4.1.1 Builder :

Builder, a Windows-based application, helps engineers create input files for CMG reservoir simulators – IMEX, GEM, STARS. Through the use of 3D and 3D visualization, and efficient keyword input, Builder helps reservoir engineers realize im-mediate time savings by efficiently navigating them through the complex process of building reservoir simulation models. Builder simplifies the creation of simulator mod-els by providing a framework for data integration and workflow management between CMG's reservoir simulators

and the "outside world". Its intuitive interface and numerous process wizards make reservoir simulation accessible to all organizations, even those with limited modeling experience. CMG's reservoir simulators and the "outside world". Its intuitive interface and numerous process wizards make reservoir simulation accessible to all organizations, even those with limited modeling experience[155].

4.4.2 Simulator

4.4.2.1 Generalized Equation-of-State Model Reservoir Simulator (GEM)

GEM is a full equation-of-state compositional reservoir simulator with advanced features for modeling recovery processes where the fluid composition affects recovery. GEM also models asphaltenes, coal bed methane and the geochemistry of the sequestration of various gases including acid Gases and CO_2[156].

4.4.2.2 IMplicit-Explicit -Three-Phase, Black Oil Simulator (IMEX):-

IMEX is a full -featured three-phase, four-component black oil reservoir simulator for modelling primary depletion and secondary recovery processes in conventional oil and gas reservoirs. IMEX also models pseudo-miscible and polymer injection in conventional oil reservoirs, and primary depletion of gas condensate reservoirs, as well as the behavior of naturally or hydraulically fractured reservoirs[157].

3.4.2.3 Steam, Thermal and Advanced processes Reservoir Simulator (STARS)

STARS is a thermal, K-value compositional, chemical reaction and geomechanics reservoir simulator ideally suited for advanced modelling of

recovery processes involving the injection of steam, solvents, air and chemicals [158].

4.5 Building and Simulation Core Flood Model :

Flow chart below represents the steps of creating the numerical model through the use of CMG software are shown in Figure4.4 and 4.5.

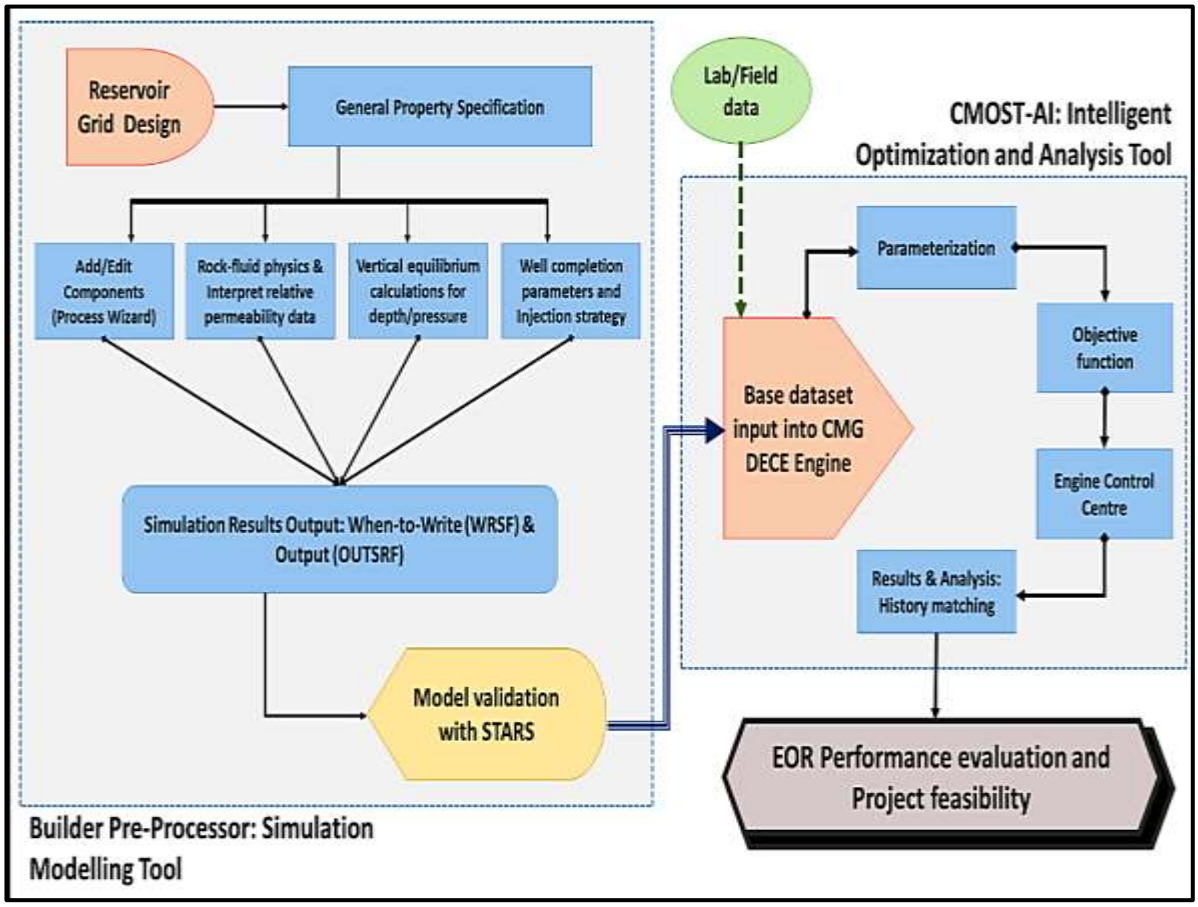

Figure 4.4:- Work Flow Illustration For Compositional Simulation Of Flooding System [158].

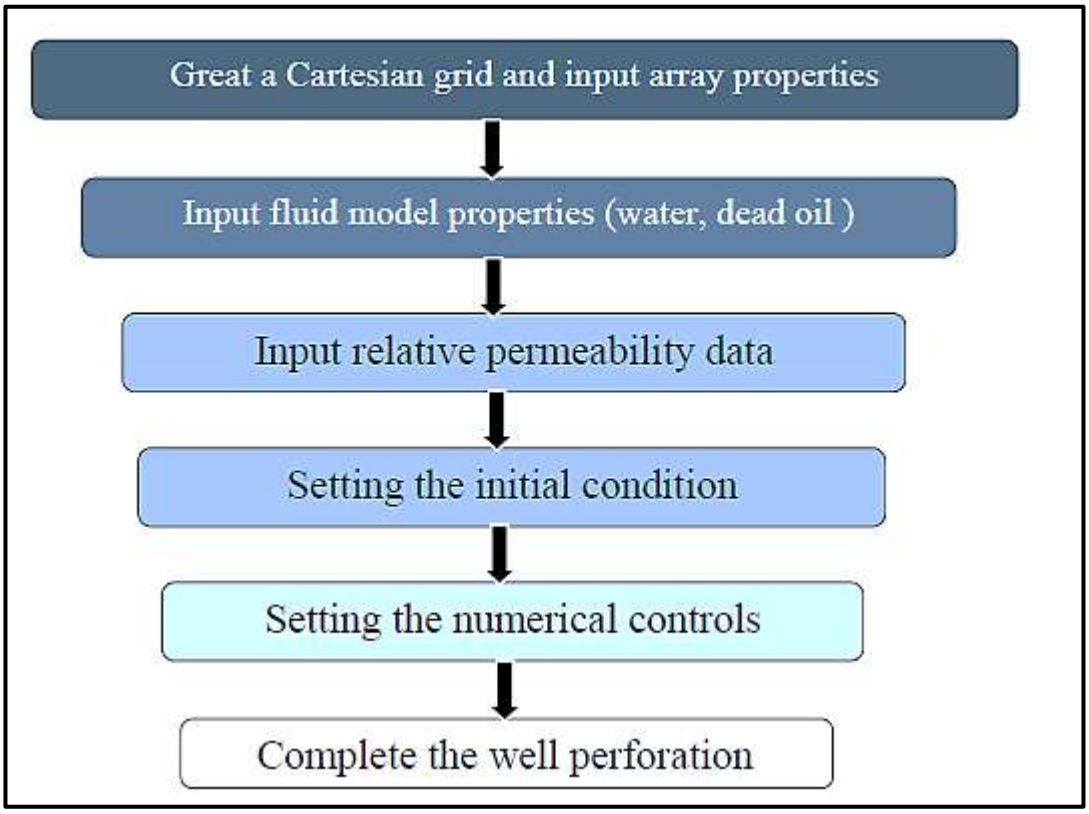

Figure 4.5:- Steps of Building Numerical Model [158]

4.5.1 Cartesian Grid

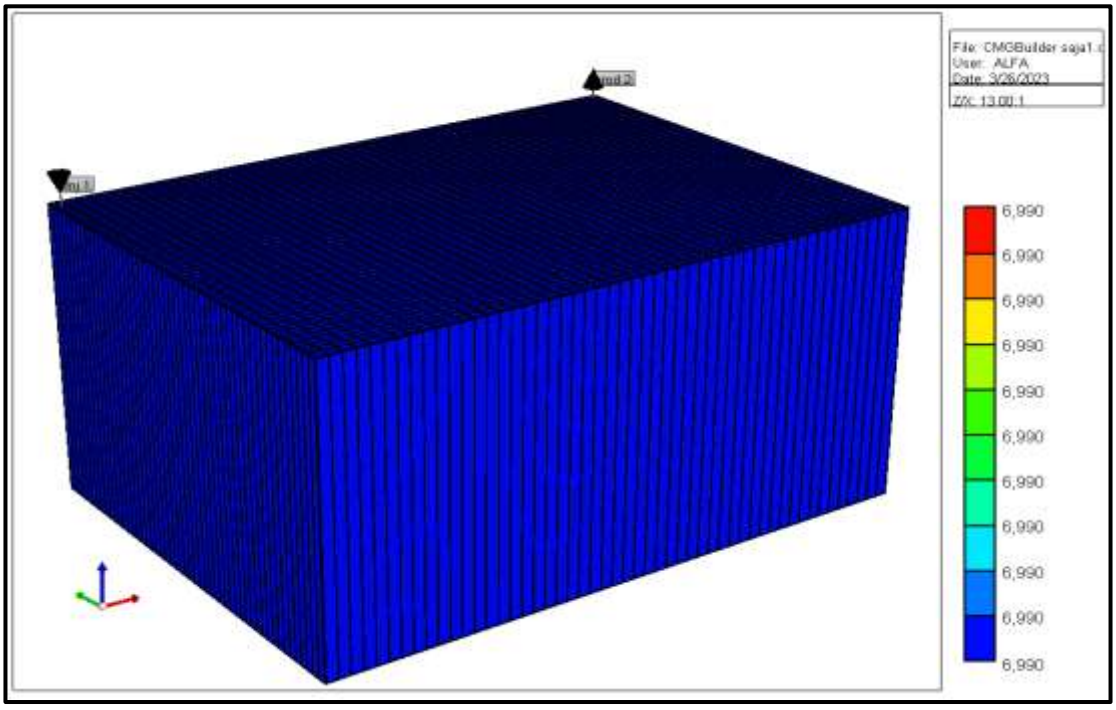

Figure 4.6:- Cartesian Grid Pattern for Flooding Simulation

Table 4.3:- Core Sample Characteristic by CMG

Properties	Core1	Core2	Core3	Core4	Core5
Grid size(x),cm	0.082	0.082	0.082	0.082	0.082
Diameter, cm	3.8	3.8	3.8	3.8	3.8
Length, cm	5.2	5.2	5.2	5.2	5.2
Grid	100	100	100	100	100
Porosity, %	15	13	16	20	22
Permeability, mD	51	41	48	55	61
Core type	Carbonate	Carbonate	Carbonate	Sandstone	Sandstone
Temperature, ℃	25	25	25	25	25
Pressure, Psi	150	160	130	135	125

4.5.2 Fluid Properties

Table 4.4:- Fluid Properties

<table>
<tr><th>Properties</th><th>Data</th></tr>
<tr><td>Brine viscosity, (Cp)</td><td>2.3</td></tr>
<tr><td>Oil Viscosity, (Cp)</td><td>5.6</td></tr>
<tr><td>1500ppm HAPAM /Brine Water Viscosity, (Cp)</td><td>8</td></tr>
<tr><td>IFT / oil + brine water, (N/m)</td><td>18.3</td></tr>
<tr><td>IFT/ oil + 1500ppm HAPAM solution ,(N/m)</td><td>4.1</td></tr>
<tr><td>Permeability, (mD)</td><td>
<table>
<tr><td>Core Samples</td><td>Gas Permeability (Ka), mD</td><td>Liquid Permeability (Kl), mD</td><td>Oil Permeability (Ko), mD</td></tr>
<tr><td>Core 1</td><td>51</td><td>30</td><td>120</td></tr>
<tr><td>Core 2</td><td>41</td><td>9</td><td>11</td></tr>
</table>
</td></tr>
</table>

	Core 3	48	33	15
	Core 4	55	44	18
	Core 5	61	53	23

4.5.3 Initial Condition

The STARS simulator package in CMG is widely employed compositional tool in the petroleum industry, with the capacity to develop reservoir models. No difference in the data-results were seen, thereby confirming the validity of the grid-based simulation. A Cartesian grid system with 100 specified divisions along X axis was developed to model the carbonate and sandstone core and simulate flooding data. Prior to running the CMG simulation, the following initial condition were made to obtain accurate findings.

(a) The reservoir initially consists of two phases, namely, oil and brine water or oil and polymer solution and no mass exchange occurred between them.

(b) The amount of free gas/solvent gas in the core model is assumed as zero.

(c) A grid-based core model is considered, with uniform properties and no geological complexities/heterogeneities.

(d) Fluid flow in radial direction is negligible as compared to that in axial direction.

(e) Salinity effect on phase behavior is ignored.

(f) Chemical reactions do not occur.

(g) Oil and brine water flowing or oil and HAPAM solution through porous media(Core sample) obeys the Darcy's Law.

(h) The mixture of brine water and polymer (HAPAM) was ideal, and was presented only in the water phase.

(I) The fluids were compressible, and the rock was not only compressible but anisotropic.

(J) The flow was isothermal, and Newtonian flow for brine water and non-Newtonian flow was advised for polymer solution .

4.5.4 Numerical Simulation And Mathematical Model

Compared to water flooding, the polymer flooding process is more complicated and is accompanied by complex parameter changes. This is especially true for polymer flooding in heavy oil reservoirs. More parameter changes need to be considered and mainly include the viscosity changes of the water phase, polymer adsorption, the permeability reduction of the water phase, inaccessible pore volumes, and the threshold pressure gradient (TPG) of heavy oil.

The viscosity of the water phase changes with the injection of the polymer solution and is affected by the mixing degree of the water and the injected polymer solution, polymer concentration, and a shear rate. First, the Todd-Long staff mixing parameter was introduced to describe the mixing degree of the water and the injected polymer solution [39,40]. In this study, the Flory–Huggins equation was applied to treat the relationship between the viscosity of the polymer solution at the zero shear rate and the concentration of the polymer and salt, which was written as [159]:

$$\mu_p^0 = \mu_w \left[1 + \left(a_{p1} c_p + a_{p2} c_p^2 + a_{p3} c_p^3\right)\ c_s^{s_p}\right] \text{.....(4.7)}$$

where, μ_p^0 : viscosity of the polymer solution at the zero shear rate , Pa.s; μ_w : water viscosity , Pa.s; a_{p1}, a_{p2} and a_{p3} : parameters in $(kg/m3)^{-1}$; C_p : polymer

concentration , kg/m^3; C_s : salt concentration in kg/m^3; s_p : slope between $(\mu_p^0 - \mu_w)/\mu_w$ and c_p on a log-log plot. Here, the effect of the salt concentration was neglected by setting s_p to zero. In addition, the dependence of the polymer solution viscosity on shear rate was modeled by power law model equation 2.4.

The relationship between the equivalent shear rate and the Darcy velocity of the polymer solution [160].

$$\dot{\gamma}_{eq} = 4\left(\frac{3n+1}{4n}\right)^{\frac{n}{n-1}} \frac{v_p}{\sqrt{8k\emptyset\sigma}} \quad \text{.....(4.8)}$$

Where, n : flow behavior index; $\boldsymbol{v_p}$: Darcy velocity of the polymer solution , m/s; k : permeability of rock , m^2; ϕ : porosity; and $\boldsymbol{\sigma}$: tortuosity of pores.

During the flow of polymer solution through the rock, some polymer molecules will inevitably be adsorbed on the inner surfaces of pores in the rock . Here, the Langmuir adsorption isotherm model was applied to treat polymer adsorption [161]:

$$c_{ap} = c_{apmax} \frac{b_p c_p}{1 + b_p c_p} \quad \text{.....(4.9)}$$

Where, c_{ap} : adsorbed concentration of polymer , kg/kg; c_{apmax} : maximum adsorbed concentration of polymer , kg/kg; and $b_p$is the adsorption coefficient.

The adsorbed polymer molecules will cause a permeability reduction of the water phase .Here, the permeability reduction of the water phase was implemented by a factor of R_k, which is [162]:

$$R_k = 1 + (RRF - 1)\frac{c_{ap}}{c_{apmax}} \quad \text{.....(4.10)}$$

where RRF is the residual resistance factor, defined as the ratio between the brine permeability measured before and after the polymer solution flows through the core.

Polymer cannot enter some small pores when the polymer solution flows through the rock, which results in an inaccessible pore volume [163]. Here, the inaccessible pore volume is treated by a factor of f_{ipv}, which is given as:

$$f_{ipv} = \frac{V_i}{V_p} \quad \text{.....(4.11)}$$

where V_i is the polymer inaccessible pore volume in m^3 and V_p is the pore volume in m^3.

Equations

The flow of the water phase was in accordance with Darcy's law, and its flow equation was [164]:

$$\vec{v}_w = \frac{\vec{k}k_{rw}}{\mu_{wp}R_k}\nabla\Phi_w \quad \text{.....(4.12)}$$

Where, $\vec{v}_w$: water phase velocity tensor , m/s; $\vec{k}$: absolute permeability tensor , m^2; k_{rw} : relative permeability of brine; μ_{wp} : viscosity of the water phase , Pa.s; and ∇ is the gradient operator. $\Phi_w = p_w - \rho_w g D$, Pa; p_w : pressure of the water phase , Pa; ρ_w : density of the water phase in kg/m^3, g : gravitational acceleration , m/s^2; and D : vertical height of m.

Because the heavy oil flow through the rock no longer follows Darcy's law, the oil phase flow equation had to be corrected with consideration of the Threshold pressure gradient (TPG) of heavy oil [165]:

$$\vec{v}_0 = \begin{cases} \frac{\vec{k}k_{ro}}{\mu_o}(\nabla\Phi_0 - G) & if \nabla\Phi_0 > G \\ O & if \quad \nabla\Phi_0 \le G \end{cases} \text{.....Eq.(4.13)}$$

Where, $\vec{v}_0$: oil phase velocity tensor , m/s; k_{ro} : relative permeability of the oil phase; and μ_o: viscosity of the oil phase , Pa.s.

According to the conservation of mass, the continuity equations of all components in ground standard conditions can be obtained by combing the flow equations[166]:

for water :

$$\nabla.\left(\frac{\overrightarrow{v_w}}{B_w}\right) + q_w = \frac{\partial}{\partial t}\left(\frac{\emptyset s_w}{B_w}\right) \quad \text{.....(4.14)}$$

for polymer:

$$\nabla.\left(\frac{\vec{v}_w}{B_w}\right) + q_w c_p = \frac{\partial}{\partial t}\left[\frac{\emptyset\left(1-f_{ipv}\right)s_w c_p}{B_w}\right] + \frac{\partial[\left(1-f_{ipv}\right)(1-\emptyset)\rho_r c_{ap}]}{\partial t} \quad \text{.....(4.15)}$$

for oil:

$$\nabla.\left(\frac{\overrightarrow{v_0}}{B_0}\right) + q_o = \frac{\partial}{\partial t}\left(\frac{\emptyset s_o}{B_o}\right) \quad \text{.....(4.16)}$$

Where, B_w and B_o : water and oil phase formation volume factors , m^3/m^3respectively; q_w and q_o : source/sink terms for the water and oil phases , m^3/(s.m3) respectively. The source term is negative, and the sink term is positive. ∂ : symbol used to denote partial derivatives, t : time , s; s_w and s_o : water and oil phase saturations respectively; ρ_r : rock density , kg/m^3.

Although the flow and continuity equations described the basic flow characteristics, the interrelationship between some physical quantities in the equations needed to be additionally described by the auxiliary equation and the equations of state. The auxiliary equations included[167]:

$$S_w + S_o = 1 \quad \text{.....(4.17)}$$

$$p_{cow}(S_w) = p_o - p_w \quad \text{.....(4.18)}$$

where $P_{cow}(sw)$ is the capillary pressure in the water-oil system in Pa, which is a function of the water phase saturation.

The equations of fluids, rock and rock-fluids included[168]:

$$k_{ro} = k_{ro}(s_w) \text{ .....(4.19)}$$

$$k_{rw} = k_{rw}(s_w) \text{.....(4.20)}$$

$$\rho_0 = \rho_0(p_o) \text{.....(4.21)}$$

$$\rho_w = \rho_w(p_w) \text{.....(4.22)}$$

$$\emptyset = \emptyset(p_r) \text{.....(4.23)}$$

where P_r : reservoir pressure , Pa.

4.6 Simulation of Brine Water flooding

For brine water flooding, the core samples and fluids properties have been given in Table 4.3 and 4.4 respectively. The core sample were modeled with 100 blocks as appear in Figure 4.6. Thus, a Cartesian grid was prepared in brine water system. Injection and production wells were located in first block and end block, respectively. Components were added in the component section with their respective properties.After completion of flooding. Simulation was run for a total of 60 second,. Injection rate constraint was fixed at 6 cm^3/min.

4.7 Simulation of polymer flooding

Table 4.3 and 4.4 show the core samples and flouid conditions are used for1500ppm HAPAM/brine water. The same grid pattern was used as in case of brine water flooding figure 4. 6. The grid size in X direction was fixed at

3.8 cm. Injection and production wells were located in first block and end block, respectively. Components were added in the component section with their respective properties. Simulation was run for a total of 60 second. Injection rate constraint was fixed at 6 cm^3/min.

Chapter Five

Result and Discussion

5.1 Rheological Properties

5.1.1. Concentration

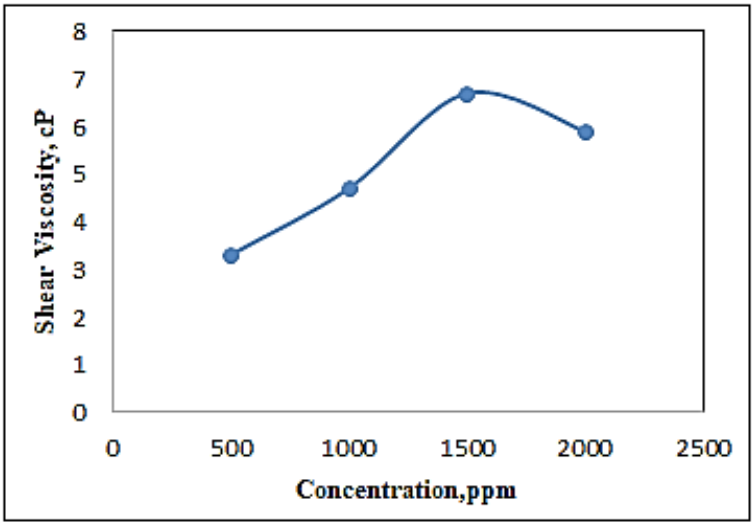

Figure 5.1:- Shear viscosity with concentration curve for HAPAM solutions with different concentration

Figure 5.1 show the relationship between the shear viscosity of brine water and concentrations of HAPAM ranging from 500 to 2000 ppm. HAPAM viscosity rises in response to increasing polymer concentrations up to around 1500 ppm, then decreases slidly up to 2000 ppm. This example exemplifies HAPAM's remarkable viscosifying abilities. A concentration of 1500 ppm is also considered to be the sweet spot for this chemical. By raising the concentration of HAPAM, the surface-active characteristics for polymer solution are strengthened, and the size of the macromolecular chains is decreased, resulting in lower viscosity [169]. In order to do this, the surface-active characteristics for polymer solution are improved.

5.1.2 Effect of Viscosity

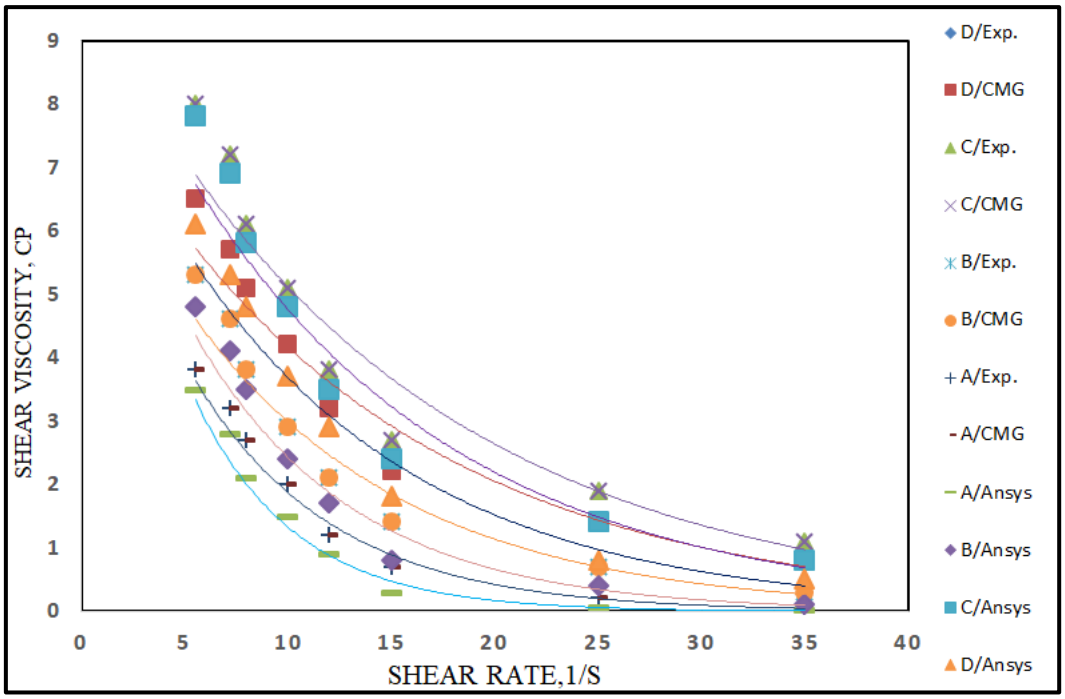

Figure 5.2:- Comparison between Experimental and Numerical Simulation of shear viscosity vs. shear rate for HAPAM/brine water at 25℃ with Concentrations A:(500), B:(1000), C:(1500), and D:(2000) ppm Respectively.

Figure 5.2 demonstrates how increasing shear rate significantly reduces the viscosity of polymeric solutions in brine. (A-D). C enhances the shear thinning feature of a brine solution as opposed to A, B, and D. The bulk of the solutions showed shear thinning at shear rates between 5 and 25 s^{-1}. We discover that the data are well-fit by the power law model based on Figure 5.2, which also depicts the shear thinning behavior of high concentration solutions (which have a steeper slope than low concentration solutions) utilizing the important fitting parameters in Table 5.1. It's necessary to make reference to this phrase. As a result, as polymer concentration increases, n, the index of flow behavior, decreases. In reality, as demonstrated in Table 5.1, the consistency index K value declines with increasing distance. This happens because working with solutions that are highly concentrated presents a number of difficulties. There

is a little drop in viscosity with increased flow rates because polymer molecules are more responsive to applied shear rates, which also reduce degree of entanglements [170].

This is accurate since shear rates also result in less entanglements. Shear viscosities are higher in polymers with increasing molecular weights or concentrations [171]. Nevertheless the viscosity of the material decreases as HAPAM content rises. At a shear rate of 7.2 s^{-1}, the shear viscosities of brine solutions A, B, C, and D were measured to be 3.20, 4.60, 7.20, and 5.70 Cp. The ideal shear rate for a reservoir has been determined by research to be 7.3 s^{-1}. More hydrodynamic volume and charge density result from an increase in Mw, which increases viscosity.

Nonetheless, the increase in molecular density may be to blame for the concentration-dependent rise in viscosity [172]. The result is an increase in the attraction and repellent forces between negatively charged polymer molecules. The conclusions of the modeling analysis and the experimental investigation are compatible with this curve. The numerical and experimental shear thing characteristics of several HAPAM solutions were studied by Ansys and CMG. Where appropriate. A potent tool for simulating non-Newtonian polymer flow in porous environments is the CMG and Ansys software.

Table 5.1:- HAPAM Solutions Characteristic by Experimental and Numerical Simulation at shear rate 7.3 s^{-1}

HAPAM Concentration (ppm)	Shear Viscosity (Cp)			Power. Law. Index .n , (dimension less)			Consistency. Index. K, ($Cp.s^{n-1}$)		
	Exp.	CMG	Ansys	Exp.	CMG	Ansys	Exp.	CMG	Ansys
500	3.2	3	2.8	0.8	0.81	0.85	4.794	3.68	2.86
1000	4.5	3.2	2.9	0.66	0.68	0.71	8.316	7.22	6.75
1500	7.2	6.9	6.4	0.5	0.55	0.59	19.31	18.11	17.5
2000	5.7	5.4	5.1	0.6	0.63	0.66	13.21	12.1	11.84

In Table 5.1, the shear viscosity, flow index (n), and consistency index (k) obtained experimentally , and numerically by Ansys and CMG for HAPAM solutions in core flooding were approximately convergence. The shear viscosity and consistency index (k) increase ,while flow index (n) decrease for 500, 1000, and 1500 ppm concentration. The change in behavior occurs at 2000 ppm concentration , where the shear viscosity and consistency index (k) decrease, while flow index (n) increase. These results confirmed with experimental behavior in viscosity and flow curve.

5.1.3 Shear Resistance

Shear resistance characteristics were evaluated after a second viscosity measurement was completed under the same conditions as the first. Because of these effects, HAPAM viscosities returned to their original levels (i.e., they retained their viscosity even at increasing shear rates and displayed pseudoplastic performance), indicating a dynamic equilibrium between intermolecular association and dissociation. The rheological characteristics of polyacrylamide were improved by the incorporation of a hydrophobic chain

into the macromolecular backbone structure of the molecule [173]. The formation of intramolecular and intermolecular hydrogen bonds, as well as the formation of hydrophobically correlated linkages between the intramolecular and intermolecular associations.

5.1.4 Shear Stress Effect

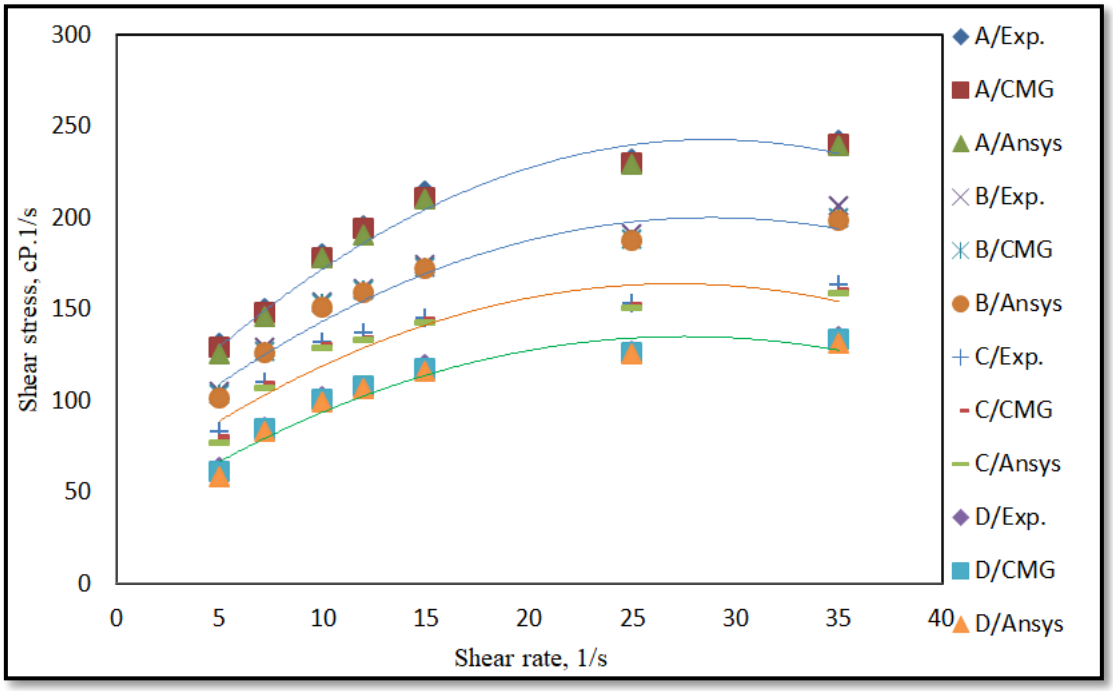

Figure 5.4:- Comparison between Experimental and Numerical Simulation of shear stress and shear rate curves for HAPAM/brine water at 500, 1000, 1500, and 2,000 ppm from (A-D) Respectively.

Figure 5.4 Chemical flooding agents frequently employ pseudoplastic behavior since it is typical of non-Newtonian fluids [174]. The deviation from a Newtonian state is what distinguishes non-Newtonian fluids. Even though they are non-Newtonian, these fluids are perfect for polymer flooding such as EOR because of their high viscosity and high strength (pseudo plastic). This is demonstrated by the fact that the C solution yielded n = 0.5. We obtained the

values of (n, k) in table 5.1 by linearly fitting the power law model for graph processing; these values are in excellent agreement with those in [175].

In Figure 5.4, appears smooth validation of shear stress behavior in HAPAM solutions, that was determined by numerical and experimental analysis in CMG and Ansys. With an increase in shear rate, the shear stress rises and stabilizes after 30 S^{-1}. This indicates that the flow changed to Newtonian and the chain was successfully untangled

5.1.5 Temperature

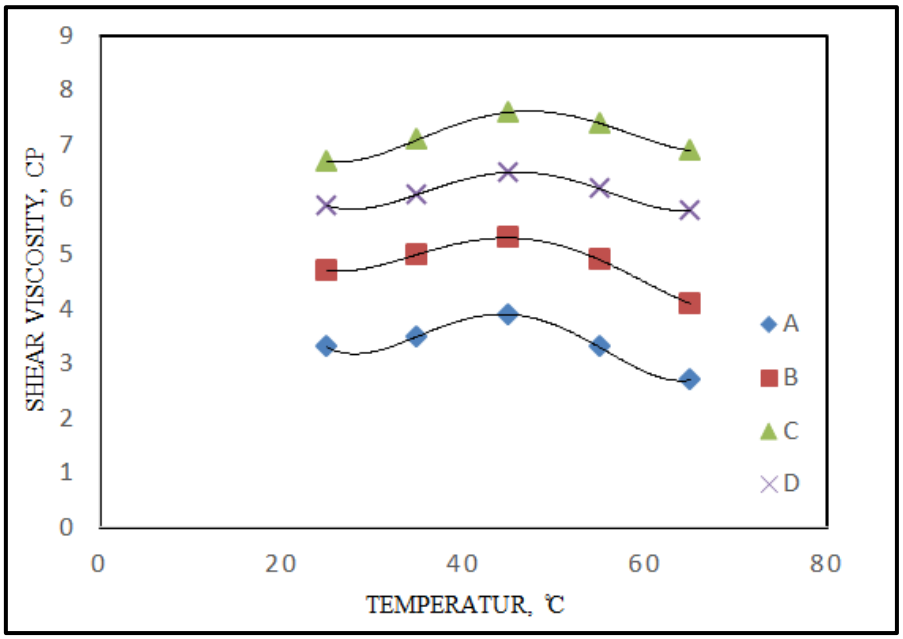

Figure 5.5:- Effect of temperature. on the viscosity of HAPAM and brine water at concentrations of 500, 1000, 1500, and 2000 ppm is demonstrated at a shear rate of 7.2 S-1for (A-D) respectively

Figure 5.5, shows that the viscosity of HAPAM polymer solutions progressively increases with temperature, peaks at around 55 degrees Celsius, and then decreases as temperature continues to rise. Increases in intermolecular hydrophobic association with rising temperature may be

attributed, at least in part, to the fact that this process is endothermic and, as a result, increases entropy [176].The increase in viscosity occurs for all HAPAM solutions in the (45-55) ºC. The stability of viscosity values was better.

5.1.6 Aging Time

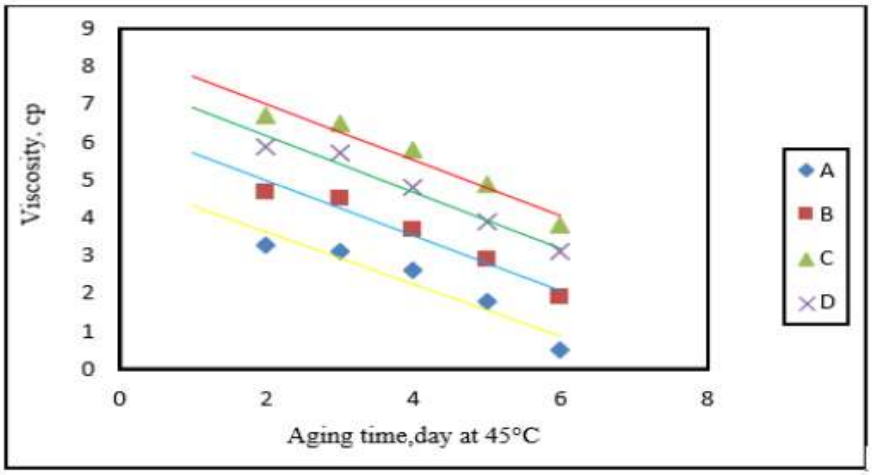

Figure 5.6:- Shear viscosity with Aging Time of HAPAM/brine water over a range of concentrations (500, 1000, 1500, and 2000 ppm) for (A-D) respectively

In Figure 5.6, we observe a linear relationship between age and the viscosity of HAPAM/brine water which illustrating how the viscosity of materials changes over time as they age. Aged HAPAM solutions become less viscous than younger ones, but to varying degrees. Age increases the viscosity of A, B, and D relative to C, which has the lowest viscosity. HAPAM solutions viscosity decreases with aging time at 45ºC. The stability in the behavior of 1500 ppm as the best depending on the rheological behavior which compatabe with the structure of HAPAM.

The results demonstrate that the addition of a hydrophobic group significantly improves the thermostability of HAPAM. The sulfonate group in HAPAM has two purposes; first, it increases the stability of the main chain, and second, it decreases the rate at which HAPAM degrades [177]. Adding a sulfonate group

to the HAPAM associative polymer would be fantastic for increasing its solubility. Hydrogen bonding is strengthened by the presence of the sulfonate group, therefore this is the case. The electrostatic repulsion between the A-D polymer chain segment is the strongest because of the strong electrolyte group given by sulfonate. When a section of a chain interacts with electrostatic repulsion, it stretches, creating new, uncoiled chains, which leads to an increase in viscosity [178].

5.2 Physical Properties

5.2.1 Interfacial Tension

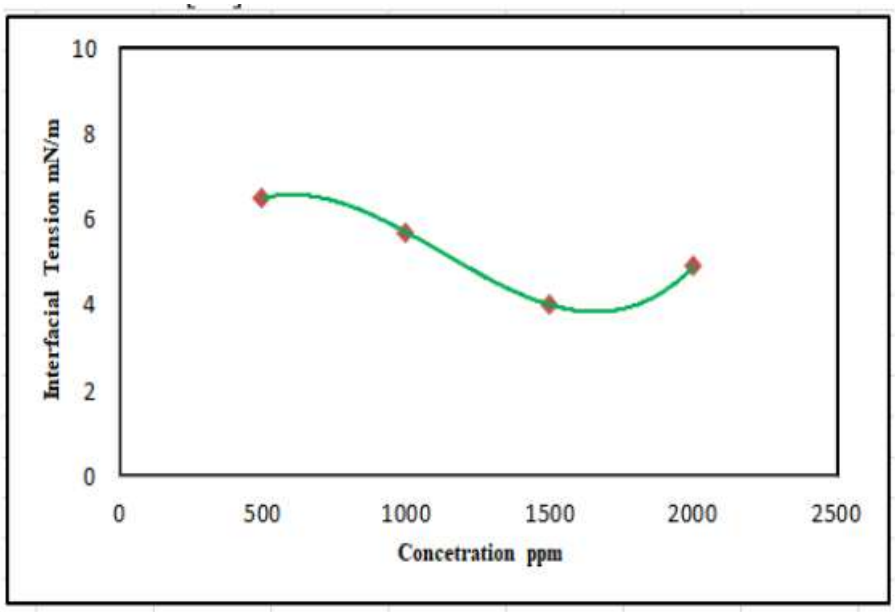

Figure 5.7:- The interfacial tension curve of a brine solution that has been combined with HAPAM at concentrations of 500, 1000, 1500, and 2,000 ppm, respectively, at a temperature of 25 degrees Celsius.

A solution of oil and brine has a substantially lower interfacial tension than water and HAPAM figure 5.7. Their amphiphilic structure, which includes both hydrophilic and hydrophobic clusters, encourages the formation of polymolecular micelles and intermolecular hydrophobic interactions, both of

which serve to lower interfacial tension. Micelles can form because the copolymer's backbone structure contains hydrophobic clusters. The molecules end up having less contact with the liquid as a result. As a result of their ability to penetrate surfaces, they help reduce tension between layers of a material [179]. In high-salt conditions, reservoir displacement efficiency can be improved by including HAPAMs into an EOR design as agents that reduce interfacial tension.

5.2.2 Surface Tension

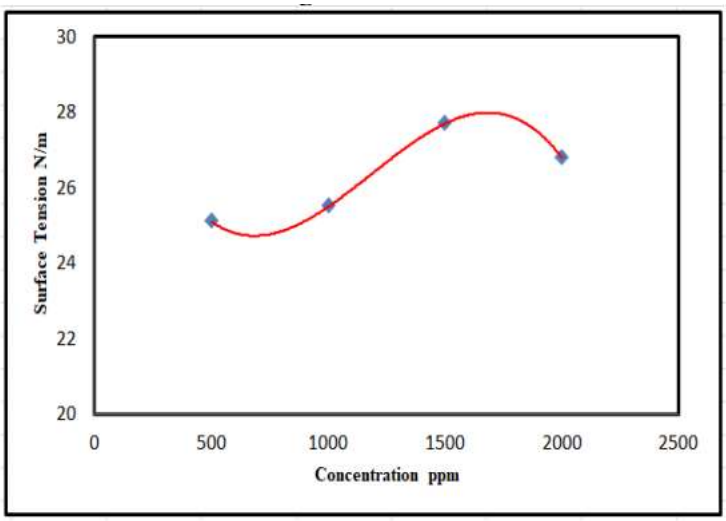

Figure 5.8:- Surface tension vs HAPAM concentration in brine water at 25 ° C for 500, 1000, 1500, and 2000 ppm

Figure 5.8, illustrates that when the concentration of HAPAM grows from 500 to 1000 to 1500 ppm, the surface tension also increases. Following that drop, at a concentration of 2000 ppm HAPAM/brine water, the decline started in comparison to other concentrations . As can be seen in Figure 5.8, the density of HAPAM and brine water increases with increasing ppm levels, from 500 to 1000 to 1500. After then, the density of the water in the 2000 ppm HAPAM brine started to drop. Increases in the ages of the interlinks between chains are indicative of high densities [180].

The surface tension of brine water is just 0.09 N/m, whereas that of water is 0.072 N/m. Because of the attraction forces present in a fluid water-air combination, this is linked to the development of surface tension. When NaCl is added, it immediately separates into its component parts, Na^+ and Cl^- ions. These ions have a much stronger attraction to water molecules due to this process, which is called hydration. In hydration, the positive H^+ ends of water molecules cluster at Na+, and the negative H- ends of water molecules cluster around Cl^-. Surface tension increases with increasing NaCl injection because of a rise in net attractive forces between hydrated charged species [181].

5.2.3 Density

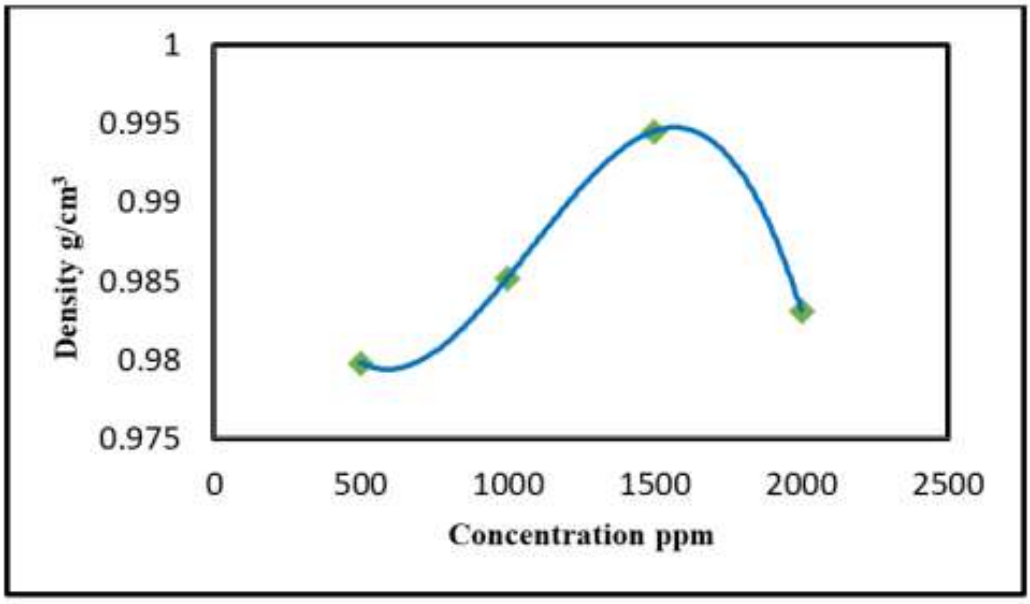

Figure 5.9:- The density of brine water / HAPAM at 25 degrees Celsius and 500, 1000, 1500, and 2000 ppm concentrations.

Density increases with concentration (500,1000and 1500)ppm HAPAM as appear in Figure 5.9. After that decrease at 2000 ppm HAPAM/brine water began decease as compared with other concentrations . High density referred by increase interlink ages between chains [182].

5.3 Petro physical Properties

5.3.1 Structure Properties of Cores

5.3.1.1 Porosity Measurement

Table 5.2 :- Core Sample Porosity

Core Samples	Area	Dry Weight	Saturated Weight	Pore Volume (Pv)	Bulk Volume (Vb) ,cm^3	Porosity %
Core1	11.3	371.8	395.1	0.09	59	0.15
Core 2	11.3	381.4	389.5	0.08	59	0.13
Core 3	11.3	375.11	385.11	0.1	59	0.16
Core 4	11.3	378.12	390.11	0.12	59	0.20
Core 5	11.3	381.3	394.1	0.13	59	0.22

5.3.1.2Absolute Permeability

Table 5.3:- Core Samples Permeability

Core Samples	Gas Permeability (Ka) mD	Liquid Permeability (Kl) mD	Oil Permeability (Ko) mD
Core 1	51	30	120
Core 2	41	9	11
Core 3	48	33	15
Core 4	55	44	18
Core 5	61	53	23

Table 5.4:- Core Sample Saturation

Core Samples	Water Volume (Vw) ,ml	Oil Volume (Vo) ,ml	Irreducible Water Saturation (Swi), %	Initial Oil Saturation (Soi), %	Residual Oil Saturation (Sor) ,%	
					Brine Water	HAPAM Solution
Core 1	3.2	12.8	0.15	0.8	37.5	6
Core 2	2.08	11	0.16	0.84	38	5
Core 3	3	17	0.15	0.85	34	4.6
Core 4	3.22	20	0.14	0.86	33	3
Core 5	2.86	19.3	0.13	0.87	37	2

5.4 Relative Permeability

When flooding with brine water is injected, this happens. Permeability measurements indicate that both brine water (krw) and oil (kro) have relative permeability lower than 0.5. Since a mobility ratio (M) of larger than one indicates the existence of viscous fingering, it is assumed that brine water will exhibit this property. This event occurs because of this cause. Precedent evidence has established that this deposit contains oil. The amount of water that may flood a given area is thus determined by capillary forces. When oil sticks to a rock's surface, water is pushed in the opposite direction through the porous rock. The oil in the reservoir is also very thick. This results in water smearing its way through the oil before dripping from the center pores [183].

Figure5.10 demonstrates the degree of agreement between the results of experimental studies and those of modeling studies. In addition to that, the flow rate in each of these situations was 6 cm^3/min. If the water relative

permeability (krw) is less than half that of the oil relative permeability (kro), then the mobility ratio is less than 1 and the polymer solution wets the surface of the porouss media. Furthermore, outside of the. The solution of HAPAM in saline water is shown at 1500 ppm in Figure 5.10. Chemical tertiary recovery in a wet reservoir is made possible by this solution [184]. The actual core's circular cross section was transformed into a square cross section with the same cross sectional area in order to construct a numerical simulation model of core flooding. A visual representation of this shift is shown in Figure 4.4. The numerical simulation model called for a minimum bottom entire pressure of 120 psi due to the fact that core flooding would expose a production end to air pressure.

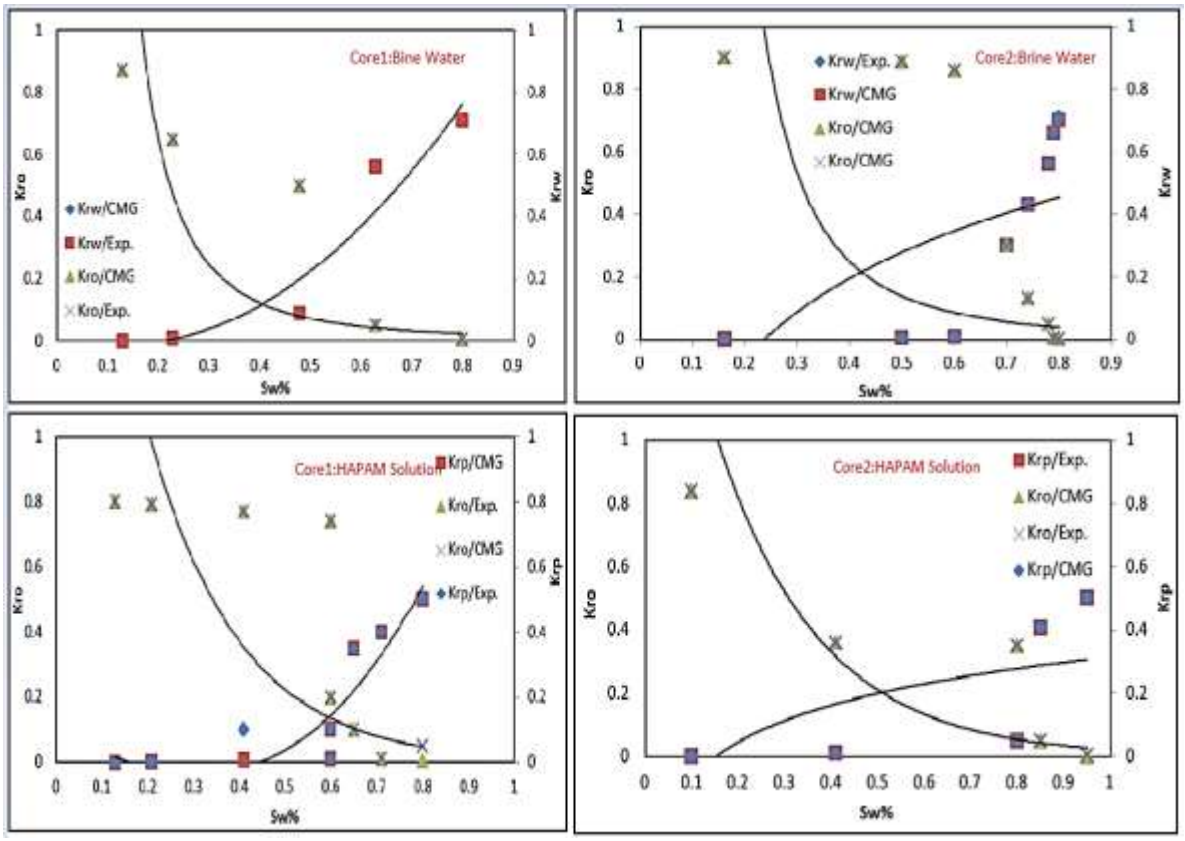

(a)

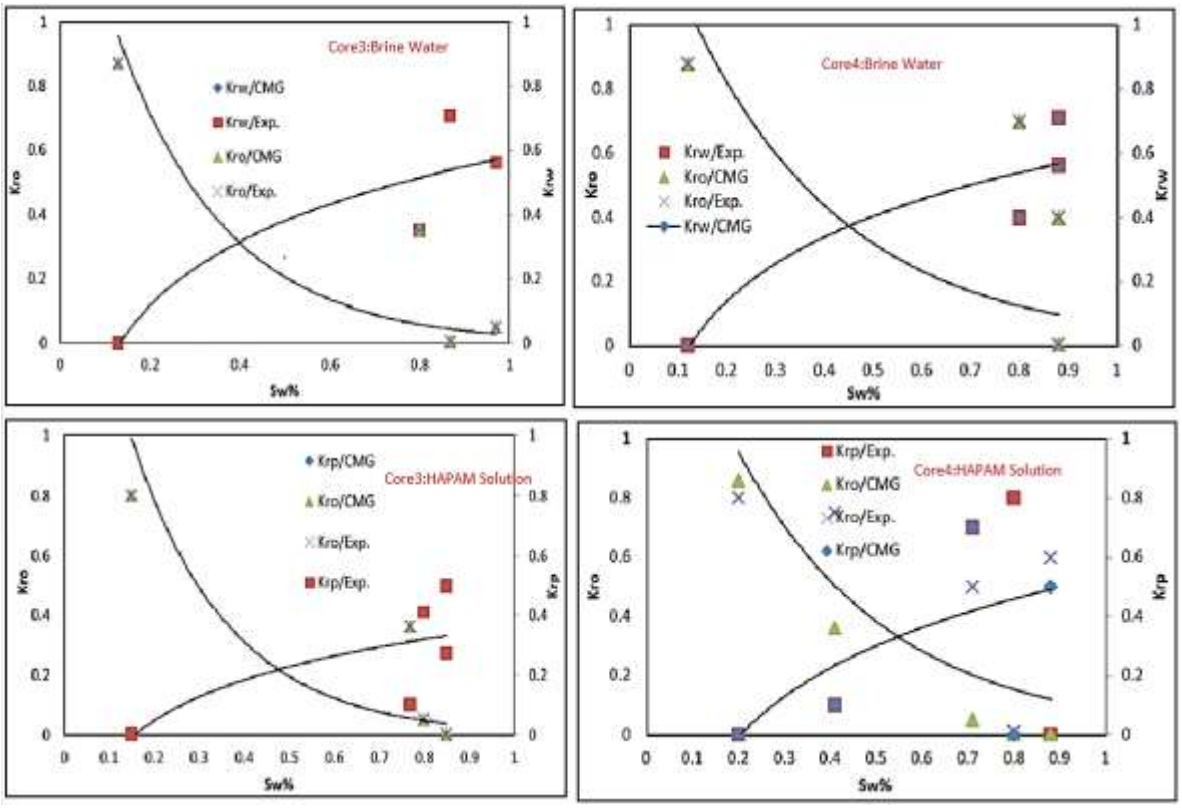

(b)

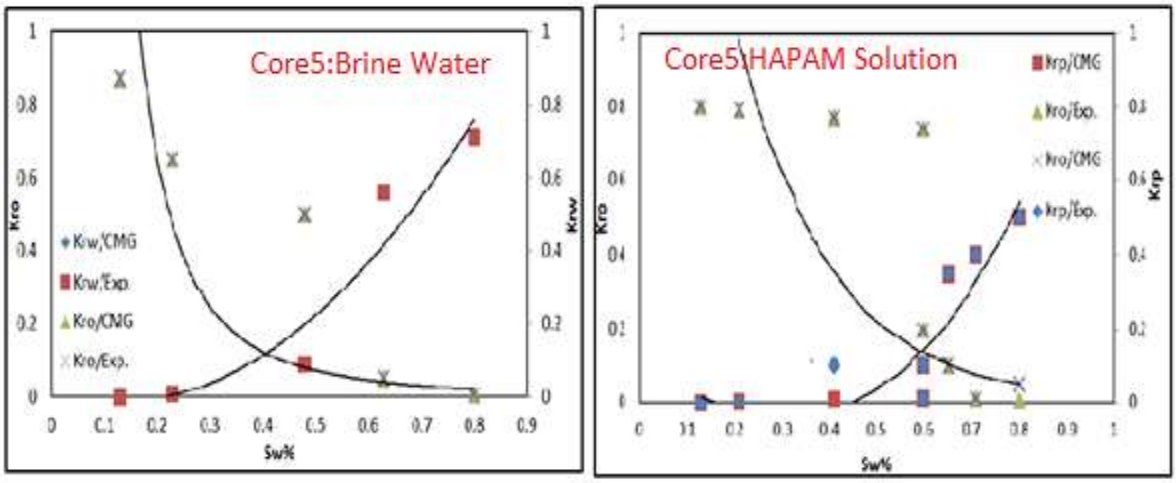

(c)

Figure 5.10 (a,b,and c):-Comparison between Experimental and Numerical Simulation of relative permeability against water saturation for brine water and 1500 ppm HAPAM/brine water in Core1,2,3,4, and 5 respectively.

5. 5 Capillary Number

Capillary number values are less than 10^{-6} for all polymeric solutions of HAPAM. On the other hand brine water is greater and its value ranges between (2.5-4) $x10^{-3}$. Which indicates a high velocity within the porous medium and its inability to pass through the narrow pores of the Core 1,2,3,4,and 5. The percentage of oil extraction is low compared to the polymeric solutions.

For low capillary numbers ($<10^{-5}$), capillary forces dominate the flow in porous media, whereas for high capillary numbers, capillary forces are negligible compared to viscous forces. The flow through the pores in the oil tank has capillary number values in the range less than 10^{-6}.The capillary number plays a role in the dynamics of the poetic flow; In particular, it controls the dynamic contact angle of a flowing droplet at an interface [185]

Figure 5.11, shows how the velocity increase affects the capillary number of Core 1,2,3,4, and 5. Where the experimental results showed that all the values of the capillary number are less than 10^{-6}, which indicates the ability of the polymeric solution of 1500ppm HAPAM/brine was to enter the smallest details of Core1,2,3,4,and 5 . Capillary number decreases and has a high susceptibility to wetting the rock, which improves the ability to extract oil.

On the other hand, we note that all the values of the capillary number of brine are greater than 10^{-6}, which indicates the ability to extract oil in a lesser way. When comparing the behavior of the capillary number with the increase in velocity in salt water, we notice that the curve is fast at the beginning, then it is regular at an average speed of $6x10^{-2}$ cm/s, and then the increase becomes almost uniform.

As for 1500ppmHAPAM/Brine water, the behavior of the capillary number curve with increasing veloity is very regular and clear, as it begins with a slow

and regular increase and then stabilizes at a velocity rate of $5.50x10^{-2}$ cm/s, Then the curve becomes very stable and regular. The capillary number increases with the increase in velocity. This phenomenon is useful in the process of extracting the remaining oil from the porous media, as the low speed allows it to pass through the most accurate pores of the core to extract the largest possible amount of oil.

Core1,2,3,4, and 5 was analyses in the lab, CMG and Ansys programs using brine water and 1500ppm HAPAM/brine water solution, and it was determined that residual oil could be retrieved if the viscous forces acting on the trapped residual oil blobs were greater than the capillary retention forces compared to the saline water. It was discovered that the capillary factor is dependent on the recovery factor [186]. In comparison to brine water, capillary number is 8cP of 1500 ppm HAPAM gives larger capillary number. This gives excellent correlations of mobilization oil with widely varying viscosities. In addition to this, a high rate of oil recovery and a reduced residual oil saturation.Through the results, the comparison between the experimental and simulation results using CMG and Ansys programs is very close. This indicates the need to use numerical simulation programs to shorten time, effort and cost.

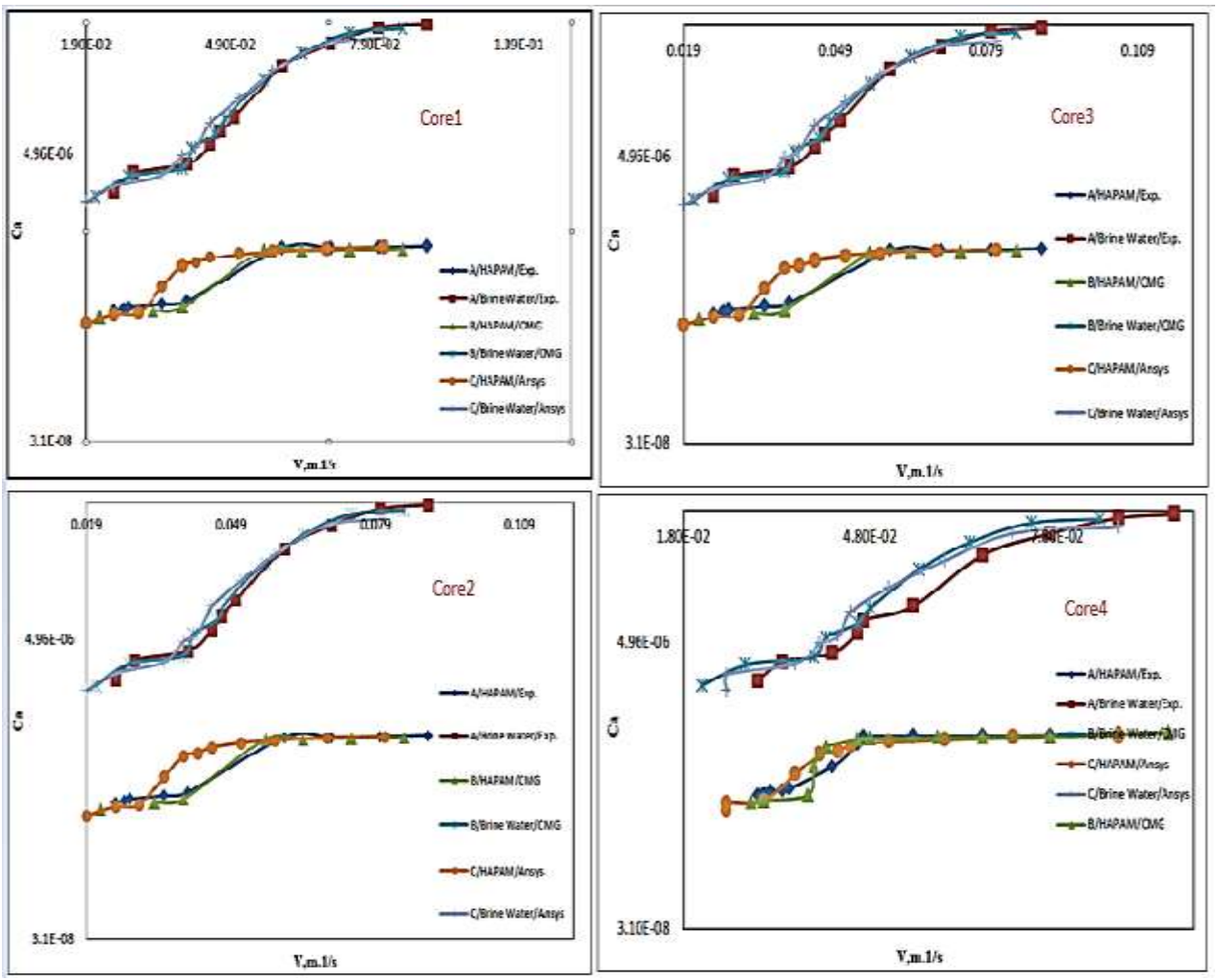

(a)

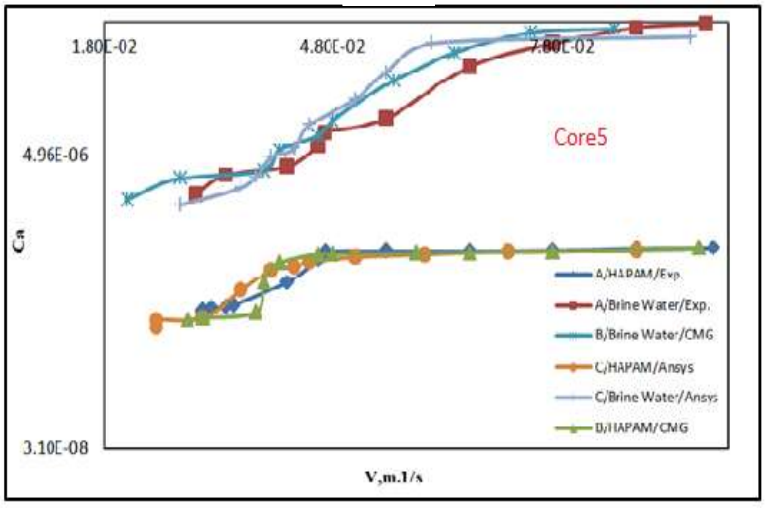

(b)

Figure 5.11(a,and b):- Comparison between Experimental and Numerical Simulation of Capillary number with Darcy Velocity for Core1,2,3,4,and 5.

5.6 Apparent Viscosity and Shear Viscosity with Shear Rate

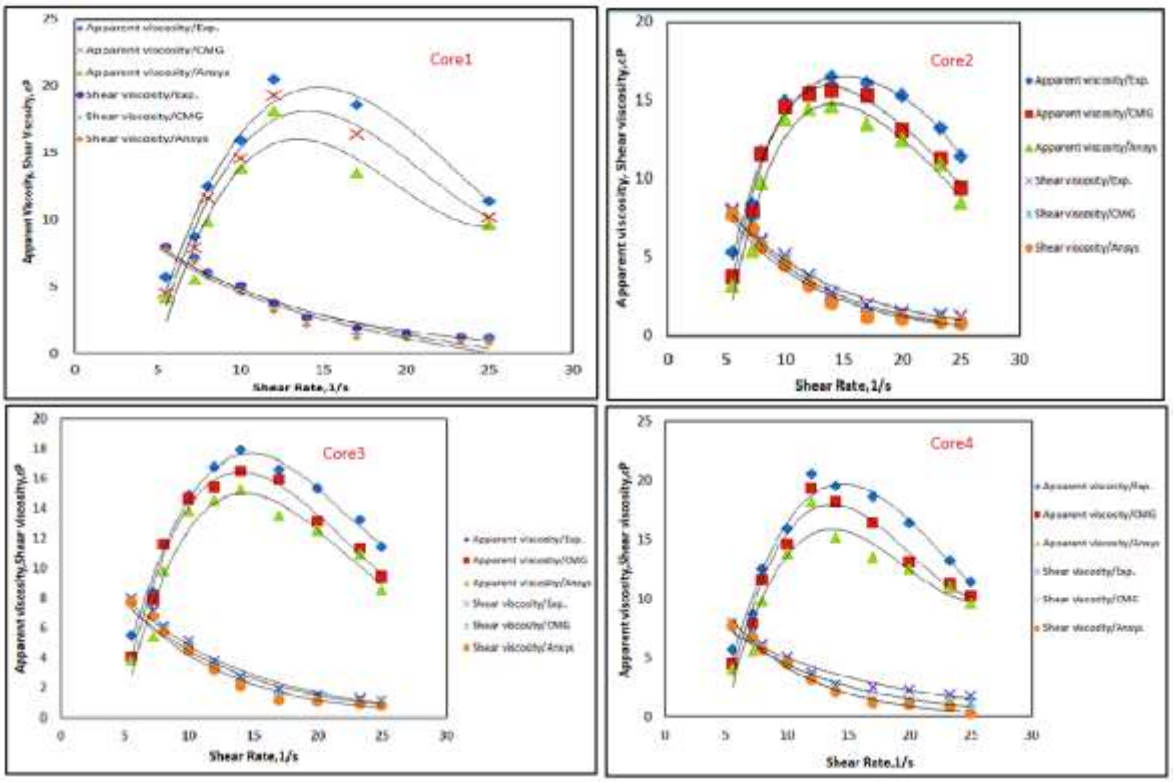

(a)

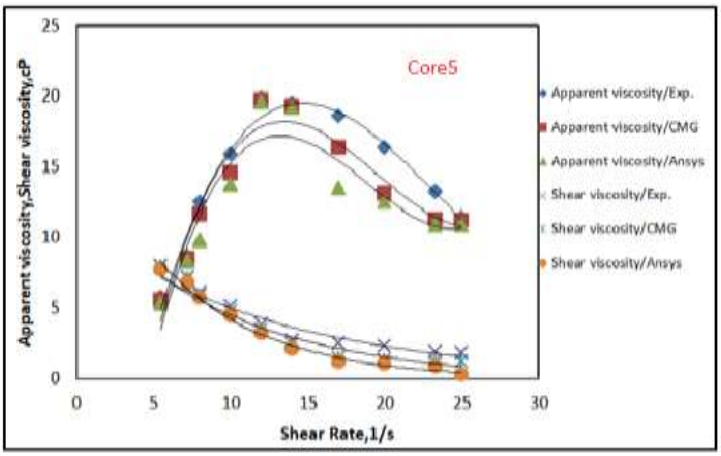

(b)

Figure 5.12(a,and b):- Comparison between Experimental and Numerical Simulation of Apparent and Shear Viscosity with shear Rate for Core1,2,3,4,and 5.

The relationship between Ansys, CMG, and experimental research on the flow behavior of 1500 ppm HAPAM/brine water is shown in Figure 5.12, which also compares the apparent viscosity measured by the core flooding test to the shear viscosity inside the cone-plate viscometere device, which represents the bulk case. The findings demonstrated the behavior of 1500 ppm HAPAM/brine water, which is typical for this solution.Non-Newtonian shear thinning behavior at high shear rates is usually linear and deteriorates over time.

On the other hand, the behavior of this solution's apparent viscosity starts to rise above 7.3 s^{-1} shear rate and continues to do so until (12-16) s^{-1} shear rate.

Figure 5.12, show Ansys and CMG's experimental and simulation programs analyze the findings of the flow behavior in relation to the rheological characteristics of the porous media. On the other hand, he is able to examine the polymeric solution's flow behavior, illustrate the events that take place in the porous medium, and show how they affect procedures for increasing oil production. We were able to get good agreement between experimental and numerical simulation methodologies for EOR through this[187].

Figure 5.12, show the efficiency of experimental and simulation program related to the Ansys and CMG program in analyzing the results of the flow behavior in relation to the rheological properties within the porous medium. On the other hand, he is able to analyze the flow behavior of the polymeric solution and demonstrate the phenomena that occur within the porous medium and demonstrate their impact on the processes of improving oil production. Through this we obtained good agreement between experimental and numerical simulation methods for EOR [188].

5.7 Apparent viscosity with Darcy velocity and shear rate

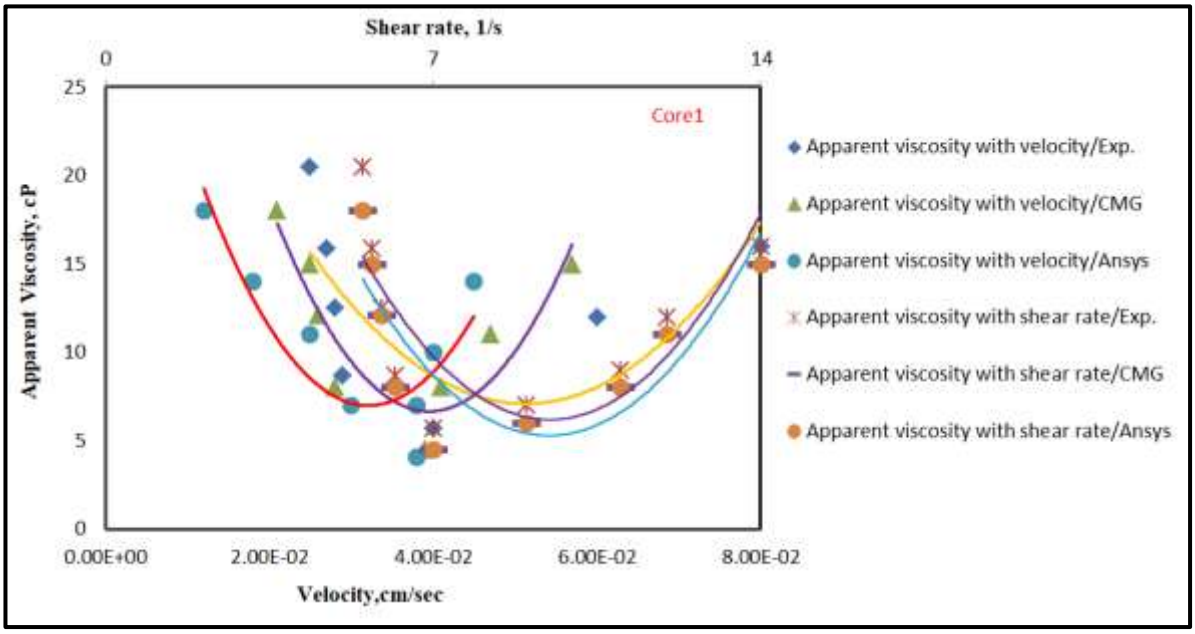

(a)

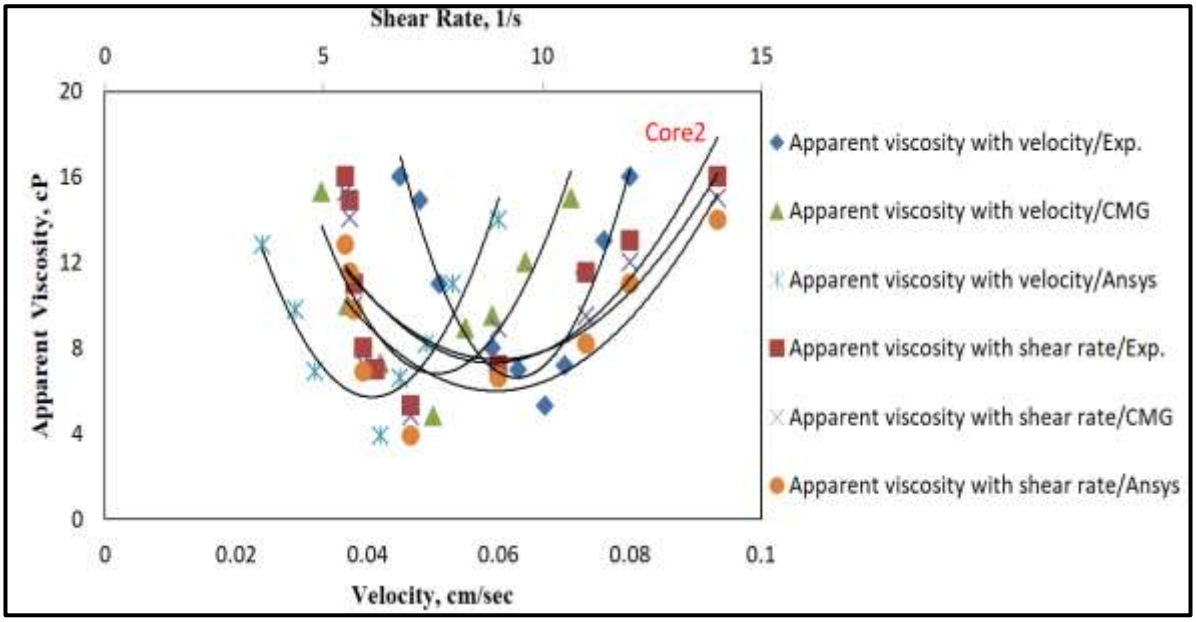

(b)

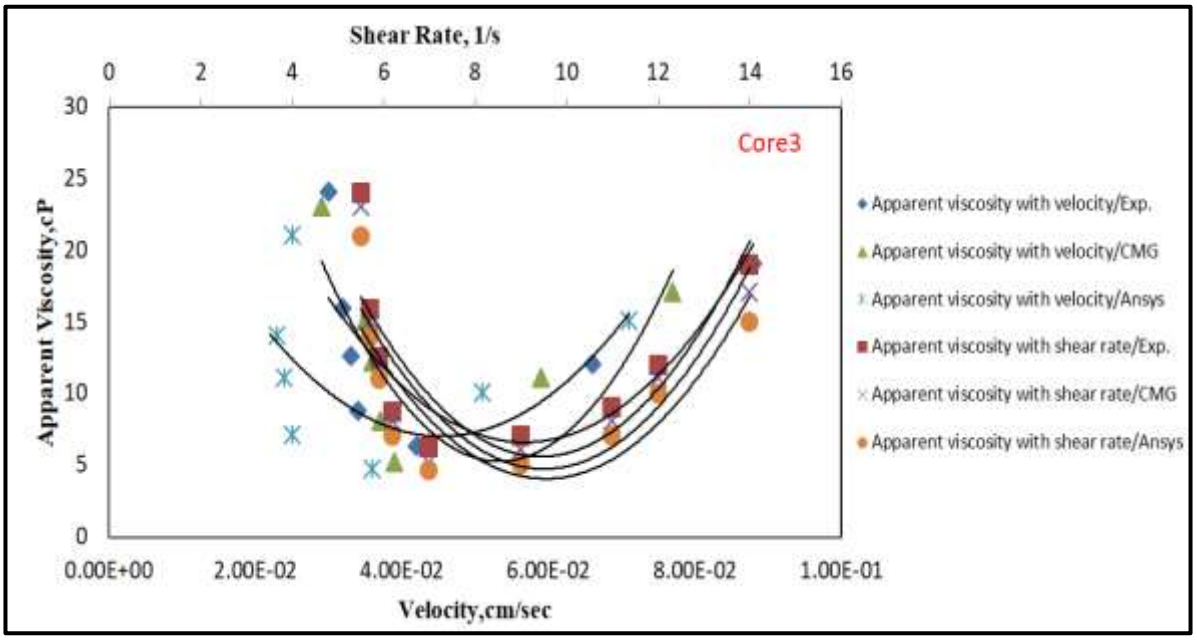
Shear Rate, 1/s
0
2
4
6
8
10
12
14
16
Core3
Apparent Viscosity,cP
30
25
20
15
10
5
0
0.00E+00
2.00E-02
4.00E-02
6.00E-02
8.00E-02
1.00E-01
Velocity,cm/sec
Apparent viscosity with velocity/Exp.
Apparent viscosity with velocity/CMG
Apparent viscosity with velocity/Ansys
Apparent viscosity with shear rate/Exp.
Apparent viscosity with shear rate/CMG
Apparent viscosity with shear rate/Ansys

(c)

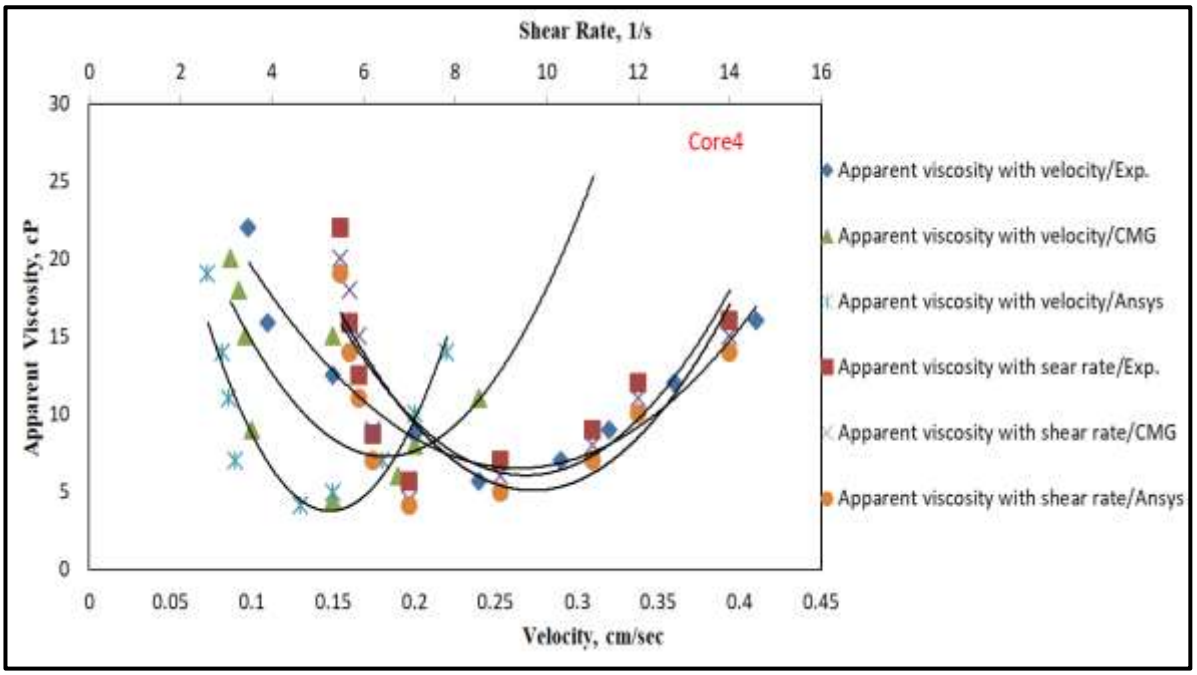
Shear Rate, 1/s
0
2
4
6
8
10
12
14
16
Core4
Apparent Viscosity, cP
30
25
20
15
10
5
0
0
0.05
0.1
0.15
0.2
0.25
0.3
0.35
0.4
0.45
Velocity, cm/sec
Apparent viscosity with velocity/Exp.
Apparent viscosity with velocity/CMG
Apparent viscosity with velocity/Ansys
Apparent viscosity with sear rate/Exp.
Apparent viscosity with shear rate/CMG
Apparent viscosity with shear rate/Ansys

(d)

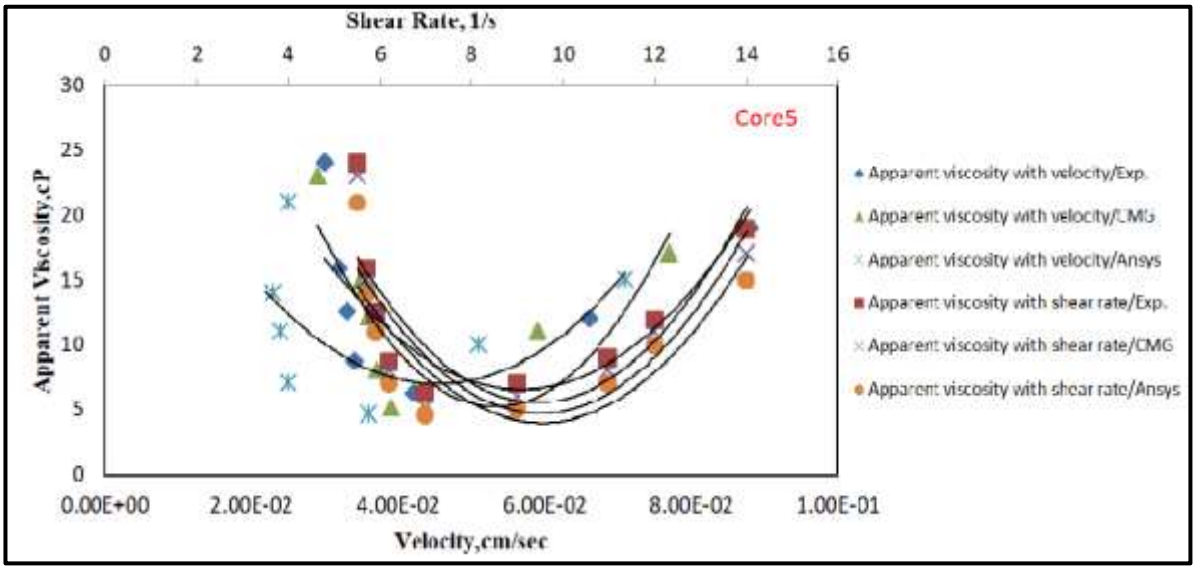

(e)

Figure 5. 13 (a-d) :- Comparison between Experimental and Numerical Simulation of Apparent viscosity with Darcy velocity and Shear rate due to flow 1500 ppm HAPAM/brine water in Core1,2,3,4,and 5 respectively.

Figure 5.13 show quantitative numerical simulations using (FEM) and (FDM) by Ansys and CMG, respectively. It has been linked with experimental results in this curve.The results showed the effect of shear thickening apparent viscosity with Darcy velocity. in both experimental and computational investigations, to address polymer apparent viscosity. There were three created curves. The obtained curves display a mixed shear thinning and thickening effect that decreases as Darcy velocity rises. when the apparent viscosity reaches 7.3 s^{-1} shear rate and begins to exhibit non-Newtonian behavior. The outcomes of simulations with rate and/or concentration steps will demonstrate how sensitive a 1500 ppm HAPAM solution is when it interacts with various intricate rheological segments based on anticipated Darcy velocity values at each shear rate.The results showed the extent of compatibility and convergence with practical and numerical results, which saves time and effort and yields great economic benefits [189].

5.8 Differential Pressure

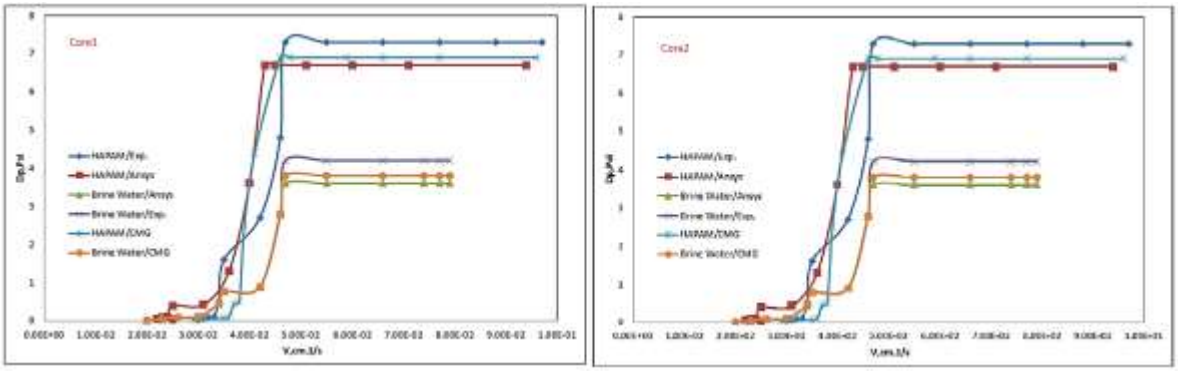

(a)

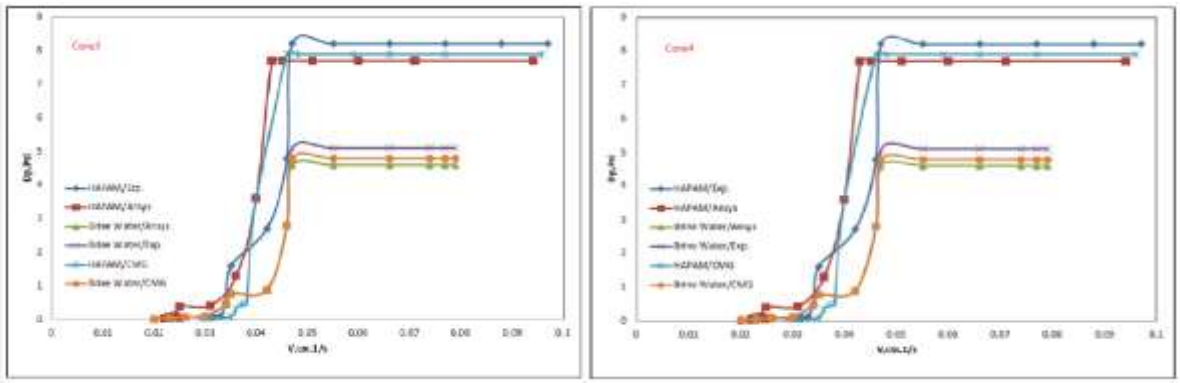

(b)

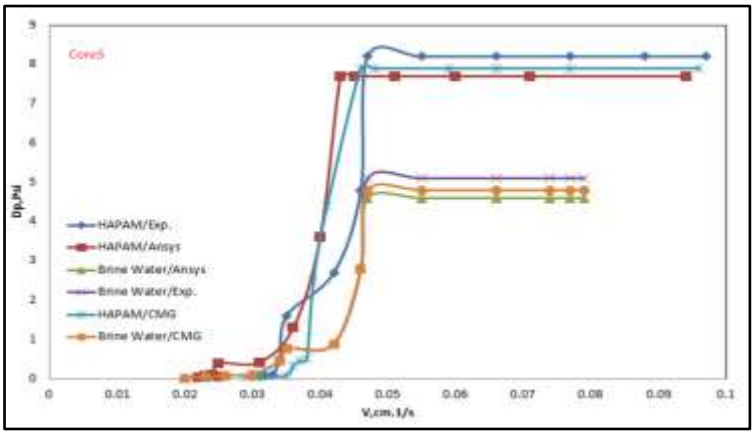

(c)

Figure 5.14(a-c):- Comparison between Experimental and Numerical Simulation of Differential Pressure with Darcy Velocity in Core1,2,3,4,and 5.

Figure 5.14, the experimental results were linked by the core flooding test with numerical simulation in (FEM) and (FDM) with Ansys and CMG, respectively. The process of convergence between the practical results and the numerical simulation proves the importance of using the latter as shown in the figure. In addition to saving time, effort and cost.

Through figure 5.14, achieve the behavior of the brine water curve begins with a rapid increase of the pressure difference at low velocity, then it increases regularly and then stabilizes. As for the brine water curve with the addition of 1500 ppm HAPAM, the pressure difference is stable and does not have any increase with the increase in velocity, then it tends to increase quickly and regularly, then it stabilizes with the increase in velocity. This is due to the elongation of the polymeric chains inside the porous medium with increasing pressure [190].

5.9 Oil Recovery

The oil production by each core samples were calculated, and the results are shown in Figure 5.15 Not surprisingly, the percentages of the oil production are the highest in core 5 with 1500 ppm HAPAM as compared with other cores . The strong performance of the HAPAM flooding in the oil production mainly comes from the enhanced sweep efficiency. On the one hand, the HAPAM solution with a high viscosity can reach the residual oil blocks that are not effectively affected by brine water flooding. The oil blocks are locally restricted at the concave blind end of the throat and the edge area of the micro porous network structure. On the other hand, the low IFT of the HAPAM solution favors

of the trapped crude oil after brine water flooding to form oil droplets; then the oil droplet is further separated to smaller oil droplets, facilitating the mobility of the crude oil to pass through micropores and narrow throats [191]. The performance in oil displacement is greatly and eventually enhanced by the synergistic effects between the HAPAM solution with sandstone and carbonate core samples. Then ultralow IFT by 1500 ppm HAPAM/brine water, which is required to obtain a much higher capillary number for an effective oil displacement. The ultralow IFT can be obtained by using polymer solution [192]. The effect of the overall flooding process on the core samples before and after flooding by brine water and HAPAM solution was evaluated and reported in Table 5.5.

One of the major drawbacks of most mobility polymers is the tendency for the polymer to be retained on rock surfaces/pores, thereby reducing the area open to flow and consequentially permeability impairment which results in additional pressure drop. The amount of retention has a direct connection to the level of permeability impairment, such that high permeability impairment after flooding most times implies high polymer retention [393]. The observed low retention with the use of HAPAM can be attributed to the presence of the negatively charged carboxylic group in the polymer structure which leads to repulsion on the surface of the negatively charged sandstone or carbonate cores [193].

In Core1, displacement experiments were conducted at 25 °C. visually investigate the mechanisms of brine water and HAPAM solution under reservoir conditions. Oil displacement by brine water and chemical solution was continuously injected into the core 1 with Sw = 0.15% after oil saturation. The brine water and polymer flooding systems have a concentration of 20% Nacl and 1500 ppm respectively. At these

concentrations, shear viscosity values of brine water and polymer solution is 2.3 and 8 cP. respectively. A 1500 ppm HAPAM concentration was used to focus on the viscosity effect of injected solutions during an oil displacement.

a large amount of residual oil can be observed in the pores and throats of core 1 after oil saturation. Generally, the flow of brine water or polymer solution at the pore-scale level is affected by the flow velocity, microscopic heterogeneity, wettability, and IFT between two solution . During the flooding, some oil blocks were bypassed by the injected fluid due to the size of the micropore and a difference of flow velocity at various directions. The mobility of isolated oil blocks was restricted by the capillary pressure at the oil−water interface; the oil was trapped and stuck in the core 1 to become residual oil. 63% and 94% oil recovery with brine water and HAPAM solution. with a higher solution viscosity by HAPAM , this can improve the volumetric sweep efficiency of the displacement [194].

In Core2, less residual oil trapped is 5 and 38 respectively by 1500 ppm HAPAM solution and brine water. Also, it can be seen that the residual oil zones are more less, this resulting from the injected polymer solution [93].the 1500 ppm HAPAM/ brine water have the largest viscosity 8cP. at 25°C. Suggesting that a higher volumetric sweep efficiency is obtained used as a flooding system for oil displacement [195].Indeed, oil displacement process by an HAPAM flooding after an injection proceeded homogeneously [196]. Most of the oil saturated in the Core2 was affected by the flooding solution, the phenomenon of finger structures that appear in brine solutions, with an increase in the addition of polymeric concentrations leads to a clear decrease of this phenomena, and this is what was noticed when adding 1500 ppm HAPAM, through the results of Ansys simulations with quantitative in the form of, the oil displacement ratio was improved to from 63% to 95%

compared to brine water without polymer adding. According to the result obtained from a rheological investigation, 2.3 and 8 cP. shear viscosity of brine water and HAPAM solution respectively. An injection of this viscous solution leads to an enlarged oil area that was swept by the HAPAM flooding during the displacement process.

Table 5.5 :- Oil Recovery

Core Samples	Incremental Oil Production, ml				Oil Recovery, %				Additional Oil Recovery,%	
	Brine Water		HAPAM Solution		Brine Water		HAPAM Solution		HAPAM Solution	
	Exp.	CMG	Exp.	CMG	Exp.	CMG	Exp.	CMG	Exp.	CMG
Core 1	50	49.5	75	74.6	63	62.83	94	93.68	31	30.85
Core 2	52	51.7	80	79.8	62	61.72	95	94.75	33	33.03
Core 3	56	55.6	82	81.6	66	65.65	96.4	96.12	30.4	30.47
Core 4	58	57.6	83	82.5	67	66.83	97	96.71	30	29.88
Core 5	60	59.5	85	84.6	69	68.85	98	97.82	29	28.97

In Core3, 96.4% oil recovery obtained when an HAPAM flooding system was injected into the porous media , the HAPAM targeted the crude oil by inserting its hydrophobic tail into the oil block to decrease the IFT between oil and HAPAM solution. Thus, a bulky oil block was gradually “melted”, and it collapsed to form dispersive oil-in-water (O/W) and movable oil droplets [197], which stabilized the dispersion system via the electrostatic repulsion

between the emulsions or the droplets. Subsequently, the spherical oil droplets with low IFT can be easily deformed and stretched into long and narrow strips to pass through smaller pores and throats, further facilitating the mobility of the crude oil.

In Core4, When the oil blocks were displaced by a flooding solution containing a HAPAM, very thin oil layers attached onto the surface of the pores, and throats were usually observed as residual oil. The oil membranes formed by HAPAM flooding solutions which occur. This phenomenon was barely observed during polymer flooding when the oil was displaced in the form of piston-like flow by the injected slug.

In a HAPAM based displacement, alteration of an oil−water interface resulted in an inhomogeneous distribution of flow velocity when a fluid containing polymer solution flowed through the pore channels. The flow gained the largest velocity at the center of a pore channel and the lowest velocity along channel edge due to wet oil micro model surface. Then the oily layer was stripped off Layer by layer, as it becomes thinner and thinner, by flow Inject the HAPAM solution . Because of a high viscosity resulting from HAPAM solution, the microflowing behavior of the this solution inside the core 4 channel was hindered, leading to an extension of the communication time between HAPAM solution and residual oil; so jobs polymer solution in reducing IFT and changing the properties of oil and water then the interface is meticulously developed. Displacement fluid with a decrease in IFT the absorption of the oil film on is weakened pore surface the oil film is gradually expelled, stripped and, subsequently, carried away by the displacement fluid [198].The amount of oil release is 67 % and 98% in core 4 by brine water and 1500 ppm HPAM/brine water.

In Core5, the brine water has the characteristics of heterogeneous and discontinuous, and the mechanism of oil displacement is concluded as the brine water droplets are temporarily stacked and blocked at the pore throat to expand the swept volume, retention at the wall surface of the large pore; reducing the flow area and increasing the flow resistance, gather into a large oil film; forming a local vesicle-shaped aggregation of brine water and increasing the flow resistance[199]. The EOR mechanism of emulsion mainly depends on whether the injected solution can increase the flow resistance and expand the swept volume .Meanwhile, the lower IFT of the solution can increase the washing efficiency of the swept area. Therefore, 98% oil recovery by 1500 ppm HAPAM. On the other hand , 69% oil produced from core 5 by brine water.

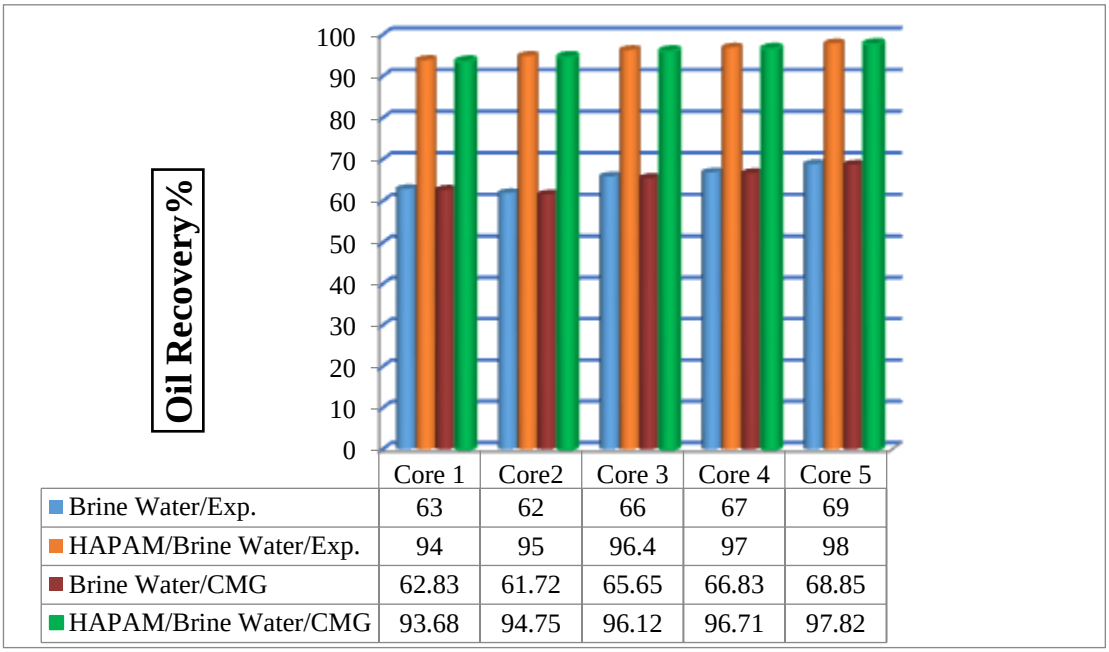

	Core 1	Core2	Core 3	Core 4	Core 5
Brine Water/Exp.	63	62	66	67	69
HAPAM/Brine Water/Exp.	94	95	96.4	97	98
Brine Water/CMG	62.83	61.72	65.65	66.83	68.85
HAPAM/Brine Water/CMG	93.68	94.75	96.12	96.71	97.82

Figure 5.15 :- Oil Recovery Curve by brine water and HAPAM/brine water in Core1,2,3,4, and 5.

Qualitative Numerical Result by Ansys

5.10 Oil Volume Fraction Contour

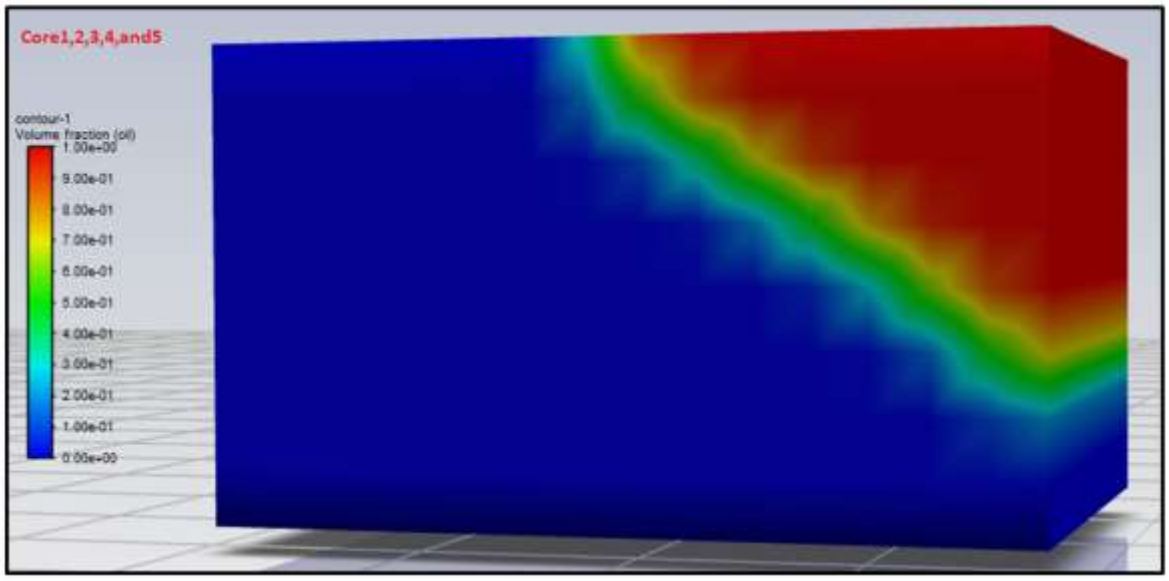

(a)

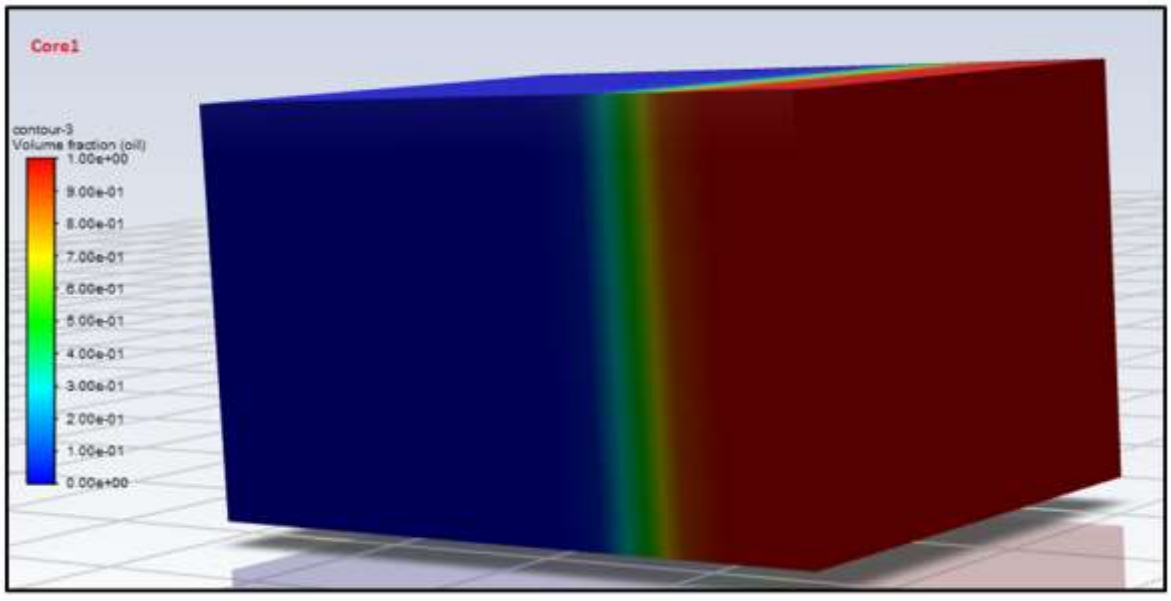

(b)

The simulation oil that was discharged from porous medium was viscous to varying degrees fluid that has been injected. For the modeling of the core1,2,3,4,and 5, acting as a porous medium, the viscosity of the aqueous

solution was an important factor. Along with the interfacial tension, the influence on the wettability of the core surface was also examined .Oil has a viscosity of 5.6 cP.s, making it more viscous than brine water, which has a viscosity of 2.3 cP and an interfacial tension of 4.1 mN/m. As a result, oil has a high mobility ratio, can easily move through porous media, does not form slug solutions, has a high permeability when oil is being pushed forward, and its ability to wet the surface was reduced.

Figure 5.16 a, depicts a viscous finger that is transparent and has an unstable contact zone between the injected brine water and the local oil. This finding, which is analogous to [200], depicts a clear interface region between two fluids that has a number of pointed fingers as a direct consequence of the low viscosity of the liquid. The parabolic velocity profile of the brine water sped up the process of reaching the break through point, which resulted in a lower amount of oil being retrieved, a lower sweep efficiency, and a greater amount of oil remaining in the core 1,2,3,4, and5.

When water is used to flood viscous oil reservoirs, a particularly unstable displacement front is formed as a result injected water. This results in viscous fingering and channelling as well as poor sweep efficiency. It doesn't take long for preferential flow routes to form themselves between the injector and the producer. These channels transport the majority of the water, but they don't recover a substantial quantity of oil.

The mobility ratio decreased as a result of a concentration of 1500 ppm HAPAM in the brine water. This resulted in the discharge of high oil volumes, an increase in slug for solutions, and a decrease in permeability while pushing oil forward. Figure 5.16 b,c,d, and e for Core 1,2,3,4, and 5. Increase in concentration of HAPAM that add to brine water results in viscous finger not found along with a stable contact zone between the injected fluid and the local oil. Similar results were seen in [320], where steady oil displacement was

achieved with a less viscous finger when the injected fluid had a higher viscosity than oil.A decrease in n values, as shown in Tables 5.1, leads to a high plug of velocity profile region, and higher concentrations of HAPAM to brine water are added, which slower the amount of time it takes to reach the break through point and increases oil recovery . This agree with [201].

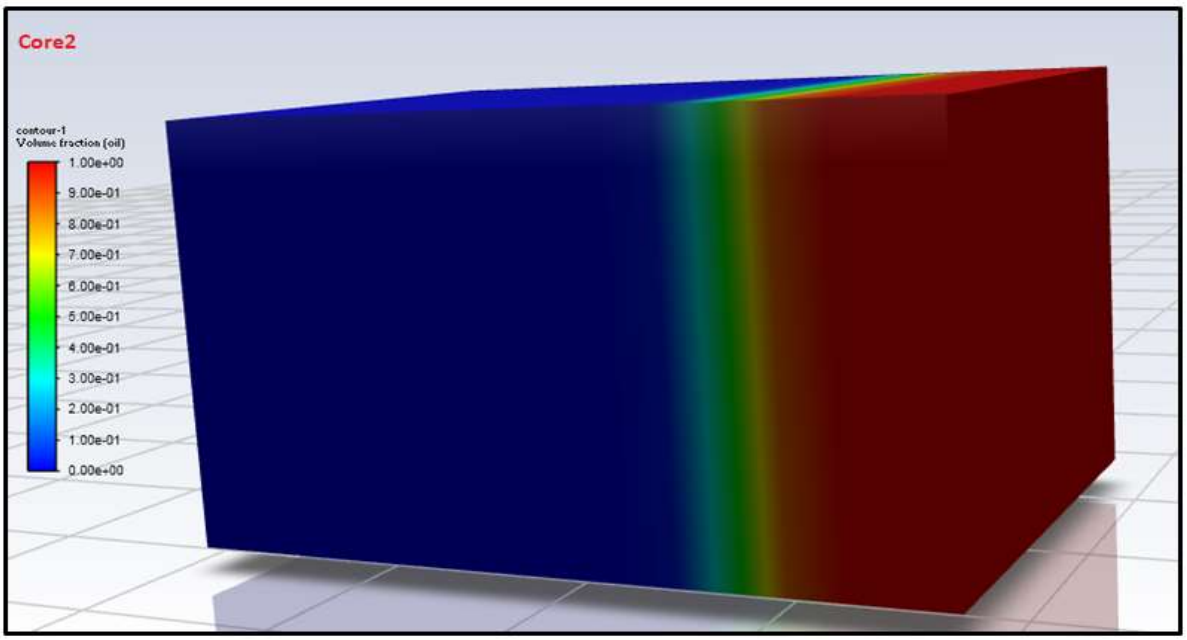

(c)

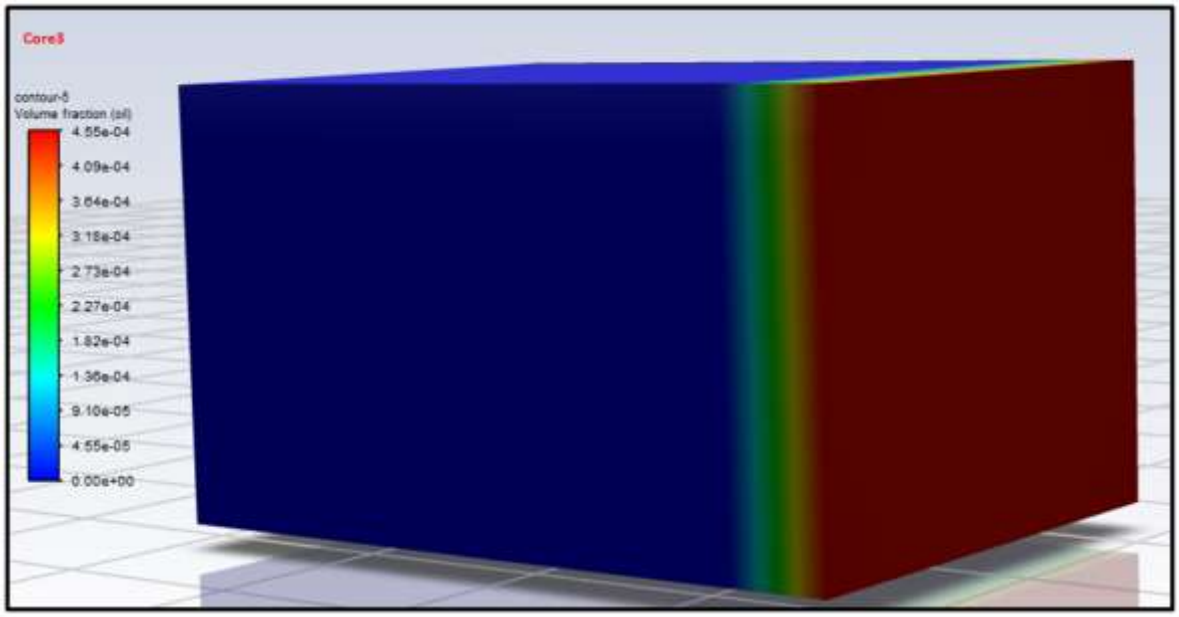

(d)

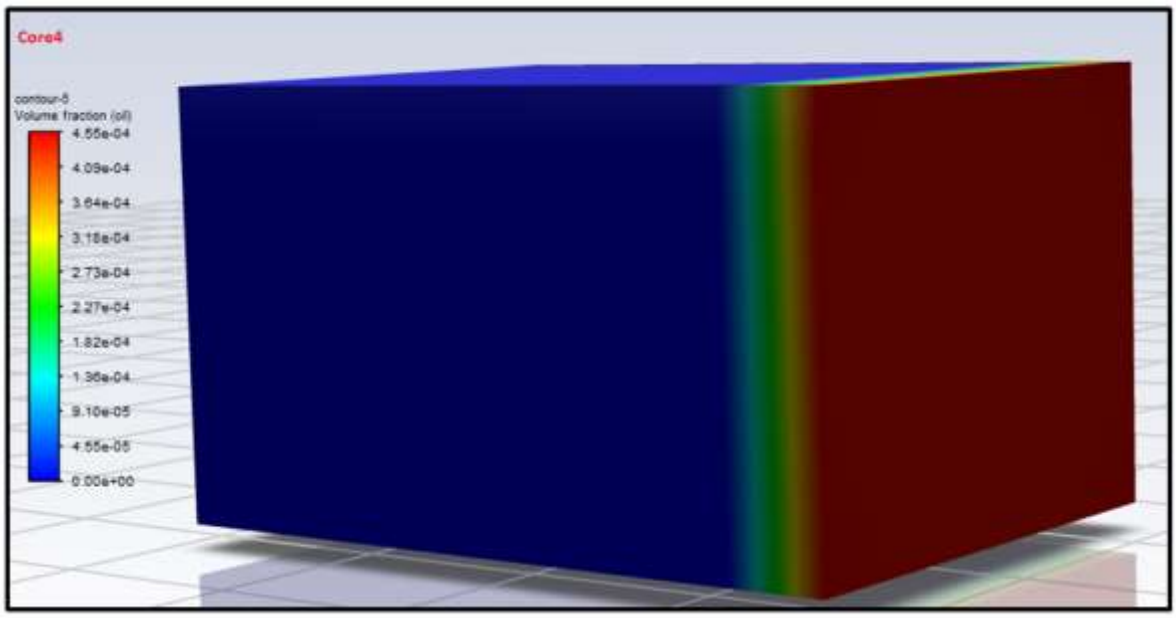

(e)

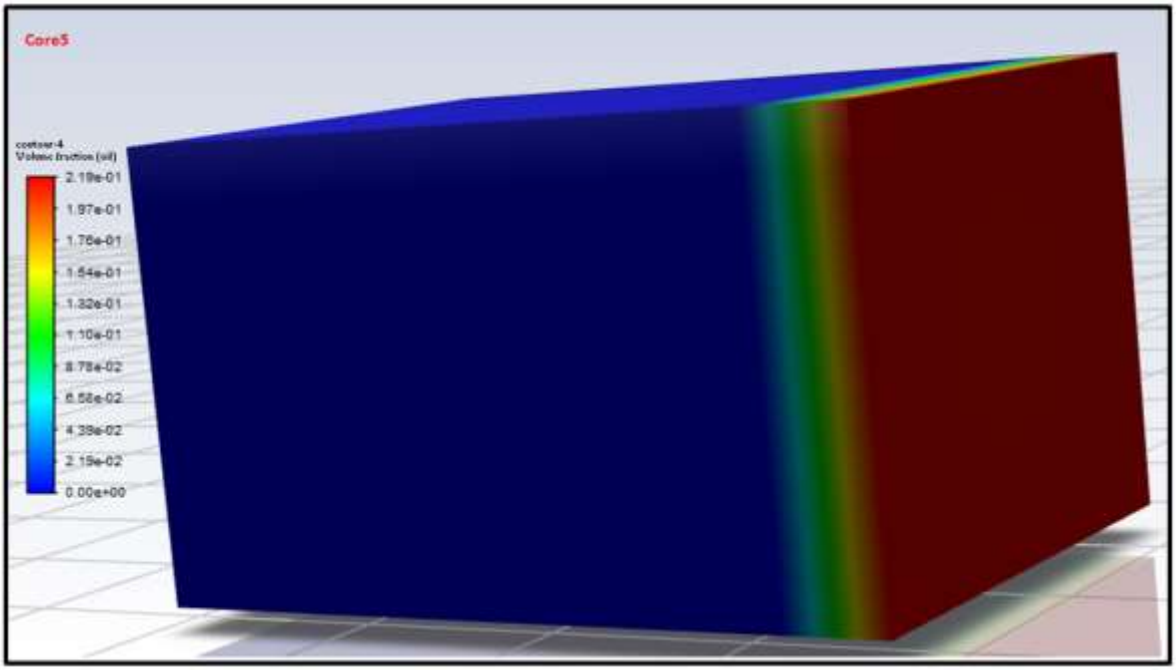

(f)

Figure 5.16:- Oil Volume Fraction contour for Core1,2,3,4,and 5 injected by a): brine water and b,c,d, and e): 1500 ppm HAPA/brine water

Qualitative Numerical Result by CMG

5.11 Oil Saturation and Oil Recovery

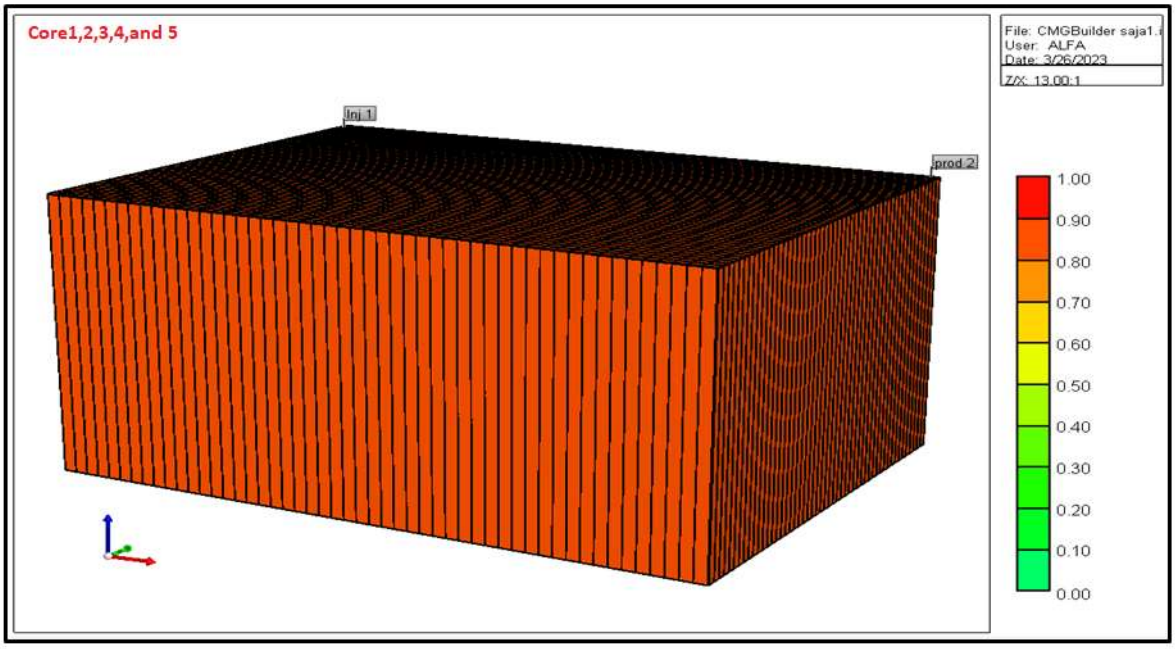

(a)

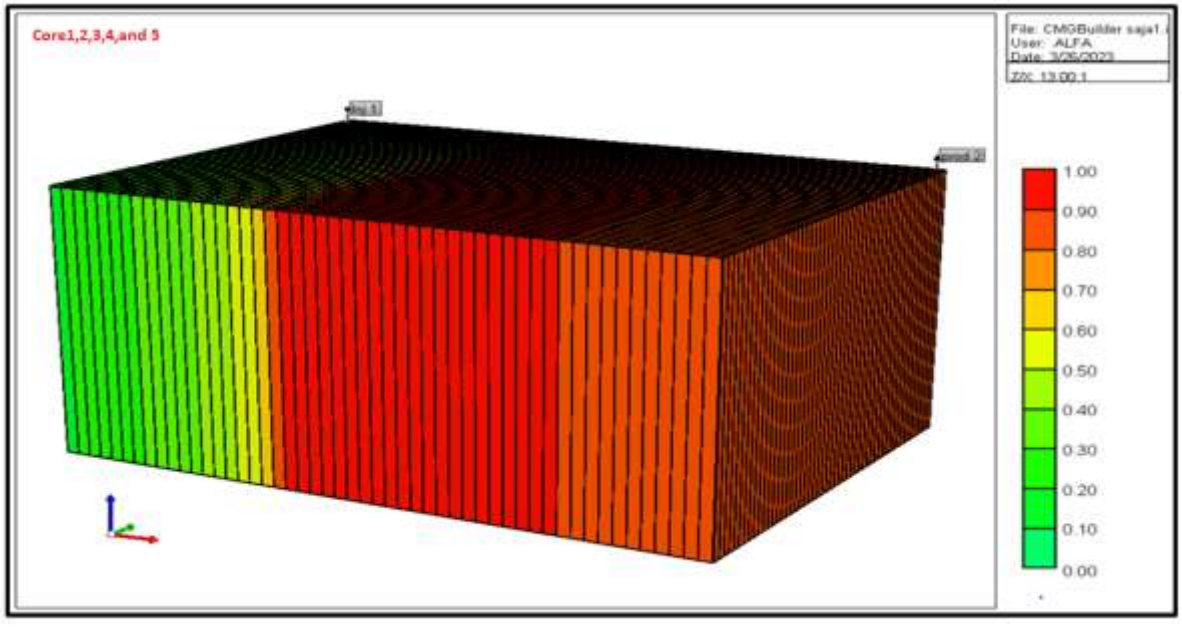

(b)

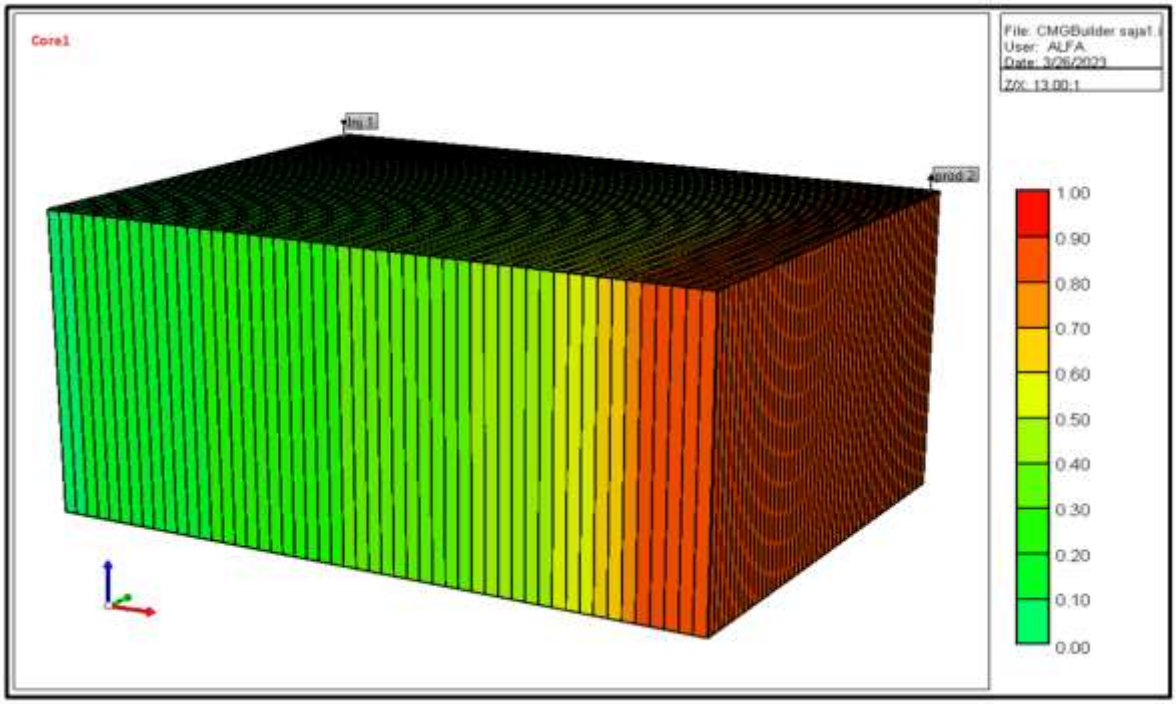
Core1
inj 1
prod 2
File: CMGBuilder saja1.
User: ALFA
Date: 3/26/2023
Z/X: 13.00:1
1.00
0.90
0.80
0.70
0.60
0.50
0.40
0.30
0.20
0.10
0.00

(c)

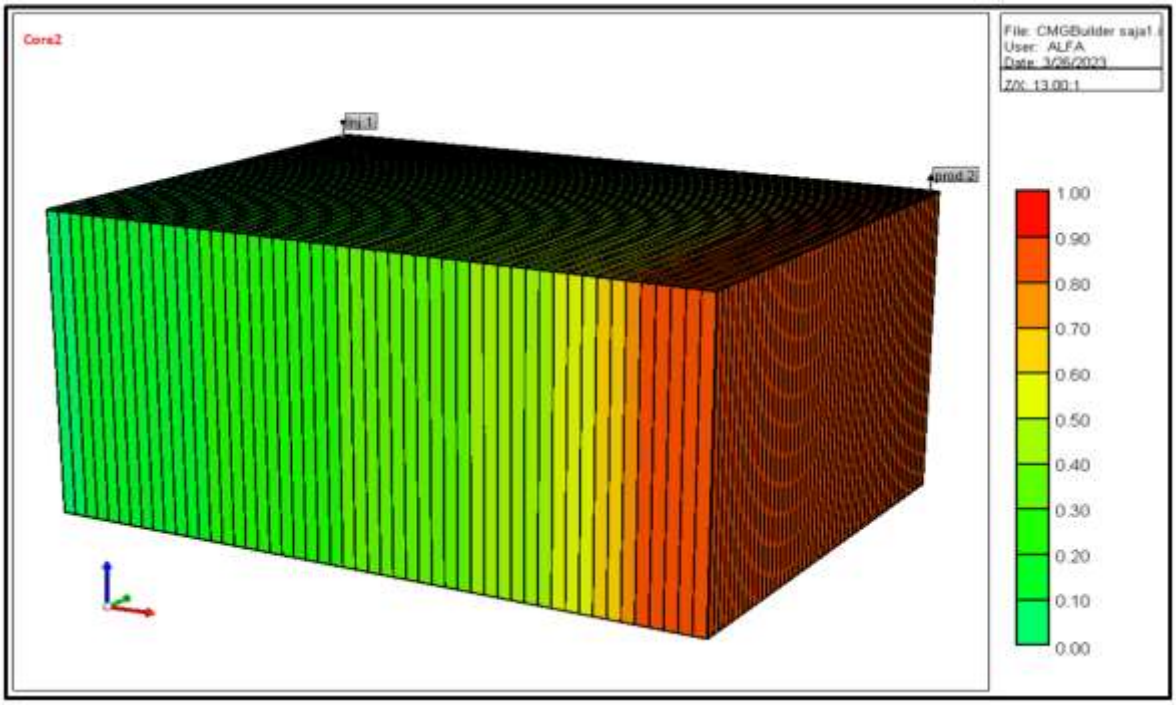
Core2
inj 1
prod 2
File: CMGBuilder saja1.
User: ALFA
Date: 3/26/2023
Z/X: 13.00:1
1.00
0.90
0.80
0.70
0.60
0.50
0.40
0.30
0.20
0.10
0.00

(d)

The oil saturation map shows a uniformity overall the grid Figure 5.17 a .This represents initial oil saturation in Core1,2,3,4, and 5. When brine water flooding is started into Core 1,2,3,4,and 5.It first pushes the oil near the injector well toward the producer well . after completion of brine water flooding , the oil saturation map looks like at Figure 5.17 b, it has been noticed that sweeping of oil is non homogenous in the Core 1,2,3,4, and 5. Maximum oil swept belongs to the region near injector well. 1500ppm HAPAM/brine water was introduced into the Core1,2,3,4,and 5 separately. It improves the sweep efficiency by IFT reduction mechanism, and now, oil far away from the injector well is also pushed to the producer well Figure 5.17 c,d,e, f and g.

With the introduction of brine water flooding in Core1,2,3,4,and 5 water cut increases progressively resulting in a decreasing oil cut. while, in case of HAPAM has been introduced for Core 1,2,3,4, and 5.It reflects that this leads to a decrease in water cut and increased oil cut and also cumulative oil increases sharply. Initial oil saturation in the Core1,2,3,4,and 5 was found to be 102,105,101, 100,103 and 105 ml respectively by volume. According to Figure 5.17 b, total oil recovered at the end of brine water flooding is 62.83, 61.72,65.65, 66.83, and 68.85%. At HAPAM flooding obtained as show in Figure 5.17 c,d,e,f, and g, total oil recovered is 93.68, 94.75,96.12, 96.71,and 97.82 % respectively. Thus, the additional recovery by using HAPAM flooding is 31, 33.03, 30.47, 29.88, and 28.97 % respectively .This agree with [202].

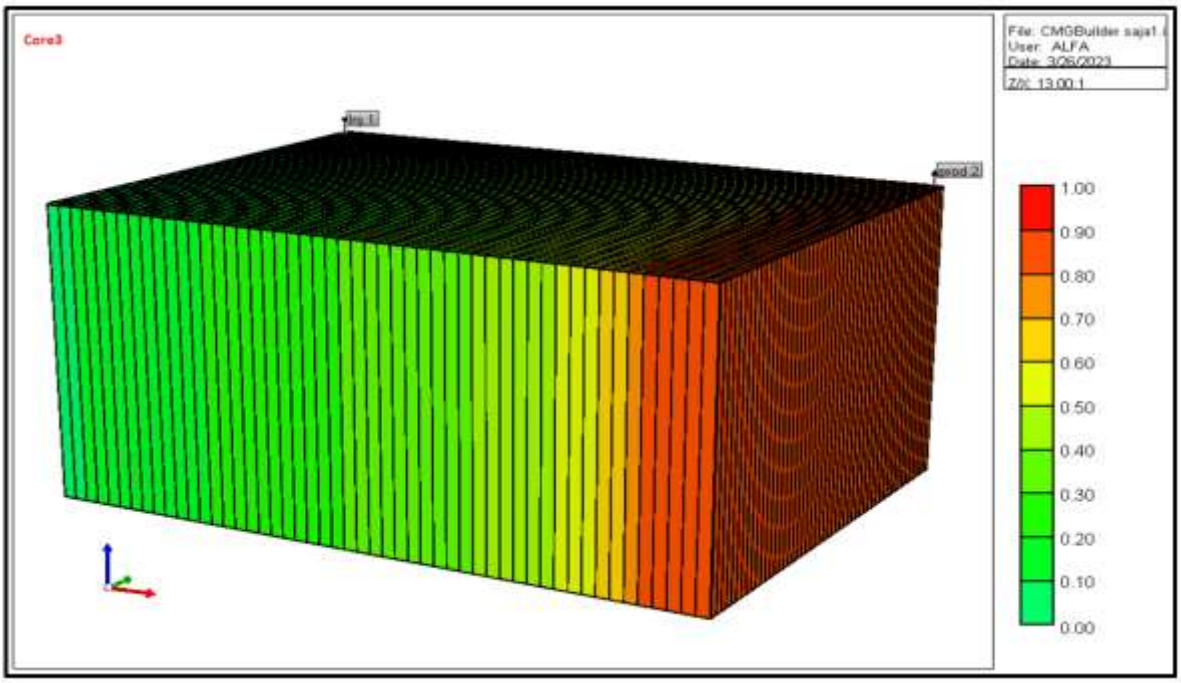
Core3
File: CMGBuilder saja1.
User: ALFA
Date: 3/26/2023
Z/X: 13.00:1
1.00
0.90
0.80
0.70
0.60
0.50
0.40
0.30
0.20
0.10
0.00

(e)

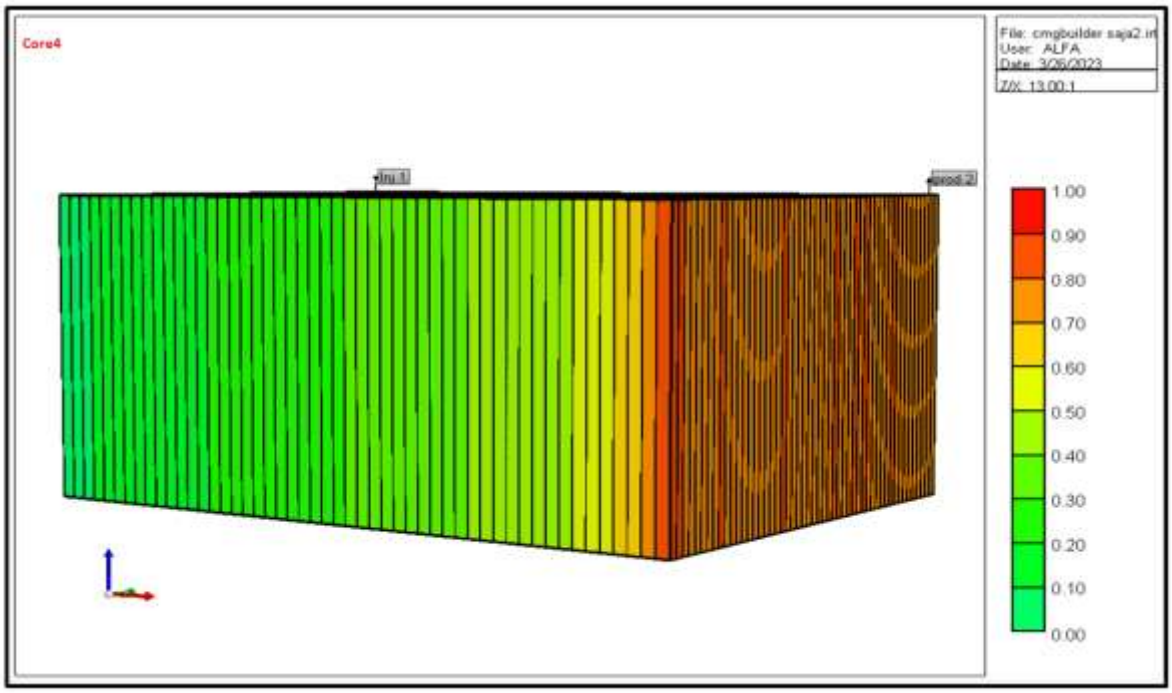
Core4
File: cmgbuilder saja2.in
User: ALFA
Date: 3/26/2023
Z/X: 13.00:1
1.00
0.90
0.80
0.70
0.60
0.50
0.40
0.30
0.20
0.10
0.00

(f)

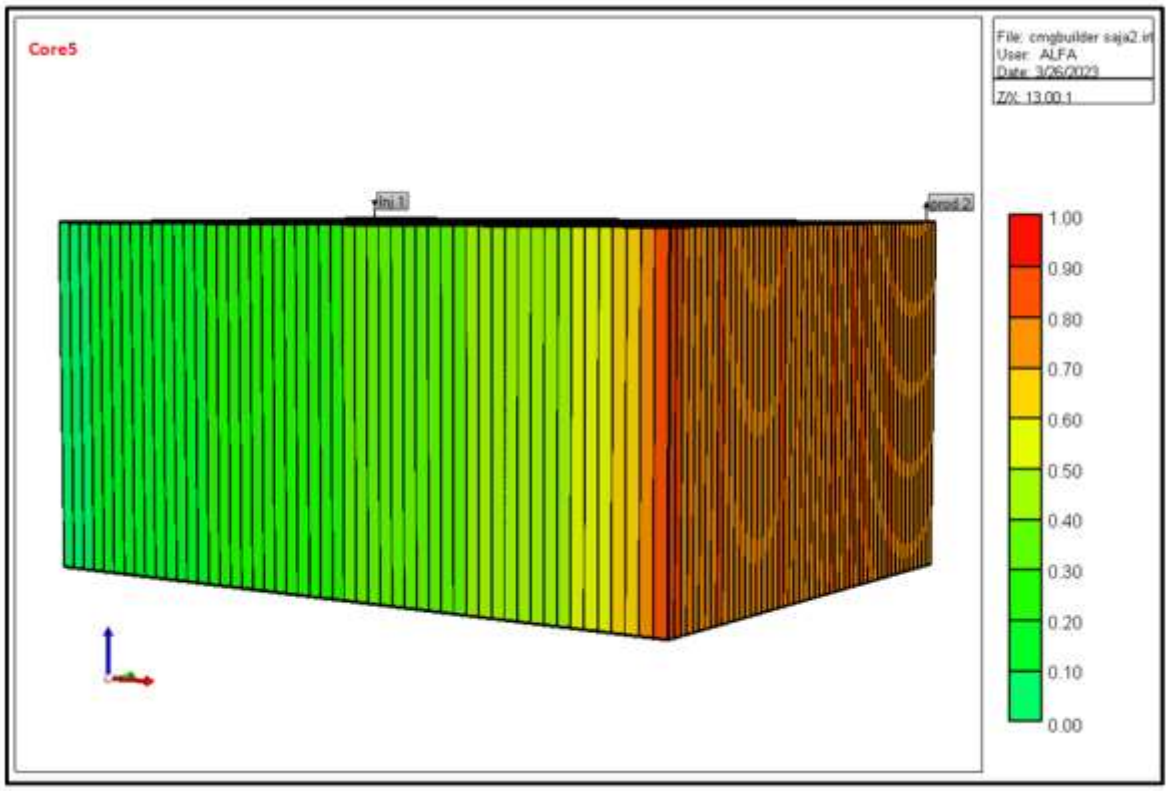

(g)

Figure 5.17 :- Numerical Simulation by CMG of oil saturation for (a) before brine water (b) after brine water ,and (c,d,e,,f and g)after1500ppm HAPAM solution injection in Core1,2,3,4,and 5.

Chapter Six

Conclusion and Recommendation

6.1Conclusion

The section focusses on investigative research for the development, formulation, and performance analysis of polymer systems for application in enhanced oil recovery (EOR). This is performed via a wide range of experimental studies, mechanistic discussions, and simulation models to serve as useful tools for systematic analyses of different EOR routes. The major conclusions of the study are presented as follows:

1- All HAPAM solutions have non-Newtonian flow, Shear thinning behavior appears clear and it was compared with the power law model.

2- The shear viscosity decreases and the shear stress increases with the shear rate above 7.3 S^{-1}.

3- HAPAM viscosities returned to their original levels (i.e., they retained their viscosity even at increasing shear rates and displayed pseudoplastic performance), indicating a dynamic equilibrium between intermolecular association and dissociation.

4- As the HAPAM concentration increases from 500 to 1500ppm, the power low index n drops and the viscosity consistency K increases.

5- 1500 ppm HAPAM solution has higher viscosity, density, surface tension, shear resistance, thermal stability, aging time, consistency index(k) and improved wettability. In addition, less flow index (n) and interfacial tension.

6- At 1500 ppm HAPAM/brine water, the IFT is low as compared with other solutions. This can significantly improve the sweep efficiency with a high solution viscosity. Thus, a higher oil recovery efficiency was obtained for all samples.

7- lower Darcy velocity and capillary number as compared with brine water for 1500ppm HAPAM, this reflect on increase trapped oil to extract from Core samples.

8- The relative permeability curves for brine water and HAPAM solution contain oil wet and water wet components, respectively. This conclusion is supported by experimental data and numerical result from CMG-STARS.

9- The impacts of oil displacement efficiency were investigated using core flooding tests, which demonstrate that flooding with 1500ppm HAPAM/brine water performs significantly better than flooding with brine water alone.

10- At high flow velocities, similar to those experienced in the near wellbore area of an injector,polymer flow history plays a substantial role for HPAM in situ viscosity. Solutions exposed to high rates were mechanically degraded and showed delay in onset of shear thickening and reduction in apparent viscosity compared to the solutions exposed to low shear rate.

11- Mechanical degradation is beneficial for the polymer types and concentrations investigated here since injection pressures are reduced and reservoir apparent viscosities are constant.

12- HAPAM flowing in porous medium at low velocities (e.g., reservoir velocities) show predominantly newtonian behavior followed by shear thickening at higher flow velocities (e.g., at wellbore area).Both flow

behaviors are absent in rheometer measurements that demonstrate a predominantly shear thinning behavior at comparable flow rates.

13- Good agreement between experimental and numerical simulation with CMG and Ansys Fluent.

14- HAPAM solution flooding is a promising technique for chemical EOR. This is because, as compared to brine water flooding.

6.2 Recommendation

Recommendation for further studies show below:-

1-Use sodium dodecyl polyacrylamide in EOR.

1- Use other type of chemical material to show effect of them on

extract oil from porous media.

2-Use other type core like limestone .

3-Use other rheological models to study the behavior of polymer .

4- Evaluate oil recovery from porous media by modeling pore throat, oil

film on rock surface and oil in dead ends.

References

[1] Kang, X., Zhang, J., Sun, F., Zhang, F., Feng, G., Yang, J., ... & Xiang, W. (2011, July). A review of polymer EOR on offshore heavy oil field in Bohai Bay, China. In SPE enhanced oil recovery conference. OnePetro.

[2] Wang, W., Liu, Y., & Gu, Y. (2003). Application of a novel polymer system in chemical enhanced oil recovery (EOR). Colloid and Polymer Science, 281(11), 1046-1054.

[3] Olajire, A. A. (2014). Review of ASP EOR (alkaline surfactant polymer enhanced oil recovery) technology in the petroleum industry: Prospects and challenges. Energy, 77, 963-982.

[4] Firozjaii, A. M., & Saghafi, H. R. (2020). Review on chemical enhanced oil recovery using polymer flooding: Fundamentals, experimental and numerical simulation. Petroleum, 6(2), 115-122.

[5] Lee, S., Kim, D. H., Huh, C., & Pope, G. A. (2009, October). Development of a comprehensive rheological property database for EOR polymers. In SPE Annual Technical Conference and Exhibition. OnePetro.

[6] Han, M., Xiang, W., Zhang, J., Jiang, W., & Sun, F. (2006, December). Application of EOR technology by means of polymer flooding in Bohai Oilfields. In International oil & gas conference and exhibition in China. OnePetro.

[7] Beteta, A., Nurmi, L., Rosati, L., Hanski, S., McIver, K., Sorbie, K., & Toivonen, S. (2020, August). Polymer Chemical Structure and its Impact on EOR Performance. In SPE Improved Oil Recovery Conference. OnePetro.

[8] Kamal, M. S., Shakil Hussain, S. M., & Sultan, A. S. (2016). Development of novel amidosulfobetaine surfactant–polymer systems for EOR applications. Journal of Surfactants and Detergents, 19(5), 989-997.

[9] Kalpakci, B., Arf, T. G., Barker, J. W., Krupa, A. S., Morgan, J. C., & Neira, R. D. (1990, April). The low-tension polymer flood approach to cost-effective chemical EOR. In SPE/DOE Enhanced Oil Recovery Symposium. OnePetro.

[10] Co, L., Zhang, Z., Ma, Q., Watts, G., Zhao, L., Shuler, P. J., & Tang, Y. (2015). Evaluation of functionalized polymeric surfactants for EOR applications in the Illinois Basin. Journal of petroleum Science and Engineering, 134, 167-175.

[11] Zeyghami, M., Kharrat, R., & Ghazanfari, M. H. (2014). Investigation of the applicability of nano silica particles as a thickening additive for polymer solutions applied in EOR processes. Energy Sources, Part A: Recovery, Utilization, and Environmental Effects, 36(12), 1315-1324.

[12] Zhu, Y. (2015, August). Current developments and remaining challenges of chemical flooding EOR techniques in China. In SPE Asia Pacific enhanced oil recovery conference. OnePetro.

[13] Meng, L. W., Kang, W. L., Zhou, Y., Wang, Z. W., Liu, S. R., & Bai, B. J. (2008). Viscoelastic rheological property of different types of polymer solutions for enhanced oil recovery. Journal of Central South University of Technology, 15(1), 126-129.

[14] Feng, Y., Billon, L., Grassl, B., Bastiat, G., Borisov, O., & François, J. (2005). Hydrophobically associating polyacrylamides and their partially

hydrolyzed derivatives prepared by post-modification. 2. Properties of non-hydrolyzed polymers in pure water and brine. Polymer, 46(22), 9283-9295.

[15] El-Hoshoudy, A. N., Desouky, S. E. M., Al-Sabagh, A. M., Betiha, M. A., MY, E. K., & Mahmoud, S. (2017). Evaluation of solution and rheological properties for hydrophobically associated polyacrylamide copolymer as a promised enhanced oil recovery candidate. Egyptian Journal of Petroleum, 26(3), 779-785.

[16] Argillier, J. F., Audibert, A., Lecourtier, J., Moan, M., & Rousseau, L. (1996). Solution and adsorption properties of hydrophobically associating water-soluble polyacrylamides. Colloids and Surfaces A: Physicochemical and Engineering Aspects, 113(3), 247-257.

[17] Wan, T., Li, R., Wu, D., Hu, Z., Xu, M., Cheng, W., & Zou, C. (2014). Rheological behaviors and structure of hydrophobically associating AM–SMA copolymers synthesized by microemulsion polymerization. Polymer bulletin, 71(11), 2819-2831.

[18] El-Hoshoudy, A. N., Desouky, S. E. M., Elkady, M. Y., Alsabagh, A. M., Betiha, M. A., & Mahmoud, S. (2015). Investigation of optimum polymerization conditions for synthesis of cross-linked polyacrylamide-amphoteric surfmer nanocomposites for polymer flooding in sandstone reservoirs. International Journal of Polymer Science, 2015.

[19] Hassan, A. M., Al-Shalabi, E. W., Alameri, W., Kamal, M. S., Patil, S., & Hussain, S. M. S. (2022). Manifestations of surfactant-polymer flooding for successful field applications in carbonates under harsh conditions: A comprehensive review. Journal of Petroleum Science and Engineering, 111243.

[20] Cardoso, O. R., Lima Vidal, R. R., de Lima, B. V., & de Carvalho Balaban, R. (2016, September). Polymer Flooding: The Influence of Polymer Chemical Structure and the Porous Medium. In Macromolecular Symposia (Vol. 367, No. 1, pp. 30-41).

[21] Fülöp, M. T., Breaz, T. O., Raita, G., & Bugnariu, A. D. (2020). More Confidence Of The Financial And Non-Financial Information With The Assurance Of Sustainability Reporting. Annales Universitatis Apulensis-Series Oeconomica, 22(2).

[22] Dordzie, G., & Dejam, M. (2021). Enhanced oil recovery from fractured carbonate reservoirs using nanoparticles with low salinity water and surfactant: a review on experimental and simulation studies. Advances in Colloid and Interface Science, 293, 102449.

[23] Maneeintr, K., Chewaroungroaj, J., & Boonpramote, T. (2020, March). Enhanced oil recovery: potential for oil production development in Fang oilfield, Thailand. In IOP conference series: earth and environmental science (Vol. 463, No. 1, p. 012063). IOP Publishing.

[24] Mohammed, M., Lin, L., Istratescu, G., Babadagli, T., Bademchi Zadeh, A., Anderson, M., & Patterson, C. (2020, September). Underlying Physics of Heavy Oil Recovery by Gas Injection: An Experimental Parametric Analysis when Oil Exists in the Form of Oil Based Emulsion. In SPE Canada Heavy Oil Conference. OnePetro.

[25] Yang, Z., Zhihua, G., JingChun, W., & Hanqing, S. (2022). Construction and Performance Evaluation of Dual-Metabolite Oil-Producing Engineering Bacteria Suitable for Low-Permeability Reservoir. Lithosphere, 2022(Special 12), 8427896.

[26] Arifin, I., Kadja, G. T. M., & Radiman, C. L. (2021). Improving the Viscosity of Partially Hydrolyzed Polyacrylamide (PHPAM) Solution for Enhanced Oil Recovery (EOR) Application. In Key Engineering Materials (Vol. 874, pp. 45-49). Trans Tech Publications Ltd.

[27] Lesage, N., Foraison, H., Lafourcade, J., Jouanolou, M., Munduru, G., Sagne, C., ... & Cordelier, P. (2019, April). EOR Back Produced Water Treatment: Media Selection to Improve Filtration Efficiency. In IOR 2019–20th European Symposium on Improved Oil Recovery (Vol. 2019, No. 1, pp. 1-9). European Association of Geoscientists & Engineers.

[28] Vishnumolakala, N., Zhang, J., & Ismail, N. B. (2020, September). A comprehensive review of enhanced oil recovery projects in Canada and recommendations for planning successful future EOR projects. In SPE Canada Heavy Oil Conference. OnePetro.

[29] Priyanto, S., Salsabila, F. F., Pusakawati, R., Kusworo, T. D., Pramudono, B., Untoro, E., & Ratu, P. (2020, January). Hydrodynamic study: The best injection pressure in enhanced oil recovery (EOR) using surfactant sodium ligno sulfonate (SLS) from black liquor. In AIP Conference Proceedings (Vol. 2197, No. 1, p. 080005). AIP Publishing LLC.

[30] Xu, Z. X., Li, S. Y., Li, B. F., Chen, D. Q., Liu, Z. Y., & Li, Z. M. (2020). A review of development methods and EOR technologies for carbonate reservoirs. Petroleum Science, 17(4), 990-1013.

[31] Anderson, T. I., Li, Y., & Kovscek, A. R. (2021, April). Predicting Heavy Oil Combustion Kinetics with Machine Learning. In SPE Western Regional Meeting. OnePetro.

[32] Al-Ghamdi, A., Haq, B., Al-Shehri, D., Muhammed, N. S., & Mahmoud, M. (2022). Surfactant formulation for Green Enhanced Oil Recovery. Energy Reports, 8, 7800-7813.

[33] Durward-Akhurst, S. A., Schultz, N. E., Norton, E. M., Rendahl, A. K., Besselink, H., Behnisch, P. A., ... & McCue, M. E. (2019). Associations between endocrine disrupting chemicals and equine metabolic syndrome phenotypes. Chemosphere, 218, 652-661.

[34] Steyrleuthner, R., Schubert, M., Jaiser, F., Blakesley, J. C., Chen, Z., Facchetti, A., & Neher, D. (2010). Bulk Electron Transport and Charge Injection in a High Mobility n-Type Semiconducting Polymer. Advanced Materials, 22(25), 2799-2803.

[35] Tsubaki, J., Kato, M., Miyazawa, M., Kuma, T., & Mori, H. (2001). The effects of the concentration of a polymer dispersant on apparent viscosity and sedimentation behavior of dense slurries. Chemical engineering science, 56(9), 3021-3026.

[36] Wang, D., Seright, R. S., Shao, Z., & Wang, J. (2008). Key aspects of project design for polymer flooding at the Daqing Oilfield. SPE Reservoir Evaluation & Engineering, 11(06), 1117-1124.

[37] Santis, F. D., Pantani, R., Speranza, V., & Titomanlio, G. (2010). Analysis of shrinkage development of a semicrystalline polymer during injection molding. Industrial & engineering chemistry research, 49(5), 2469-2476.

[38] Stormonth-Darling, J. M., Pedersen, R. H., How, C., & Gadegaard, N. (2014). Injection moulding of ultra high aspect ratio nanostructures using

coated polymer tooling. Journal of Micromechanics and Microengineering, 24(7), 075019.

[39] Hassan, H. (2013). An experimental work on the effect of injection molding parameters on the cavity pressure and product weight. The International Journal of Advanced Manufacturing Technology, 67(1), 675-686.

[40] Sortino, M., Totis, G., & Kuljanic, E. (2014). Comparison of injection molding technologies for the production of micro-optical devices. Procedia Engineering, 69, 1296-1305.

[41] Ayirala, S., AlSofi, A., AlYousef, Z., Wang, J., Alsaud, M. A., & AlYousef, A. (2022). SmartWater based synergistic technologies for enhanced oil recovery. Fuel, 316, 123264.

[42] Santamaria, O., Lopera, S. H., Riazi, M., Minale, M., Cortés, F. B., & Franco, C. A. (2021). Phenomenological study of the micro-and macroscopic mechanisms during polymer flooding with SiO2 nanoparticles. Journal of Petroleum Science and Engineering, 198, 108135.

[43] Yoo, H., & Lee, J. (2020). Impact of design parameters on oil recovery performance in polymer flooding with low-salinity water-flooding. Geosystem Engineering, 23(2), 63-72.

[44] Skauge, T., Vik, B. F., Ormehaug, P. A., Jatten, B. K., Kippe, V., Skjevrak, I., ... & Skauge, A. (2014, March). Polymer flood at adverse mobility ratio in 2D flow by X-ray visualization. In SPE EOR Conference at Oil and Gas West Asia. OnePetro.

[45] Firozjaii, A. M., & Saghafi, H. R. (2020). Review on chemical enhanced oil recovery using polymer flooding: Fundamentals, experimental and numerical simulation. Petroleum, 6(2), 115-122.

[46] Iyer, A. K., Khaled, G., Fang, J., & Maeda, H. (2006). Exploiting the enhanced permeability and retention effect for tumor targeting. Drug discovery today, 11(17-18), 812-818.

[47] Maeda, H., Bharate, G. Y., & Daruwalla, J. (2009). Polymeric drugs for efficient tumor-targeted drug delivery based on EPR-effect. European journal of pharmaceutics and biopharmaceutics, 71(3), 409-419.

[48] Mishra, S., Bera, A., & Mandal, A. (2014). Effect of polymer adsorption on permeability reduction in enhanced oil recovery. Journal of Petroleum Engineering, 2014.

[49] AlSofi, A. M., Wang, J., Leng, Z., Abbad, M., & Kaidar, Z. F. (2017, April). Assessment of polymer interactions with carbonate rocks and implications for EOR applications. In SPE Kingdom of Saudi Arabia Annual Technical Symposium and Exhibition. OnePetro

[50] Lozinsky, V. I., Galaev, I. Y., Plieva, F. M., Savina, I. N., Jungvid, H., & Mattiasson, B. (2003). Polymeric cryogels as promising materials of biotechnological interest. TRENDS in Biotechnology, 21(10), 445-451.

[51] Taylor, K. C., & Nasr-El-Din, H. A. (2007, June). Hydrophobically associating polymers for oil field applications. In Canadian International Petroleum Conference. OnePetro.

[52] Foucault, S., Ascanio, G., & Tanguy, P. A. (2005). Power characteristics in coaxial mixing: Newtonian and non-Newtonian fluids. Industrial & engineering chemistry research, 44(14), 5036-5043.

[53] Ji, Y., Kang, W., Liu, S., Yang, R., & Fan, H. (2015). The relationships between rheological rules and cohesive energy of amphiphilic polymers with different hydrophobic groups. Journal of Polymer Research, 22(3), 1-7.

[54] Biedermann, F., Nau, W. M., & Schneider, H. J. (2014). The Hydrophobic Effect Revisited—Studies with Supramolecular Complexes Imply High-Energy Water as a Noncovalent Driving Force. Angewandte Chemie International Edition, 53(42), 11158-11171.

[55] Feng, Y., Billon, L., Grassl, B., Bastiat, G., Borisov, O., & François, J. (2005). Hydrophobically associating polyacrylamides and their partially hydrolyzed derivatives prepared by post-modification. 2. Properties of non-hydrolyzed polymers in pure water and brine. Polymer, 46(22), 9283-9295.

[56] Li, X., Shu, Z., Luo, P., & Ye, Z. (2018). Associating polymer networks based on cyclodextrin inclusion compounds for heavy oil recovery. Journal of Chemistry, 2018.

[57] Ezeh, O., Ikiensikimama, S. S., & Akaranta, O. Critical Review of Polymer Flooding in Daqing Field and Pelican Field: Case Studies of the World's Largest Polymer Flooding in Light and Heavy Oil Reservoirs, Respectively.

[58] Yousfi, M., Alix, S., Lebeau, M., Soulestin, J., Lacrampe, M. F., & Krawczak, P. (2014). Evaluation of rheological properties of non-Newtonian fluids in micro rheology compounder: Experimental

procedures for a reliable polymer melt viscosity measurement. Polymer testing, 40, 207-217.

[59] Jian-xin, L., Yong-jun, G., Jun, H., Jian, Z., Xing, L., Xin-ming, Z., & Ping-ya, L. (2012). Displacement characters of combination flooding systems consisting of gemini-nonionic mixed surfactant and hydrophobically associating polyacrylamide for bohai offshoreoilfield. Energy & Fuels, 26(5), 2858-2864.

[60] Saboorian-Jooybari, H., Dejam, M., & Chen, Z. (2016). Heavy oil polymer flooding from laboratory core floods to pilot tests and field applications: Half-century studies. Journal of Petroleum Science and Engineering, 142, 85-100.

[61] Meng, L. W., Kang, W. L., Zhou, Y., Wang, Z. W., Liu, S. R., & Bai, B. J. (2008). Viscoelastic rheological property of different types of polymer solutions for enhanced oil recovery. Journal of Central South University of Technology, 15(1), 126-129.

[62] El-Hoshoudy, A. N., Desouky, S. E. M., Al-Sabagh, A. M., Betiha, M. A., MY, E. K., & Mahmoud, S. (2017). Evaluation of solution and rheological properties for hydrophobically associated polyacrylamide copolymer as a promised enhanced oil recovery candidate. Egyptian Journal of Petroleum, 26(3), 779-785.

[63] Afolabi, R. O., Oluyemi, G. F., Officer, S., & Ugwu, J. O. (2019). Hydrophobically associating polymers for enhanced oil recovery–Part A: A review on the effects of some key reservoir conditions. Journal of petroleum science and engineering, 180, 681-698.

[64] Pu, W. F., Liu, R., Li, B., Jin, F. Y., Peng, Q., Sun, L., ... & Yao, F. S. (2015). Amphoteric hyperbranched polymers with multistimuli-

responsive behavior in the application of polymer flooding. RSC advances, 5(107), 88002-88013.

[65] Fradette, L., Thomé, G., Tanguy, P. A., & Takenaka, K. (2007). Power and mixing time study involving a Maxblend® impeller with viscous Newtonian and non-Newtonian fluids. Chemical engineering research and design, 85(11), 1514-1523.

[66] da Veiga, H. B., & Yang, J. (2019). On the energy equality for solutions to Newtonian and non-Newtonian fluids. Nonlinear Analysis, 185, 388-402.

[67] Markgraf, W., Horn, R., & Peth, S. (2006). An approach to rheometry in soil mechanics—structural changes in bentonite, clayey and silty soils. Soil and Tillage Research, 91(1-2), 1-14.

[68] Shi, L., Zhu, S., Ye, Z., Zhang, J., Xue, X., & Zhao, W. (2020). The seepage flow characteristics of hydrophobically associated polymers with different aggregation behaviours in porous media. Royal Society open science, 7(1), 191270.

[69] Ezeh, O., Ikiensikimama, S. S., & Akaranta, O. Critical Review of Polymer Flooding in Daqing Field and Pelican Field: Case Studies of the World's Largest Polymer Flooding in Light and Heavy Oil Reservoirs, Respectively.

[70] Yousfi, M., Alix, S., Lebeau, M., Soulestin, J., Lacrampe, M. F., & Krawczak, P. (2014). Evaluation of rheological properties of non-Newtonian fluids in micro rheology compounder: Experimental procedures for a reliable polymer melt viscosity measurement. Polymer testing, 40, 207-217.

[71] Wever, D. A. Z., Picchioni, F., & Broekhuis, A. A. (2011). Polymers for enhanced oil recovery: a paradigm for structure–property relationship in aqueous solution. Progress in polymer science, 36(11), 1558-1628.

[72] Sarsenbekuly, B., Kang, W., Yang, H., Zhao, B., Aidarova, S., Yu, B., & Issakhov, M. (2017). Evaluation of rheological properties of a novel thermo-viscosifying functional polymer for enhanced oil recovery. Colloids and Surfaces A: Physicochemical and Engineering Aspects, 532, 405-410.

[73] Quadri, S. M. R., Shoaib, M., AlSumaiti, A. M., & Alhassan, S. M. (2015, December). Screening of polymers for EOR in high temperature, high salinity and carbonate reservoir conditions. In International petroleum technology conference. OnePetro.

[74] Hashmet, M. R., Onur, M., & Tan, I. M. (2014). Empirical correlations for viscosity of polyacrylamide solutions with the effects of temperature and shear rate. II. Journal of dispersion science and technology, 35(12), 1685-1690.

[75] Kamal, M. S., Shakil Hussain, S. M., & Sultan, A. S. (2016). Development of novel amidosulfobetaine surfactant–polymer systems for EOR applications. Journal of Surfactants and Detergents, 19(5), 989-997.

[76] Lu, H., Feng, Y., Zhang, T., & Huang, Z. (2010). Retention behaviors of hydrophobically associating polyacrylamide prepared via inverse microemulsion polymerization through porous media. Journal of Macromolecular Science, Part A: Pure and Applied Chemistry, 47(6), 602-607.

[77] Chen, S., Han, M., & AlSofi, A. M. (2021). Synergistic effects between different types of surfactants and an associating polymer on surfactant–polymer flooding under high-temperature and high-salinity conditions. Energy & Fuels, 35(18), 14484-14498.

[78] El-Hoshoudy, A. N., Desouky, S. E. M., Al-Sabagh, A. M., Betiha, M. A., MY, E. K., & Mahmoud, S. (2017). Evaluation of solution and rheological properties for hydrophobically associated polyacrylamide copolymer as a promised enhanced oil recovery candidate. Egyptian Journal of Petroleum, 26(3), 779-785.

[79] Sarsenbekuly, B., Kang, W., Fan, H., Yang, H., Dai, C., Zhao, B., & Aidarova, S. B. (2017). Study of salt tolerance and temperature resistance of a hydrophobically modified polyacrylamide based novel functional polymer for EOR. Colloids and Surfaces A: Physicochemical and Engineering Aspects, 514, 91-97.

[80] Hassan, A. M., Al-Shalabi, E. W., & Ayoub, M. A. (2022). Updated Perceptions on Polymer-Based Enhanced Oil Recovery toward High-Temperature High-Salinity Tolerance for Successful Field Applications in Carbonate Reservoirs. Polymers, 14(10), 2001.

[81] Wang, W., Liu, Y., & Gu, Y. (2003). Application of a novel polymer system in chemical enhanced oil recovery (EOR). Colloid and Polymer Science, 281(11), 1046-1054.

[82] Afolabi, R. O., Oluyemi, G. F., Officer, S., & Ugwu, J. O. (2019). Hydrophobically associating polymers for enhanced oil recovery–Part A: A review on the effects of some key reservoir conditions. Journal of petroleum science and engineering, 180, 681-698.

[83] Quadri, S. M. R., Shoaib, M., AlSumaiti, A. M., & Alhassan, S. M. (2015, December). Screening of polymers for EOR in high temperature, high salinity and carbonate reservoir conditions. In International petroleum technology conference. OnePetro.

[84] Lee, S., Kim, D. H., Huh, C., & Pope, G. A. (2009, October). Development of a comprehensive rheological property database for EOR polymers. In SPE Annual Technical Conference and Exhibition. OnePetro.

[85] Sarsenbekuly, B., Kang, W., Yang, H., Zhao, B., Aidarova, S., Yu, B., & Issakhov, M. (2017). Evaluation of rheological properties of a novel thermo-viscosifying functional polymer for enhanced oil recovery. Colloids and Surfaces A: Physicochemical and Engineering Aspects, 532, 405-410.

[86] Shi, L. T., Zhu, S. J., Zhang, J., Wang, S. X., Xue, X. S., Zhou, W., & Ye, Z. B. (2015). Research into polymer injection timing for Bohai heavy oil reservoirs. Petroleum Science, 12(1), 129-134.

[87]-[160]

[87] Thomas, S. (2008). Enhanced oil recovery-an overview. Oil & Gas Science and Technology-Revue de l'IFP, 63(1), 9-19.

[88] Alvarado, V., & Manrique, E. (2010). Enhanced oil recovery: an update review. Energies, 3(9), 1529-1575.

[89] Sheng, J. J. (2010). Modern chemical enhanced oil recovery: theory and practice. Gulf Professional Publishing.

[90] Moritis, G. (1996). New technology, improved economics boost EOR hopes. Oil and Gas Journal, 94(16).

[91] Zhang, Y., Wei, M., Bai, B., Yang, H., & Kang, W. (2016, April). Survey and data analysis of the pilot and field polymer flooding projects in China. In SPE improved oil recovery conference. OnePetro.

[92] Wang, D., Seright, R. S., Shao, Z., & Wang, J. (2008). Key aspects of project design for polymer flooding at the Daqing Oilfield. SPE Reservoir Evaluation & Engineering, 11(06), 1117-1124.

[93] Wang, B., Chen, Y., Liu, S., Wu, H., & Song, H. (2006). Photocatalytical visbreaking of wastewater produced from polymer flooding in oilfields. Colloids and Surfaces A: Physicochemical and Engineering Aspects, 287(1-3), 170-174.

[94] Shi, L., Ye, Z., Zhang, Z., Zhou, C., Zhu, S., & Guo, Z. (2010). Necessity and feasibility of improving the residual resistance factor of polymer flooding in heavy oil reservoirs. Petroleum Science, 7(2), 251-256.

[95] Qiannan, Y. U., Yikun, L. I. U., LIANG, S., Shuai, T. A. N., Zhi, S. U. N., & Yang, Y. U. (2019). Experimental study on surface-active polymer flooding for enhanced oil recovery: A case study of Daqing placanticline oilfield, NE China. Petroleum Exploration and Development, 46(6), 1206-1217.

[96] Jingwen, M., Yi, L., Heqing, T., Yiwei, R., Lunhua, L., Taitong, N., & Pingjian, W. (2006). Determination and removal of PAM in oil-field wastewater. INDUSTRIAL WATER TREATMENT-TIANJIN-, 26(3), 77.

[97] Wever, D. A., Polgar, L. M., Stuart, M. C., Picchioni, F., & Broekhuis, A. A. (2013). Polymer molecular architecture as a tool for controlling the rheological properties of aqueous polyacrylamide

solutions for enhanced oil recovery. Industrial & Engineering Chemistry Research, 52(47), 16993-17005.

[98] Lewandowska, K. (2007). Comparative studies of rheological properties of polyacrylamide and partially hydrolyzed polyacrylamide solutions. Journal of applied polymer science, 103(4), 2235-2241.

[99] Xu, L., Che, L., Zheng, J., Huang, G., Wu, X., Chen, P., ... & Hu, Q. (2014). Synthesis and thermal degradation property study of N-vinylpyrrolidone and acrylamide copolymer. RSC advances, 4(63), 33269-33278.

[100] Wei, S., Zhang, X., Zhao, K., Fu, Y., Li, Z., Lin, B., & Wei, J. (2016). Preparation, characterization, and photocatalytic degradation properties of polyacrylamide/calcium alginate/T i O 2 composite film. Polymer Composites, 37(4), 1292-1301.

[101] Lai, N., Dong, W., Ye, Z., Dong, J., Qin, X., Chen, W., & Chen, K. (2013). A water-soluble acrylamide hydrophobically associating polymer: synthesis, characterization, and properties as EOR chemical. Journal of applied polymer science, 129(4), 1888-1896.

[102] El Karsani, K. S., Al-Muntasheri, G. A., Sultan, A. S., & Hussein, I. A. (2014). Impact of salts on polyacrylamide hydrolysis and gelation: New insights. Journal of Applied Polymer Science, 131(23).

[103] Feng, Y., Grassl, B., Billon, L., Khoukh, A., & François, J. (2002). Effects of NaCl on steady rheological behaviour in aqueous solutions of hydrophobically modified polyacrylamide and its partially hydrolyzed analogues prepared by post-modification. Polymer international, 51(10), 939-947.

[104] Deng, Q., Li, H., Li, Y., Cao, X., Yang, Y., & Song, X. (2014). Rheological properties and salt resistance of a hydrophobically associating polyacrylamide. Australian Journal of Chemistry, 67(10), 1396-1402.

[105] Levitt, D. B., Dufour, S., Pope, G., Morel, D., & Gauer, P. (2012, February). Design of an ASP flood in a high-temperature, high-salinity, low-permeability carbonate. In IPTC 2012: International Petroleum Technology Conference (pp. cp-280). European Association of Geoscientists & Engineers.

[106] Ji, Y., Lu, Q., Liu, Q., & Zeng, H. (2013). Effect of solution salinity on settling of mineral tailings by polymer flocculants. Colloids and Surfaces A: Physicochemical and Engineering Aspects, 430, 29-38.

[107] Mpofu, P., Addai-Mensah, J., & Ralston, J. (2004). Temperature influence of nonionic polyethylene oxide and anionic polyacrylamide on flocculation and dewatering behavior of kaolinite dispersions. Journal of colloid and interface science, 271(1), 145-156.

[108] Seright, R. S., Campbell, A. R., Mozley, P. S., & Han, P. (2010). Stability of partially hydrolyzed polyacrylamides at elevated temperatures in the absence of divalent cations. Spe Journal, 15(02), 341-348.

[109] Kamal, M. S., Sultan, A. S., Al-Mubaiyedh, U. A., & Hussein, I. A. (2015). Review on polymer flooding: rheology, adsorption, stability, and field applications of various polymer systems. Polymer Reviews, 55(3), 491-530.

[110] ElKarsani, K. S., Al-Muntasheri, G. A., Sultan, A. S., & Hussein, I. A. (2015). Performance of PAM/PEI gel system for water shut-off in

high temperature reservoirs: Laboratory study. Journal of applied polymer science, 132(17).

[111] Deng, Y., Dixon, J. B., White, G. N., Loeppert, R. H., & Juo, A. S. (2006). Bonding between polyacrylamide and smectite. Colloids and Surfaces A: Physicochemical and Engineering Aspects, 281(1-3), 82-91.

[112] Nwidee, L. N., Al-Anssari, S., Barifcani, A., Sarmadivaleh, M., Lebedev, M., & Iglauer, S. (2017). Nanoparticles influence on wetting behaviour of fractured limestone formation. Journal of Petroleum Science and Engineering, 149, 782-788.

[113] Karimi, A., Fakhroueian, Z., Bahramian, A., Pour Khiabani, N., Darabad, J. B., Azin, R., & Arya, S. (2012). Wettability alteration in carbonates using zirconium oxide nanofluids: EOR implications. Energy & Fuels, 26(2), 1028-1036.

[114] El-Diasty, A. I., & Aly, A. M. (2015, September). Understanding the mechanism of nanoparticles applications in enhanced oil recovery. In SPE North Africa technical conference and exhibition. OnePetro.

[115] Aliabadian, E., Sadeghi, S., Kamkar, M., Chen, Z., & Sundararaj, U. (2018). Rheology of fumed silica nanoparticles/partially hydrolyzed polyacrylamide aqueous solutions under small and large amplitude oscillatory shear deformations. Journal of rheology, 62(5), 1197-1216.

[116] Yuan, J., Liu, D., Huang, W., Li, J., Tang, H., Jia, H., ... & Jia, H. (2021). Effects of Various Nanoparticles on the Rheological Properties of Carboxylic Cellulose Nanofibers and the Compound System’s Application in Enhanced Oil Recovery. Energy & Fuels, 35(14), 11295-11305.

[117] Ahmadi, M. A., Ahmad, Z., Phung, L. T. K., Kashiwao, T., & Bahadori, A. (2016). Evaluation of the ability of the hydrophobic nanoparticles of SiO2 in the EOR process through carbonate rock samples. Petroleum Science and Technology, 34(11-12), 1048-1054.

[118] Kamal, M. S., Adewunmi, A. A., Sultan, A. S., Al-Hamad, M. F., & Mehmood, U. (2017). Recent advances in nanoparticles enhanced oil recovery: rheology, interfacial tension, oil recovery, and wettability alteration. Journal of Nanomaterials, 2017.

[119] Cheraghian, G. (2015). Effects of nanoparticles on wettability: A review on applications of nanotechnology in the enhanced Oil recovery.

[120] Saha, R., Uppaluri, R. V., & Tiwari, P. (2018). Silica nanoparticle assisted polymer flooding of heavy crude oil: emulsification, rheology, and wettability alteration characteristics. Industrial & Engineering Chemistry Research, 57(18), 6364-6376.

[121] Corredor, L. M., Husein, M. M., & Maini, B. B. (2019). Impact of PAM-Grafted nanoparticles on the performance of hydrolyzed polyacrylamide solutions for heavy oil recovery at different salinities. Industrial & Engineering Chemistry Research, 58(23), 9888-9899.

[122] Frijters, S., Günther, F., & Harting, J. (2012). Effects of nanoparticles and surfactant on droplets in shear flow. Soft Matter, 8(24), 6542-6556.

[123] Suleimanov, B. A., Ismailov, F. S., & Veliyev, E. F. (2011). Nanofluid for enhanced oil recovery. Journal of Petroleum science and Engineering, 78(2), 431-437.

[124] Khan, M. B., Khoker, M. F., Husain, M., Ahmed, M., & Anwer, S. (2018). Effects of nanoparticles on rheological behavior of polyacrylamide related to enhance oil recovery. Acad. J. Polym. Sci, 1, 1-2

[125] Haruna, M. A., Nourafkan, E., Hu, Z., & Wen, D. (2019). Improved polymer flooding in harsh environments by free-radical polymerization and the use of nanomaterials. Energy & Fuels, 33(2), 1637-1648.

[126] Sun, X., Zhang, Y., Chen, G., & Gai, Z. (2017). Application of nanoparticles in enhanced oil recovery: a critical review of recent progress. Energies, 10(3), 345.

[127] Gbadamosi, A., Junin, R., Manan, M., Agi, A., & Oseh, J. (2019). Nanotechnology Application in Chemical Enhanced Oil Recovery: Current Opinion and Recent Advances. In Enhanced Oil Recovery Processes-New Technologies. IntechOpen.

[128] Aliabadian, E., Kamkar, M., Chen, Z., & Sundararaj, U. (2019). Prevention of network destruction of partially hydrolyzed polyacrylamide (HPAM): Effects of salt, temperature, and fumed silica nanoparticles. Physics of Fluids, 31(1), 013104.

[129] CHEN, W. H., WANG, Y. F., HE, Z. P., & DING, M. C. (2020). Stability, rheology and displacement performance of nano-SiO2/HPAM/NaCl dispersion systems. Journal of Fuel Chemistry and Technology, 48(5), 568-576.

[130] Peng, B., Tang, J., Luo, J., Wang, P., Ding, B., & Tam, K. C. (2018). Applications of nanotechnology in oil and gas industry: Progress and perspective. The Canadian journal of chemical engineering, 96(1), 91-100.

[131] Seright, R. S., Fan, T., Wavrik, K., Wan, H., Gaillard, N., & Favéro, C. (2011). Rheology of a new sulfonic associative polymer in porous media. SPE Reservoir Evaluation & Engineering, 14(06), 726-734.

[132] Fathi, S. J., Austad, T., & Strand, S. (2012, April). Water-Based Enhanced Oil Recovery EOR by Smart Water in Carbonate Reservoirs. In SPE EOR conference at oil and gas West Asia. OnePetro.

[133] Hatzignatiou, D. G., Norris, U. L., & Stavland, A. (2013). Core-scale simulation of polymer flow through porous media. Journal of Petroleum Science and Engineering, 108, 137-150.

[134] Lu, J., Goudarzi, A., Chen, P., Kim, D. H., Delshad, M., Mohanty, K. K., ... & Pope, G. A. (2014). Enhanced oil recovery from high-temperature, high-salinity naturally fractured carbonate reservoirs by surfactant flood. Journal of Petroleum Science and Engineering, 124, 122-131.

[135] Shi, L. T., Zhu, S. J., Zhang, J., Wang, S. X., Xue, X. S., Zhou, W., & Ye, Z. B. (2015). Research into polymer injection timing for Bohai heavy oil reservoirs. Petroleum Science, 12, 129-134.

[136] Sakthivel, S., Gardas, R. L., & Sangwai, J. S. (2016). Effect of alkyl ammonium ionic liquids on the interfacial tension of the crude oil–water system and their use for the enhanced oil recovery using ionic liquid-polymer flooding. Energy & Fuels, 30(3), 2514-2523.

[137] Hashmet, M. R., AlSumaiti, A. M., Qaiser, Y., & S. AlAmeri, W. (2017). Laboratory investigation and simulation modeling of polymer flooding in high-temperature, high-salinity carbonate reservoirs. Energy & fuels, 31(12), 13454-13465.

[138] He, H., Fu, J., Hou, B., Yuan, F., Guo, L., Li, Z., & You, Q. (2018). Investigation of injection strategy of branched-preformed particle gel/polymer/surfactant for enhanced oil recovery after polymer flooding in heterogeneous reservoirs. Energies, 11(8), 1950.

[139] Qiannan, Y. U., Yikun, L. I. U., Liang, S., Shuai, T., Zhi, S., & Yang, Y. (2019). Experimental study on surface-active polymer flooding for enhanced oil recovery: A case study of Daqing placanticline oilfield, NE China. Petroleum Exploration and Development, 46(6), 1206-1217.

[140] Castro, R. H., Llanos, S., Rodríguez, J., Quintero, H. I., & Manrique, E. (2020). Polymers for EOR application in high temperature and high viscosity oils: Rock–fluid behavior. Energies, 13(22), 5944.

[141] Maghsoudian, A., Tamsilian, Y., Kord, S., Soulgani, B. S., Esfandiarian, A., & Shajirat, M. (2021). Styrene intermolecular associating incorporated-polyacrylamide flooding of crude oil in carbonate coated micromodel system at high temperature, high salinity condition: Rheology, wettability alteration, recovery mechanisms. Journal of Molecular Liquids, 337, 116206.

[142] Hincapie, R. E., Borovina, A., Neubauer, E., Tahir, M., Saleh, S., Arekhov, V., ... & Clemens, T. (2022). Recovery Observations from Alkali, Nanoparticles and Polymer Flooding as Combined Processes. Polymers, 14(3), 603.

[143] Shutang G, Qiang G (2010) Recent progress and evaluation of ASP flooding for EOR in Daqing oil field. SPE EOR Conference at Oil & Gas West Asia.

[144] Ambaliya, M., & Bera, A. (2023). A Perspective Review on the Current Status and Development of Polymer Flooding in Enhanced Oil Recovery Using Polymeric Nanofluids. *Industrial & Engineering Chemistry Research*, *62*(6), 2444-2459.

[145] Rai SK, Bera A, Mandal A (2015) Modeling of surfactant and surfactant–polymer flooding for enhanced oil recovery using STARS (CMG)

software. Journal of Petroleum Exploration and Production Technology 5: 1-11.

[146] Bengar A, Moradi S, Ganjeh-Ghazvini M, Shokrollahi A (2017) Optimized polymer flooding projects via combination of experimental design and reservoir simulation. Society of Petroleum Engineers.

[147] Rai, S. K., Bera, A., & Mandal, A. (2015). Modeling of surfactant and surfactant–polymer flooding for enhanced oil recovery using STARS (CMG) software. Journal of Petroleum Exploration and Production Technology, 5, 1-11.

[148] Firozjaii, A. M., & Moradi, S. (2018). Sensitivity analysis and optimization of the effective parameters on ASP flooding compared to polymer flooding using CMG-STARS. Journal of Petroleum & Environmental Biotechnology, 9(01).

[149] Firozjaii, A. M., & Saghafi, H. R. (2020). Review on chemical enhanced oil recovery using polymer flooding: Fundamentals, experimental and numerical simulation. Petroleum, 6(2), 115-122.

[150] Manzoor, A. A. (2020). Modeling and simulation of polymer flooding with time-varying injection pressure. ACS omega, 5(10), 5258-5269.

[151] Rego, F. B., Botechia, V. E., & Schiozer, D. J. (2017). Heavy oil recovery by polymer flooding and hot water injection using numerical simulation. Journal of Petroleum Science and Engineering, 153, 187-196.

[152] Mohsenatabar Firozjaii, A., Derakhshan, A., & Shadizadeh, S. R. (2018). An investigation into surfactant flooding and alkaline-surfactant-polymer flooding for enhancing oil recovery from carbonate reservoirs: Experimental study and simulation. Energy Sources, Part A: Recovery, Utilization, and Environmental Effects, 40(24), 2974-2985.

[153] Liu, J. Z., Adegbesan, K., & Bai, J. J. (2012, June). Suffield Area, Alberta, Canada–Caen Polymer Flood Pilot Project. In SPE Heavy Oil Conference Canada. OnePetro.

[154] Hazarika, K., Gogoi, S. B., & Kumar, A. (2022). Polymer flo flooding and its effects on enhanced oil recovery special reference to Upper Assam Basin. Petroleum Research.

[155] Lamas, L. F., Botechia, V. E., Schiozer, D. J., Rocha, M. L., & Delshad, M. (2021). Application of polymer flooding in the revitalization of a mature heavy oil field. Journal of Petroleum Science and Engineering, 204, 108695.

[156] Lamas, L. F., Botechia, V. E., Schiozer, D. J., Rocha, M. L., & Delshad, M. (2021). Application of polymer flooding in the revitalization of a mature heavy oil field. Journal of Petroleum Science and Engineering, 204, 108695.

[157] Wang, D., Namie, S., & Seright, R. (2022, April). Pressure barrier applicability to polymer flood design. In SPE Improved Oil Recovery Conference. OnePetro.

[158] Wang, J., & Liu, H. (2014). A novel model and sensitivity analysis for viscoelastic polymer flooding in offshore oilfield. Journal of Industrial and Engineering Chemistry, 20(2), 656-667.

[159] Rosado-Vázquez, F. J., Bashbush-Bauza, J. L., & López-Ramírez, S. (2022). Practical Mathematical Model for the Evaluation of Main Parameters in Polymer Flooding: Rheology, Adsorption, Permeability Reduction, and Effective Salinity. ACS omega, 7(29), 24982-25002.

[160] SayedAkram, N. I., & Mamora, D. (2011, May). Simulation study on surfactant-polymer flood performance in fractured carbonate reservoir. In SPE/DGS Saudi Arabia section technical symposium and exhibition. OnePetro.

[161] Dang, C. T., Chen, Z., Nguyen, N. T., Bae, W., & Phung, T. H. (2011, July). Successful story of development and optimization for surfactant-polymer flooding in a geologically complex reservoir. In SPE Enhanced Oil Recovery Conference. OnePetro.

[162] Pinto, M. S., Herrera, D. M., & Angarita, J. C. G. (2018). Production optimization for a conceptual model through combined use of polymer flooding and intelligent well technology under uncertainties. Revista Fuentes, 16(1), 37-45.

[163] Bao, P., Li, A., Luo, S., & Dang, X. (2018, February). Determination of adsorption parameters in numerical simulation for polymer flooding. In IOP conference series: earth and environmental science (Vol. 113, No. 1, p. 012070). IOP Publishing.

[164] Tunnish, A., & Henni, A. (2018). The Employment Of CMG-STARS To Simulate Alkaline/Ionic Liquid/Polymer (AILP) Flooding Results. J. Multidiscip. Eng. Sci. Stud., 4(12), 2362-2368.

[165] Jadhawar, P., & Saeed, M. (2023). Low salinity water and polymer flooding in sandstone reservoirs: Upscaling from nano-to macro-scale using the maximum energy barrier. Journal of Petroleum Science and Engineering, 220, 111247.

[166] Zechner M, Buchgraber M, Clemens T, Gumpenberger T, Castanier LM, Kovscek AR, et al. Rheological behavior within induced fractures and near-wellbore-area.SPE Annual Technical Conference and Exhibition New Orleans (USA): Society of Petroleum Engineers; 2013. https://doi.org/10.2118/166085-MS.

[167] Laoroongroj A, Gumpenberger T, Clemens T. Polymer flood incremental oil recovery and efficiency in layered reservoirs including non-

newtonian and viscoelastic effects. SPE Ann Tech Conf Exhibit Amsterdam, the Netherlands: Society of Petroleum Engineers; 2014. https://doi.org/10.2118/170657-MS.

[168] Heemskerk J, Rosmalen R, Janssen-van R, Holtslag RJ, Teeuw D. Quantification of viscoelastic effects of polyacrylamide solutions. SPE Enhanced Oil Recovery Symposium Tulsa (USA): Society of Petroleum Engineers; 1984. https://doi.org/ 10.2118/12652-MS.

[169] Delshad M, Kim DH, Magbagbeola OA, Huh C, Pope GA, Tarahhom F. Mechanistic interpretation and utilization of viscoselastic behavior of polymer solutions for improved polymer-flood efficiency. SPE Symposium on Improved Oil Recovery Tulsa (USA): Society of Petroleum Engineers; 2008. https://doi.org/10.2118/ 113620-MS.

[170] Gleasure RW. An experimental study of non-newtonian polymer rheology effects on oil recovery and injectivity. SPE Reserv Engs 1990;5(4):481–6. https://doi.org/ 10.2118/17648-PA.

[171] Buitenhuis J, Springer J. Negative thixotropy of polymer solutions. 2. A systematic study of the time-dependent viscosity of partially hydrolyzed polyacrylamide. Colloid Polym Sci 2003;281(3):260–6. https://doi.org/10.1007/s00396-002- 0769-x.

[172] Buitenhuis J, Ponitsch M. Negative thixotropy of polymer solutions. 1. A model explaining time-dependent viscosity. Colloid Polym Sci 2003;281(3):253–9. https://doi.org/10.1007/s00396-002-0768-y.

[173] Hu Y, Wang SQ, Jamieson AM. Rheological and rheooptical studies of shearthickening polyacrylamide solutions. Macromolecules 1995;28(6):1847–53. https://doi.org/10.1021/ma00110a019.

[174] Quadrat O, Bradna P, Dupuis D, Wolff C. Negative thixotropy of solutions of partially hydrolyzed polyacrylamide. 1. the influence of shear rate on time changes of flow characteristics. Colloid Polym Sci 1992;270(11):1057–9. https:// doi.org/10.1007/BF00652867.

[175] You, Q., Wen, Q., Fang, J., Guo, M., Zhang, Q., & Dai, C. (2019). Experimental study on lateral flooding for enhanced oil recovery in bottom-water reservoir with high water cut. Journal of Petroleum Science and Engineering, 174, 747-756.

[176] Maddinelli, G., Bartosek, M., Carminati, S., Moghadasi, L., Manfredini, N., & Moscatelli, D. (2020, November). Design of Thermoresponsive Polymers to Selective Permeability Reduction in Porous Media. In *Abu Dhabi International Petroleum Exhibition & Conference*. OnePetro.

[177] Sarmah, S., Gogoi, S. B., Jagatheesan, K., & Hazarika, K. (2022). Formulation of a combined low saline water and polymer flooding for enhanced oil recovery. *International Journal of Ambient Energy*, *43*(1), 1089-1097.

[178] Saha, R., Phukan, R., Pandey, L., & Tiwari, P. (2022). Optimum Formulation of Chemical Slug and Core Flooding Studies. *Microbial Enhanced Oil Recovery: Principles and Potential*, 73-99.

[179] Khamees, T., Flori, R., & Al Saba, M. (2019, October). Investigating BrightWater® as a Potential Method of Improving Sweep Efficiency in Heterogeneous Reservoirs by Numerical Modeling. In *SPE Kuwait Oil & Gas Show and Conference*. OnePetro.

[180] OLAYINKA, G. A. (2019). *APPLICATION OF POLYMERIC NANOFLUIDS FOR ENHANCED OIL RECOVERY IN MID-PERMEABILITY SANDSTONE* (Doctoral dissertation, Universiti Teknologi Malaysia).

[181] Ambaliya, M., & Bera, A. (2023). A Perspective Review on the Current Status and Development of Polymer Flooding in Enhanced Oil Recovery Using Polymeric Nanofluids. *Industrial & Engineering Chemistry Research*, *62*(6), 2444-2459.

[182] Saha, R., Phukan, R., Pandey, L., & Tiwari, P. (2022). Optimum Formulation of Chemical Slug and Core Flooding Studies. *Microbial Enhanced Oil Recovery: Principles and Potential*, 73-99.

[183] Sarmah, S., Gogoi, S. B., Jagatheesan, K., & Hazarika, K. (2022). Formulation of a combined low saline water and polymer flooding for enhanced oil recovery. *International Journal of Ambient Energy*, *43*(1), 1089-1097.

[184] Gbadamosi, A. O., Junin, R., Manan, M. A., Yekeen, N., & Augustine, A. (2019). Hybrid suspension of polymer and nanoparticles for enhanced oil recovery. *Polymer Bulletin*, *76*, 6193-6230.

[185] Xiangguo, L. U., Bao, C. A. O., Kun, X. I. E., Weijia, C. A. O., Yigang, L. I. U., ZHANG, Y., ... & ZHANG, J. (2021). Enhanced oil recovery mechanisms of polymer flooding in a heterogeneous oil reservoir. *Petroleum Exploration and Development*, *48*(1), 169-178.

[186] Kakati, A., Bera, A., & Al-Yaseri, A. (2022). A Review on Advanced Nanoparticles-Induced Polymer Flooding for Enhanced Oil Recovery. *Chemical Engineering Science*, 117994.

[187] Southwick JG, Manke CW. Molecular degradation, injectivity, and elastic properties of polymer solutions. SPE Reserv Engs 1988;3(4):193–201.

[188] Papanastasiou T, Georgiou G, Alexandrou AN. Viscous fluid flow. Boca Raton(USA): CRC Press; 1999. ISBN 978-0-84931-606-7.

[189] Guo SP, Huang YZ. Physical chemistry microscopic seepage flow mechanism. Beijing (China): Science Press; 1990.

[190] Al-Anssari, S., Ali, M., Alajmi, M., Akhondzadeh, H., Khaksar Manshad, A., Kalantariasl, A., ... & Keshavarz, A. (2021). Synergistic effect of nanoparticles and polymers on the rheological properties of injection fluids: implications for enhanced oil recovery. *Energy & Fuels*, *35*(7), 6125-6135.

[191] Bera, A., Shah, S., Shah, M., Agarwal, J., & Vij, R. K. (2020). Mechanistic study on silica nanoparticles-assisted guar gum polymer flooding for enhanced oil recovery in sandstone reservoirs. *Colloids and Surfaces A: Physicochemical and Engineering Aspects*, *598*, 124833.

[192] Levitt D, Pope GA. Selection and screening of polymers for enhanced-oil recovery. SPE symposium on improved oil recovery Tulsa (USA): Society of Petroleum Engineers; 2008. https://doi.org/10.2118/113845-MS.

[193] Gou S, Li S, Feng M, Zhang Q, Pan Q, Wen J, Wu Y, Guo Q. Novel biodegradable graft-modified water-soluble copolymer using acrylamide and konjac glucomannan for enhanced oil recovery. Ind Eng Chem Res 2017;56(4):942–51. https:// doi.org/10.1021/acs.iecr.6b04649.

[194] Sabhapondit A, Borthakur A, Haque I. Water soluble acrylamidomethyl propane sulfonate (AMPS) copolymer as an enhanced oil recovery chemical. Energy Fuels 2003;17(3):683–8. https://doi.org/10.1021/ef010253t.

[195] Gaillard N, Giovannetti B, Favero C, Caritey JP, Dupuis G, Zaitoun A. New water soluble anionic NVP acrylamide terpolymers for use in harsh EOR conditions. SPE improved oil recovery symposium Tulsa (USA): Society of Petroleum Engineers;2014. https://doi.org/10.2118/169108-MS.

[196] Gaillard N, Sanders DB, Favero C. Improved oil recovery using thermally and chemically protected compositions based on co- and ter-polymers containing acrylamide. SPE improved oil recovery symposium Tulsa (USA): Society of Petroleum Engineers; 2010. https://doi.org/10.2118/129756-MS.

[197] Sandengen K, Meldahl MM, Gjersvold B, Molesworth P, Gaillard N, Braun O, Antignard S. Long term stability of ATBS type polymers for enhanced oil recovery. J Petrol Sci Eng 2018;169:532–45. https://doi.org/10.1016/j.petrol.2018.06.001.

[198] Lara-Ceniceros AC, Rivera-Vallejo C, Jimenez-Regalado EJ. Synthesis, characterization and rheological properties of three different associative polymers obtained by micellar polymerization. Polym Bull 2007;58(2):425–33. https://doi.org/10. 1007/s00289-006-0675-3.

[199] Pancharoen M. Physical properties of associative polymer solutions MSc thesis Stanford (USA): Stanford University; 2009.

[200] Guo Y, Hu J, Zhang X, Feng R, Li H. Flow behavior through porous media and microdisplacement performances of hydrophobically modified partially hydrolyzed polyacrylamide. SPE J 2016;21(3):688–705. https://doi.org/10.2118/ 178921-PA.

[201] Tan H, Tam KC, Tirtaatmadja V, Jenkins RD, Bassett DR. Extensional properties of model hydrophobically modified alkali-soluble associative

(HASE) polymer solutions. J Nonnewton Fluid Mech 2000;92(2–3):167–85. https://doi.org/10.1016/ S0377-0257(00)00093-8.

[202] Abdala AA. Solution rheology & microstructure of associative polymers Doctoral Dissertation Raleigh (USA): North Carolina State University; 2002.

الخلاصة

يهدف هذا العمل إلى تحسين إنتاج النفط الخام المتبقي داخل الأوساط المسامية (الصخور) من خلال استخدام أسلوب غمر البوليمر بطريقة مختبرية وعددية . تم خلط بوليمر البولي اكريل امايد المترابط الكارهة للماء (HAPAM) بتراكيز (500 ، 1000 ، 1500 و 2000) جزء في المليون ، مع الماء المالح لاستخدامه في الاختبارات البوليمرية والإزاحة. تم دراسة الخصائص الانسيابية ,الفيزيائية ,البتروفيزيائية ,قابلية الترطيب ,التحلل الميكانيكي ونسبة استخلاص النفط. تم إجراء محاكاة عددية باستخدام طريقة الاختلاف المحدده (F.D.M) في برنامج مجموعة النمذجة الحاسوبية (CMG) وطريقة العناصر المحددة (F.E.M) في برنامج Ansys Fluent.

تم قياس الخواص الريولوجية حسب تغير اللزوجة مع التركيز ,معدل القص ,اجهاد القص ,مقاومة القص ودرجة الحرارة. تم اختبار الخواص الفيزيائية وفقاً للتغير في الكثافة ,الشد السطحي ,الشد البني ا بتركيزات مختلفة من HAPAM. تم تصميم وبناء جهاز الازاحة المختبرية (Core flooding) في هذه الدراسة لقياس الخصائص البتروفيزيائية ونسبة الاستخلاص المعزز للنفط. المسامية والنفاذية وسرعة دارسي وعدد الشعيرات الدموية لثلاثة أنواع من صخور الكاربونية Core 1 , 1 Core 2 , Core 3 ونوعين من الصخور الرملية Core4 و Core5 في هذا النظام.

تمت دراسة قابلية الترطيب من خلال منحنيات النفاذية النسبية مع نسبة التشبع بالماء واستخلاص النفط مع حجم المسام. تم تقدير التدهور الميكانيكي من خلال منحنيات اللزوجة الظاهرية داخل الوسط المسامي ولزوجة القص داخل مقياس الانسياب مع اختلاف معدل القص ,اللزوجة الظاهرة مع سرعة دارسي ومعدل القص بالإضافة إلى فرق الضغط مع سرعة دارسي.

تم محاكاة تجارب الازاحة المختبرية باستخدام CMG-STARS للتحقيق من النفاذية النسبية ونسبة استخراج الزيت ، كما تم استخدام النموذج الديكارتي لتطوير نهج رقمي قوي لمطابقة خصائص الغمر للسوائل التي تم تحليلها في البداية ، تم محاكاة الماء المالحي وحقن محلول HAPAM بشكل منفصل. تم استخدام Ansys Fluent لتقدير منطقة التلامس التي تشير إلى محلول ملحي مع النفط او HAPAM مع النفط كسوائل غير قابلة للامتزاج في مستطيل ثنائي الأبعاد (2D) نوعيًا. تم إجراء المحاكاة اعتمادًا على الشد السطحي والشد البيني (IFT) وتأثيرات اللزوجة.

أظهرت النتائج التجريبية أن جميع محاليل HAPAM لها تدفق غير نيوتوني ، وكان سلوك ترقق القص(shear thinning) هو المسيطر وتمت مقارنته مع موديل power law. تنخفض لزوجة

القص و إجهاد القص يزداد مع معدل القص أعلى من $7.3\ S^{-1}$ ، حيث يتميز محلول HAPAM 1500 جزء في المليون بلزوجة ,كثافة ,شد سطحي ,مقاومة القص ,استقرار حراري ,وقت تقادم ,مؤشر الاتساق (Consistency, k) وتحسين قابلية البلل ، مع انخفاض مؤشر التدفق (n) والشد البيني.إن HAPAM 1500جزء في المليون مقارنة بالمياه المالحة لديها سرعة دارسي ,عدد شعري , وقابلية للترطيب عالية بسبب تأخير نقطة اختراق النفط.ظاهرة سماكة القص والتدهور الميكانيكي عند معدل القص فوق $7.3S^{-1}$ ،تحسين قابلية استخراج النفط من (63,62,66, and67)%الى (94,95,96.4,97,and 98)% . أظهرت النتائج النوعية لـ Ansys ثباتًا عاليًا وعدم وجود أصابع لزجة في منطقة التلامس بين هذا المحلول والنفط. من خلال نتائج هذه الدراسة نلاحظ مدى التوافق ما بين النتائج المختبرية والعددية مما يوفر هذا العمل نهجًا اقتصاديًا وموفرًا للوقت لإجراء تجارب عددية في مجالات عمليات تحسين انتاج النفط.

Appendex

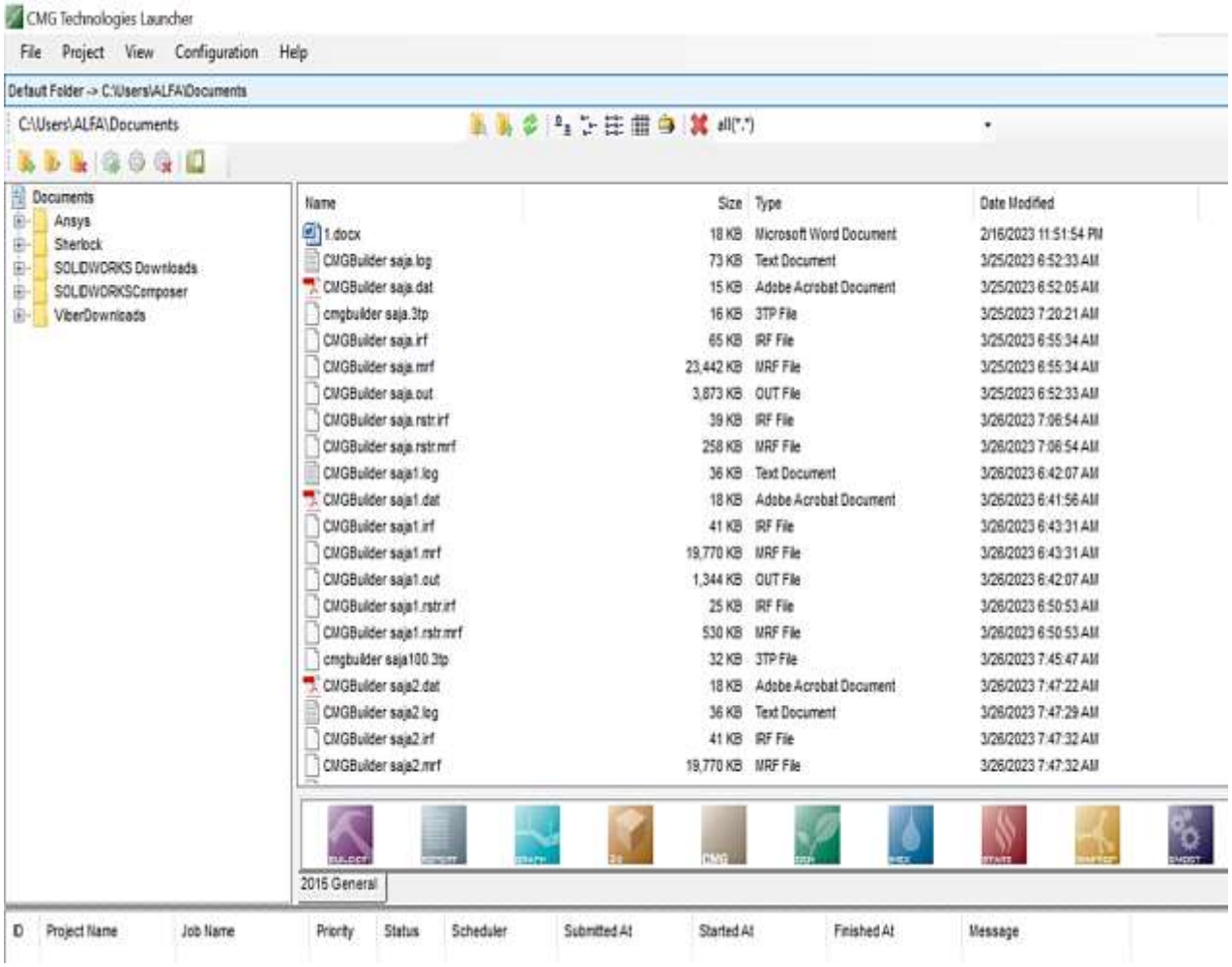
CMG Technologies Launcher
File Project View Configuration Help
Default Folder -> C:\Users\ALFA\Documents
C:\Users\ALFA\Documents
all(*.*)
Documents
Ansys
Sherlock
SOLIDWORKS Downloads
SOLIDWORKSComposer
ViberDownloads
Name Size Type Date Modified
1.docx 18 KB Microsoft Word Document 2/16/2023 11:51:54 PM
CMGBuilder saja.log 73 KB Text Document 3/25/2023 6:52:33 AM
CMGBuilder saja.dat 15 KB Adobe Acrobat Document 3/25/2023 6:52:05 AM
cmgbuilder saja.3tp 16 KB 3TP File 3/25/2023 7:20:21 AM
CMGBuilder saja.irf 65 KB IRF File 3/25/2023 6:55:34 AM
CMGBuilder saja.mrf 23,442 KB MRF File 3/25/2023 6:55:34 AM
CMGBuilder saja.out 3,873 KB OUT File 3/25/2023 6:52:33 AM
CMGBuilder saja.rstr.irf 39 KB IRF File 3/26/2023 7:06:54 AM
CMGBuilder saja.rstr.mrf 258 KB MRF File 3/26/2023 7:06:54 AM
CMGBuilder saja1.log 36 KB Text Document 3/26/2023 6:42:07 AM
CMGBuilder saja1.dat 18 KB Adobe Acrobat Document 3/26/2023 6:41:56 AM
CMGBuilder saja1.irf 41 KB IRF File 3/26/2023 6:43:31 AM
CMGBuilder saja1.mrf 19,770 KB MRF File 3/26/2023 6:43:31 AM
CMGBuilder saja1.out 1,344 KB OUT File 3/26/2023 6:42:07 AM
CMGBuilder saja1.rstr.irf 25 KB IRF File 3/26/2023 6:50:53 AM
CMGBuilder saja1.rstr.mrf 530 KB MRF File 3/26/2023 6:50:53 AM
cmgbuilder saja100.3tp 32 KB 3TP File 3/26/2023 7:45:47 AM
CMGBuilder saja2.dat 18 KB Adobe Acrobat Document 3/26/2023 7:47:22 AM
CMGBuilder saja2.log 36 KB Text Document 3/26/2023 7:47:29 AM
CMGBuilder saja2.irf 41 KB IRF File 3/26/2023 7:47:32 AM
CMGBuilder saja2.mrf 19,770 KB MRF File 3/26/2023 7:47:32 AM
2016 General
ID Project Name Job Name Priority Status Scheduler Submitted At Started At Finished At Message

جمهورية العراق

وزارة التعليم العالي والبحث العلمي

جامعة بابل

كلية هندسة المواد

قسم البوليمر والصناعات البتروكيمياوية

التمثيل العملي والمحاكاة العددية للخواص الانسيابية للبوليمرات الكارهة للماء للاستخراج المعزز للنفط

اطروحة

مقدمة الى كلية هندسة المواد/جامعة بابل وهي جزء من متطلبات نيل

درجة فلسفة الدكتوراه في هندسة المواد/ بوليمر

من قبل

سجى حيدر محمد جبار

بأشراف

أ.د. نزار جواد هادي

1444 2023